SECRET

MASTER

MND-P-3004

THIS DOCUMENT CONSISTS OF 130 ~~128~~ PAGES

NO. 40 OF 100 COPIES, SERIES A

RADIOISOTOPE FUELED AUXILIARY POWER UNIT

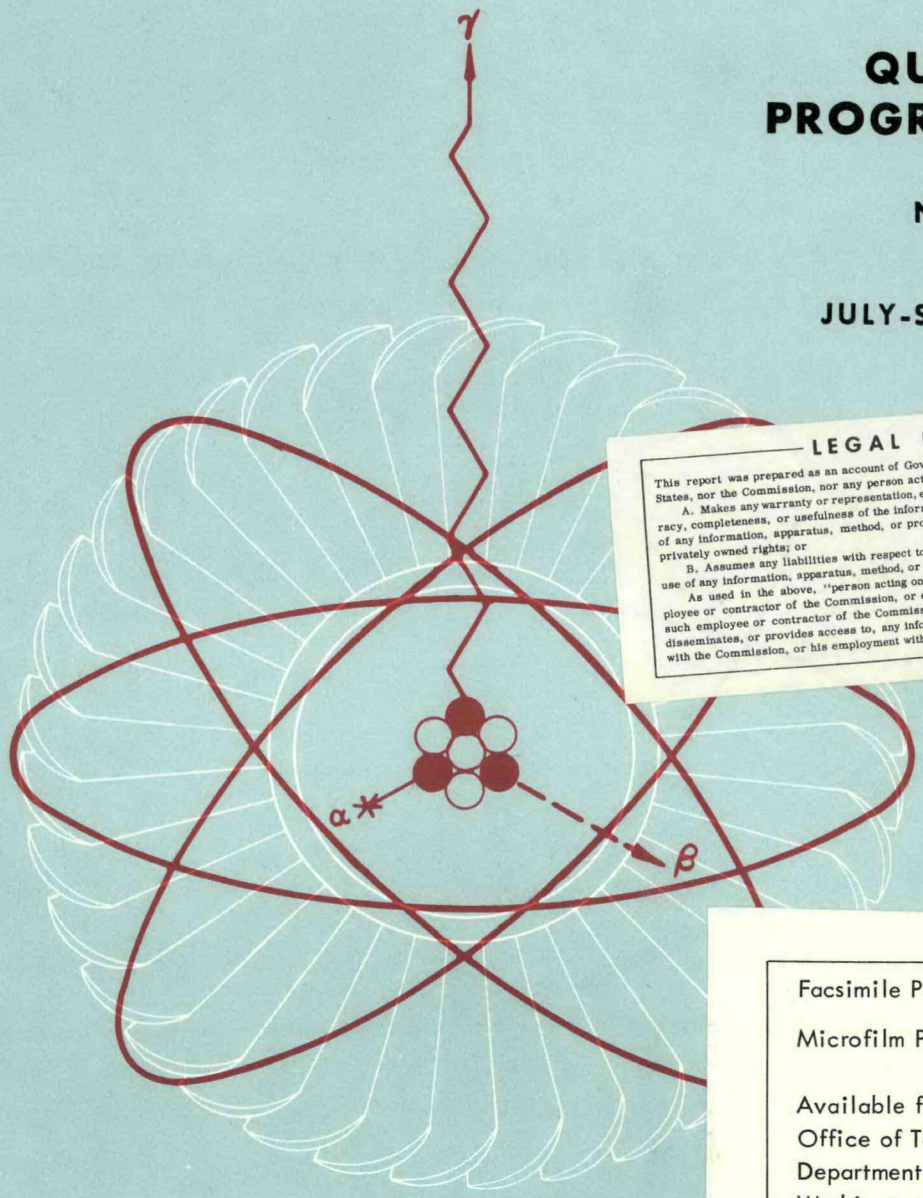

QUARTERLY PROGRESS REPORT

NUMBER 7

JULY-SEPTEMBER 1958

Facsimile Price $ 9.60

Microfilm Price $ 3.68

Available from the
Office of Technical Services
Department of Commerce
Washington 25, D. C.

MARTIN

SECRET

DISCLAIMER

DEFENSE INFORMATION

This document contains information affecting the National Defense of the United States within the meaning of the Espionage Laws, Title 18, U. S. C., Sections 793 and 794, the transmission or violation of which in any manner to an unauthorized person is prohibited by law.

This report is prepared under contract AT(30 3) 217 with the United States Atomic Energy Commission

"Special Distribution"

RADIOISOTOPE FUELED AUXILIARY POWER UNIT

QUARTERLY PROGRESS REPORT NUMBER 7

JULY - SEPTEMBER 1958

APPROVED BY Kenneth P. Johnson
Project Engineer

Research & Development

C-83

MND - P - 3004

1 4957

MARTIN
BALTIMORE

DEFENSE INFORMATION

This document contains information affecting the National Defense of the United States within the meaning of the Espionage Laws, Title 18, U.S.C., Sections 793 and 794, the transmission or violation of which in any manner to an unauthorized person is prohibited by law.

LEGAL NOTICE

This report was prepared as an account of Government sponsored work. Neither the United States, nor the Commission, nor any person acting on behalf of the Commission:

A. Makes any warranty or representation, express or implied, with respect to the accuracy, completeness, or usefulness of the information contained in this report, or that the use of any information, apparatus, method, or process disclosed in this report may not infringe privately owned rights; or

B. Assumes any liabilities with respect to the use of, or for damages resulting from the use of any information, apparatus, method, or process disclosed in this report.

As used in the above, "person acting on behalf of the Commission" includes any employee or contractor of the Commission to the extent that such employee or contractor prepares, handles or distributes, or provides access to, any information pursuant to his employment or contract with the Commission.

DISTRIBUTION LIST FOR 3215

		Copy No.
1.	Air Force Ballistic Missile Division Commander, Air Force Ballistic Missile Division Hq., Air Research and Development Command, USAF P. O. Box 262 Inglewood, California For: Major George Austin	1
2.	Air Research and Development Command Commander, Air Research and Development Command Andrews Air Force Base Washington 25, D.C. Attn: RDTAPS, Capt. W. G. Alexander	2
3.	Army Ballistic Missile Agency Commanding General Army Ballistic Missile Agency Redstone Arsenal, Alabama Attn: ORDAB-c	3,4
4.	Atomic Energy Commission, Washington U.S. Atomic Energy Commission Technical Reports Library Washington 25, D. C. Attn: Mrs. J. M. O'Leary	
	For: Lt. Col. G. M. Anderson, DRD	5
	Capt. John P. Wittry, DRD	6
	Lt. Col. Robert D. Cross, DRD	7
	R. G. Oehl, DRD	8
	Edward F. Miller, PROD	9
	Technical Reports Library	10
5.	Atomics International Atomics International Division of North American Aviation, Inc. P. O. Box 309 Canoga Park, California Attn: Dr. Chauncey Starr For: J. Wetch	11
6.	Bureau of Aeronautics Chief, Bureau of Aeronautics Washington 25, D. C. Attn: C. L. Gerhardt, NP	12

Copy No.

7. Bureau of Ordnance
Chief, Bureau of Ordnance
Dept. of the Navy, Room 4110 Main Navy Bldg.
Washington 25, D. C.
Attn: Mrs. Maryle R. Schmidt or Laura G. Myers (To be opened by addressee only)

For: Ren 13
SP 14

8. Bureau of Ships 15
Chief, Bureau of Ships
Code 1500
Department of the Navy
Washington 25, D. C.
Attn: Melvin L. Ball

9. Canoga Park Area Office 16
U. S. Atomic Energy Commission
Canoga Park Area Office
P. O. Box 591
Canoga Park, California
Attn: A. P Pollman, Area Manager

10. Chicago Operations Office 17,18
U. S. Atomic Energy Commission
Chicago Operations Office
P. O. Box 59
Lemont, Illinois
Attn: A. I Mylyck
For: T. A. Nemzek
Mr. Klein

11. Chief of Naval Operations 19
Office of the Chief of Naval Operations
Department of the Navy
Washington 25, D. C.

12. Department of the Army 20
Atomic Division
Office of Chief of Research and Development
Department of the Army
Washington 25, D. C.

13. Diamond Ordnance Fuse Laboratories 21,22,23
Commanding Officer
Diamond Ordnance Fuse Laboratories
Washington 25, D. C.
Attn: ORDTL 06.33, Mrs. M. A. Hawkins

Copy No.

14. Hanford Operations Office — 24
U. S. Atomic Energy Commission
Hanford Operations Office
P. O. Box 550
Richland, Washington
Attn: Technical Information Library

15. Lockheed Aircraft Corporation — 25,26
Asst. AF Plant Representative
Missile Systems Division
Lockheed Aircraft Corporation
P. O. Box 504
Sunnyvale, California
For: John H. Carter

16. Mound Laboratory — 27
Monsanto Chemical Company
Mound Laboratory
P. O. Box 32
Miamisburg, Ohio
Attn: Library and Records Center
For: Mr. Roberson

17. National Advisory Committee For Aeronautics, Ames — 28
National Advisory Committee For Aeronautics
Ames Aeronautical Laboratory
Moffett Field, California
Attn: Smith J. de France, Director

18. National Advisory Committee For Aeronautics, Langley — 29
National Advisory Committee For Aeronautics
Langley Aeronautical Laboratory
Langley Field, Virginia
Attn: Henry J. E. Reid, Director

19. National Advisory Committee For Aeronautics, Lewis — 30
National Advisory Committee For Aeronautics
Lewis Flight Propulsion Laboratory
21000 Brookpark Road
Cleveland 35, Ohio
Attn: George Mandel

20. Naval Ordnance Laboratory — 31,32,33
Commander, U S. Naval Ordnance Laboratory
White Oak, Silver Spring, Maryland
Attn: Eva Lieberman, Librarian

Copy No.

21. Naval Research Laboratory — 34
Director, Naval Research Laboratory, Code 1572
Washington 25, D.C.
Attn: Mrs. Katherine H. Cass

22. New York Operations Office — 35
U. S. Atomic Energy Commission
New York Operations Office
70 Columbus Avenue
New York 23, New York
Attn: Document Custodian

23. Oak Ridge National Laboratory — 36
Union Carbide Nuclear Company
X-10, Laboratory Records Department
P. O. Box X
Oak Ridge, Tennessee
Attn: Eugene Lamb

24. Office of Naval Research — 37
Office of Naval Research
Department of the Navy, Code 735
Washington 25, D. C
Attn: E. E. Sullivan
For: Code 429

25. Project Rand — 38
Director, USAF Project Rand
Via AF Liaison Office
The Rand Corporation
1700 Main Street
Santa Monica, California
Attn: F. R. Collbohm
For: Dr. John Huth

26. Rome Air Development Center — 39
Commander, Rome Air Development Center
Griffiss Air Force Base, New York
Attn: RCSG, J. L. Briggs

27. Technical Information Service Extension — 40 through 64
U. S. Atomic Energy Commission
Reference Branch
Technical Information Service Extension
P. O. Box 62
Oak Ridge, Tennessee

Copy No.

28. Thompson Products, Inc. — 65,66,67
Thompson Products, Inc.
Staff Research and Development
New Devices
P. O. Box 1610
Cleveland 4, Ohio
Attn: C. G. Martin

29. University of California Radiation Laboratory — 68
University of California Radiation Laboratory
Technical Information Division
P. O. Box 808
Livermore, California
Attn: Clovis G. Craig
For: Dr. Hayden Gordon

30. Wright Air Development Center — 69
Commander, Wright Air Development Center — 70
Wright-Patterson Air Force Base, Ohio — 71,72
Attn: WCACT
For: Capt. Clarence N. Munson, WCLPS
G. W. Sherman, WCLEE
WCOSI

31. Jet Propulsion Laboratory — 73
Commanding Officer
Jet Propulsion Laboratory
Pasadena, California
Attn: W. H. Pickering, I. E. Newlan

FOREWORD

This is the seventh quarterly progress report submitted under Contract AT(30-3)-217. It covers the period from July through September 1958.

CONTENTS

CONTENTS (Cont'd)

CONTENTS (Cont'd)

ILLUSTRATIONS

ILLUSTRATIONS (Cont'd)

ILLUSTRATIONS (Cont'd)

TABLES

SUMMARY

TASK I - OVERALL SYSTEM DESIGN

Integration of the APU module into WS-117L made it necessary to shift some of the components within the module and redesign the boiler biological shield. The shield has been divided into two compartments making it possible to sequence the draining of these compartments with respect to missile fueling. At no time during the count down is the booster overloaded or is radiation excessive.

Test results show that the scale model fuel element assemblies exposed to LOX, JP4 fire and explosion (1/10 scale Atlas) were not significantly damaged. The integrity of the fuel element under launch pad abort conditions has been demonstrated successfully.

TASK II - BOILER DESIGN

In order to provide additional volume in the fuel element, a redesign of the boiler assembly was necessary. Release of final manufacturing drawings has been delayed because of this.

Work is under way to provide ORNL with fixtures for use in the hot cell assembly of the fuel element.

TASK III - FUEL DEVELOPMENT

Tests have been conducted to determine the thermal properties of CeO_2. The following have been measured and the results reported:

1. Conductivity;

2. Expansion;

3. Specific heat.

Fabrication studies to determine the effects of calcining temperatures on compactibility and sinterability of ORNL-prepared materials were continued.

TASK IV - MATERIALS DEVELOPMENT

An analysis of the type of failure which occurred in the operation of two thermal harps (Croloy 5 Si and 5 Ti) indicates that mass transport is occurring from the hot to the cold leg of the corrosion loop. A third corrosion loop (Carpenter 20 CB) has been put in operation and work has been initiated to explore this problem intensively.

Compatibility studies of molybdenum and molten lead are continuing.

TASK V - POWER CONVERSION

Component development has continued and test runs have been made on rotating assemblies of the turbine, alternator and bearings, (TATP 1 and 2). Feasibility

of the rotating package has been demonstrated but component performance must be improved and start and stop capabilities demonstrated. A summary of demonstrated performance and future capability is listed.

PERFORMANCE ESTIMATES

Power Conversion System

Component	Design Objectives	Best Estimate	Present Achievement
Turbine			
Overall efficiency	40%	43%	37%
Output shaft power	605 W	652 W	560 W
Bearings			
Power Consumption	40 W	80 W	100 W
Pump			
Overall Efficiency	24%	22.5%	17.5%
Power Consumption	40 W	37.8 W	48.5 W
Controls			
Power Consumption	25 W	20 W	25 W
Alternator			
Overall Efficiency	90%	90%	89.5%
Power Output	525 W	480 W	368 W
Cycle			
Overall Efficiency	10%	9.2%	6.85%
Power Output	500 W	460 W	343 W

TASK VI - GROUND TEST

A conceptual design of a test facility has been prepared and hazards and shielding analyses started. Equipment to measure radiation spectrums has been purchased.

TASK VII - SNAP-III

As a result of low material efficiencies achieved by Westinghouse Electric Corporation, The Martin Company has arranged to purchase a thermo-electric generator with a minimum efficiency of five per cent under space conditions from another source. This unit will be delivered by November 27, 1958.

The Westinghouse effort will continue to the end of 1958 when delivery of an operating prototype is scheduled. This prototype will incorporate an excess heat dump control that will not be a part of the original model.

TASK VIII - GROUND HANDLING AND TRANSPORTATION EQUIPMENT

Conceptual designs of equipment, systems and techniques for transporting, handling, servicing and installing the SNAP-I module were initiated. This work has been divided into two phases; assembly which will be conducted at ORNL and The Martin Company, and installation to be accomplished at the launch site. A report covering Phase 1, has been approved by ORNL.

TASK IX - THERMIONIC CONVERSION TECHNIQUES

A general evaluation of thermionic conversion techniques has been made. Proposals have been evaluated and contracts will be awarded during the next quarter.

I. TASK I - SNAP-I SYSTEM DESIGN

A. SYSTEM INTEGRATION

The integration of the SNAP-I module into the WS-117L vehicle has been continuing. The comments of Lockheed Aircraft Company on the preliminary integration drawing, presented in the last quarterly report, has led to Vehicle Integration Drawing No. 3, shown in Fig. 1. A preliminary tubing drawing, Fig. 2, has also been forwarded to Lockheed Aircraft Company. The major improvements include:

1. Relocation of the nitrogen bottle to Vehicle Station 425, which is 20 inches forward of the SNAP-I module;

2. Location on center line of vehicle of center of mass of rotating element in turbine-alternator package;

3. Revision of support points of module;

4. Relocation of vehicle attitude rockets to avoid interference with SNAP-I;

5. Location of condenser to avoid interference with helium tank support arms.

B. BOILER HANDLING AND COUNTDOWN

The problems associated with the limited static load capacity of the Atlas booster, the weight of the full biological shield and interference with launch pad procedures and countdowns have been solved by a revised boiler shield design.

The Atlas booster has a static load carrying capacity of 11,600 pounds with a corresponding pressure of two psig in the Atlas LOX tank. The WS-117L with SNAP-I installed has a dry weight of 2820 pounds. With fuel in the third stage fuel tank, WS-117L weighs 8820 pounds leaving 2780 pounds available for the biological shield. The total weight of the biological shield is approximately 7500 pounds.

In order to overcome this problem, the following change in concept has been affected.

The proposed design for a half-power boiler consists of replacing the multiple inner radiation shields by means of a canned thermal insulator. A single radiation shield placed outside the insulation but within the original outer shield can be used to contain enough biological mercury to permit extended operation of the power conversion equipment and still allow personnel to work around the missile. The conceptual design is shown here.

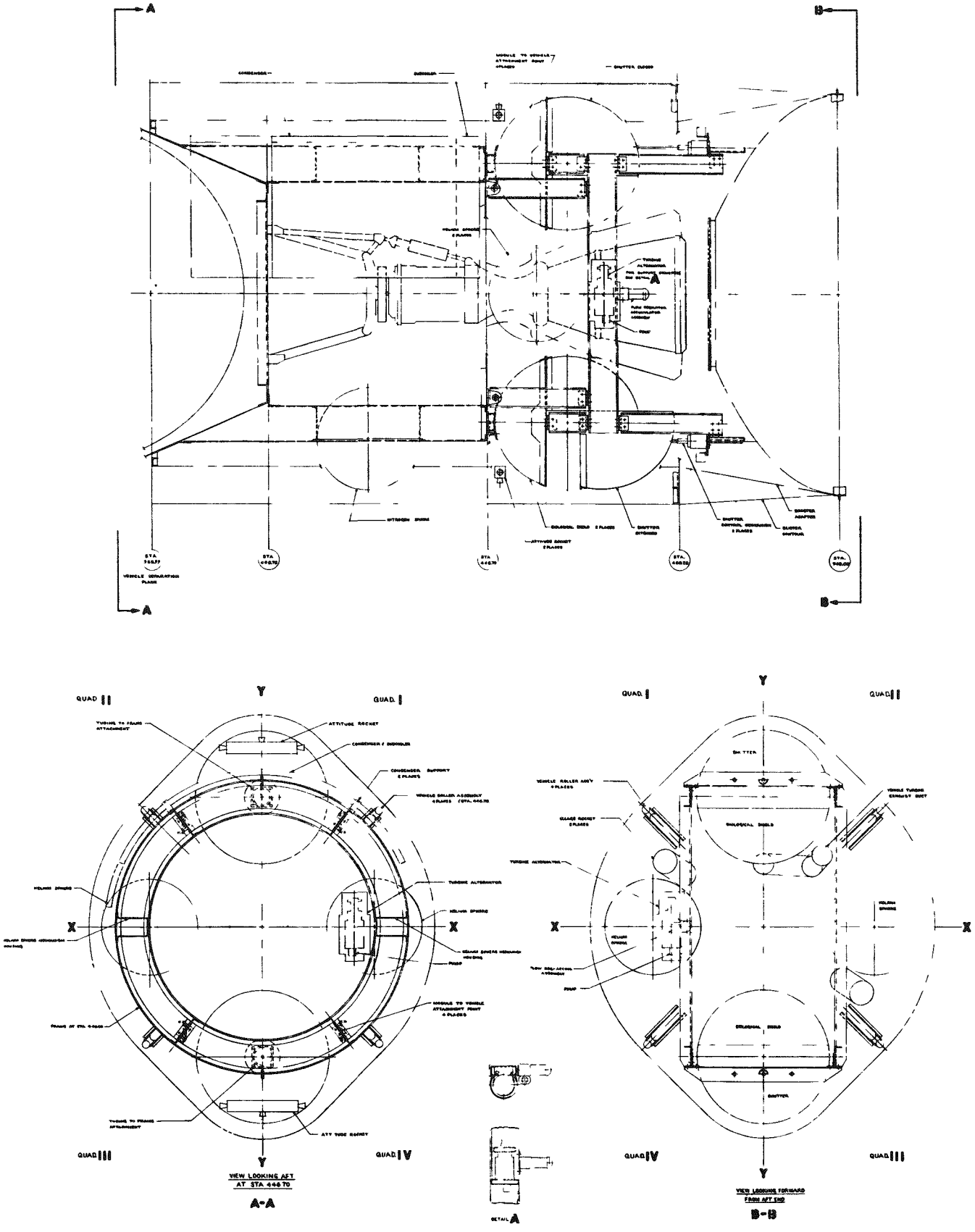

Fig. 1. Vehicle Integration Drawing

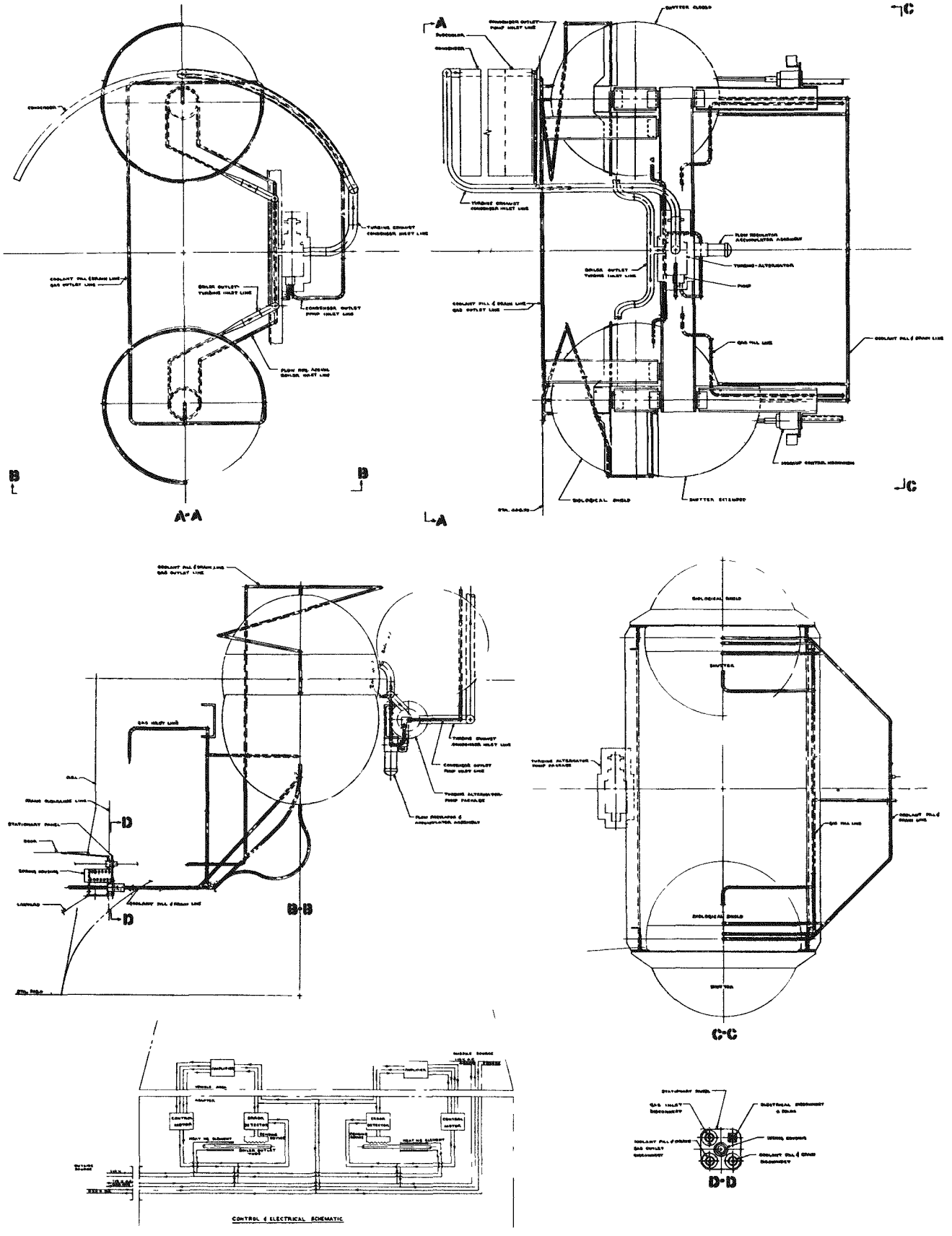

Fig. 2. Preliminary Tubing Drawing

The sequence for start-up and launch is as follows:

1. After the APU module is mounted in the WS-117L and the satellite vehicle placed on the Atlas, the APU is started at T-120 minutes by stopping the flow of coolant liquid immediately adjacent to the boiler, allowing the boiler to come up to operating temperature. The turbine is motored and started (elapsed time is 15 minutes). Excess heat is disposed of from the boiler surface by passing cooling gas over it;

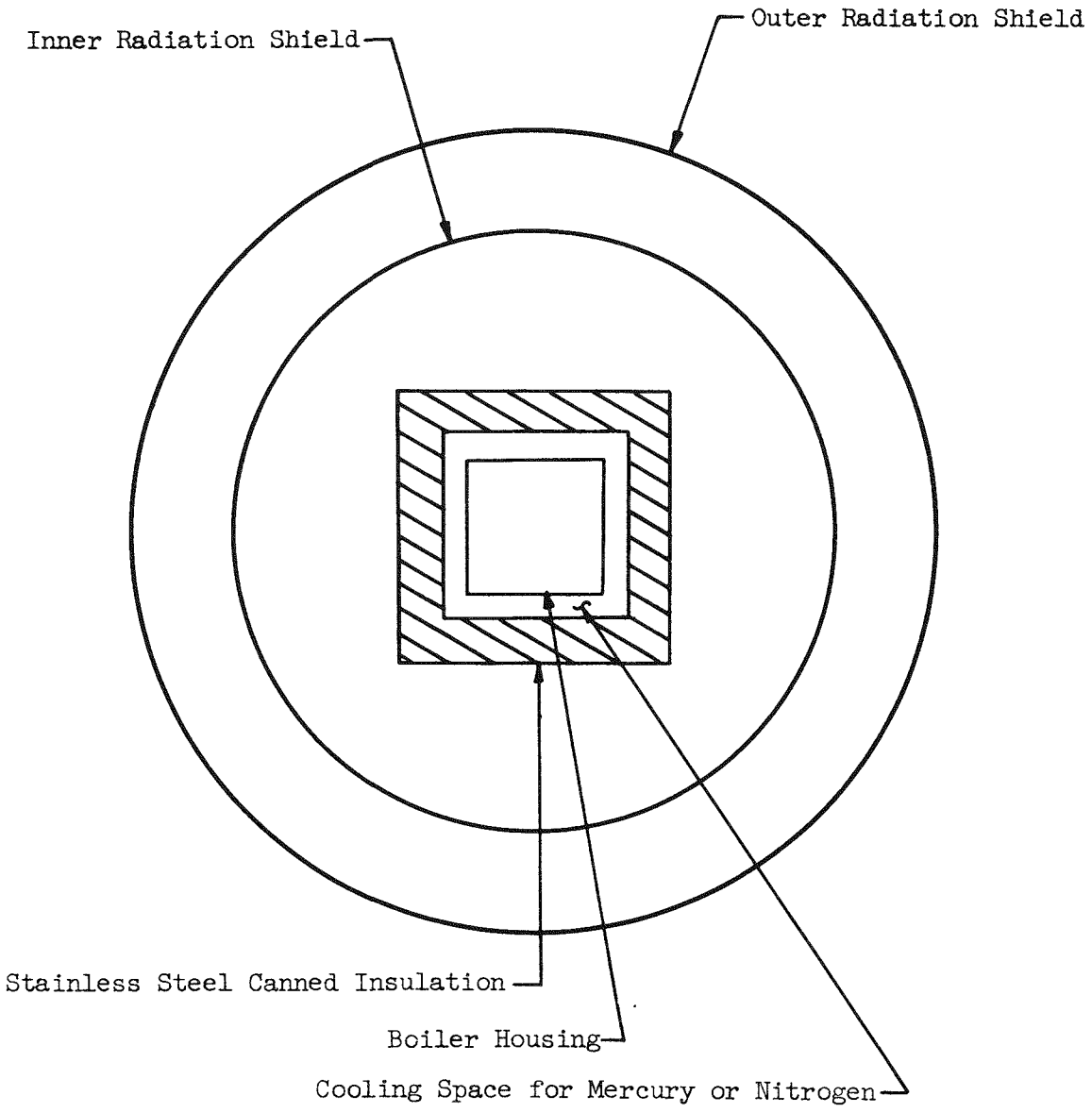

2. Prior to fueling the third stage engine, the biological shield in Region I is drained (T-45). The dose level on the ground will be approximately seven mr/hr, permitting personnel to work in the area for several hours if necessary. The weight of the biological shield will not exceed 2600 pounds and the third stage engine can be fueled;

3. At T-5, the biological shield in Region 1 will be drained;

4. Mercury biological shield lines will remain in place and be parted as the missile leaves the ground.

The amount of nitrogen gas necessary to regulate the working fluid outlet temperature is small and operation under these conditions can be carried on indefinitely.

Heat transfer calculations were made on a simplified model, neglecting the compartmentalized thermal shutter, using the following criteria:

1. Maximum heat loss through outer shield of six per cent either on the ground and operating with the inner shield full, or in space;

2. Outside surface temperature of the canned thermal insulation will not exceed 650°F;

3. The gas coolant space and the thermal insulation must be kept at a minimum so maximum advantage can be taken of the inner biological shield.

For the cooling space around the boiler housing, nitrogen cooling with spaces of 1/16, 1/8 and 1/4 inch were investigated. The smallest spacing proved most efficient and the pressure drops were reasonably low. With a 1/16 inch spacing, all the isotopic heat generated could be removed (no working fluid) and temperatures at 1350°F could be maintained by circulating 18 cfm of 100°F nitrogen. A 500°F maximum temperature is maintained by circulating 71 cfm of 100°F nitrogen. Pressure drops are approximately 0.5 and 5.6 respectively.

When operating with the working fluid at design conditions and the inner biological filled with mercury, a 0.69 inch thickness of potassium titanate will keep heat losses down to about 5 1/2 per cent while maintaining the outer can surface temperature at about 350°F. Losses in a space environment are less than 5 1/2 per cent.

Gamma ray dosage rates have been calculated and are based on a 1/8 inch cooling space and a 3/4 inch insulating can (insulator plus cladding). Results are summarized.

Inner Shield Only

Inner shield - 8 7/8 x 8 7/8 x 9 7/8 inches

Inner shield mercury - 1407 pounds

Dose rate - maximum per boiler - 22,000 mr/hr at two feet

Dose rate - maximum both boilers - 7 mr/hr at 70 feet

Inner and Outer Shield Combined

Outer shield - 11.5 x 11.5 x 12.5 inches (present design)

Total mercury weight - 3202 pounds

Dose rate - maximum per boiler - 430 mr/hr at two feet (58 mr/hr present design)

Outer shield - 12.0 x 12.0 x 13.0 inches

Total mercury weight - 3651 pounds

Dose rate - maximum per boiler - 205 mr/hr at two feet

Dose rate - maximum two boilers in transport - 260 mr/hr at three feet

Outer shield - 12.5 x 12.5 x 13.5 inches

Total mercury weight - 4137 pounds

Dose rate - maximum per boiler - 98 mr/hr at two feet

These data indicate that approximately 1/2 inch of mercury must be added to the boiler shield to bring dosage rates to a tolerable level of about 260 mr/hr at three feet to comply with shipping regulations. This represents an additional 291 pounds of mercury per boiler. Calculations for gas cooling of the boiler to shutdown temperatures give reasonable results with a 1/16 inch spacing.

C. SHIELDING ANALYSIS

1. Boiler Revision Based Upon New ORNL Information

During July, Oak Ridge National Laboratory (ORNL) informed The Martin Company that the separated Ce-144 would contain more impurities than had been anticipated. As a result, the boiler was made larger to allow for a greater fuel volume to produce the same total power and dose rates were recalculated. Because of design considerations and space limitations in the launching vehicle the outer dimensions of the biological shield were not changed.

The dimensions and weights of several ellipsodial biological shields, including the one being used, are given in Fig. 3. Dose rates at a two-foot radius from the center of the half-power boiler are also given for each of the ellipsoids. Dose rate calculations were made for an activity of 5×10^5 (one half-million) curies of Ce-144. This is assumed to be the maximum activity which the half-power boilers will contain when they are loaded at the fission product separation plant (F3P). Dose rates applicable at later times may be obtained by multiplying the given dose rates by an appropriate decay factor obtained from Fig. 4. Dose rates at the surface of a 23-inch diameter biological shield are shown in Fig. 5.

ORNL also reported[1] an experimental determination of 0.00738 watt per curie heat produced by Ce-144. This is about six per cent less than the value previously calculated using the decay scheme of Ce-144.

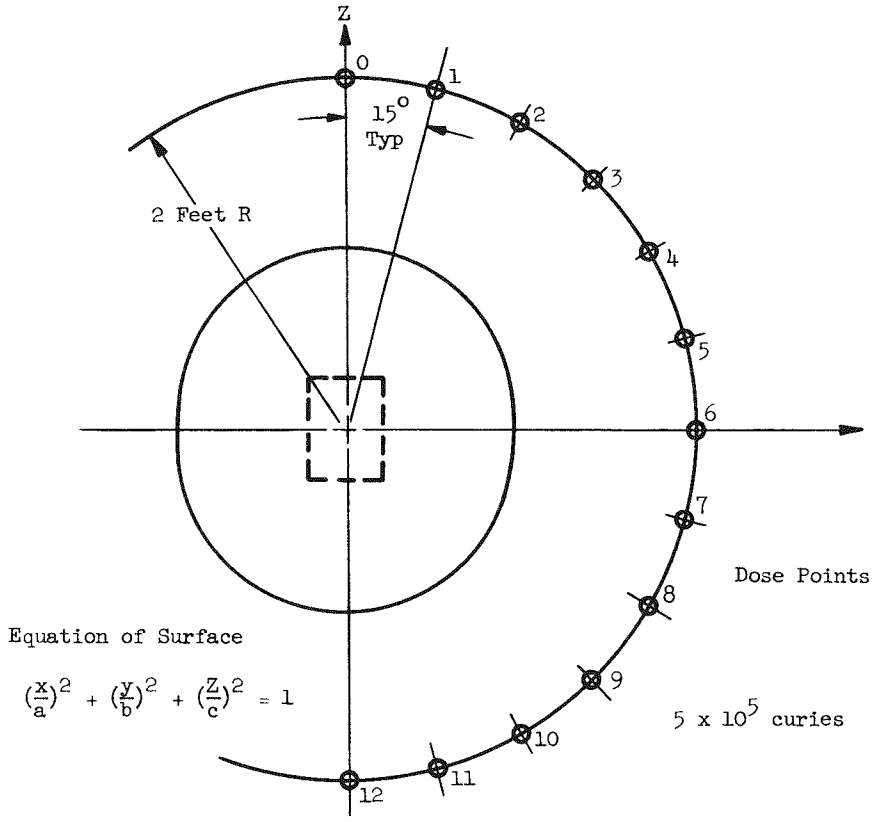

Surface Constants	(inches)	(inches)	(inches)	Present Design Surface (inches)	(inches)
a	10	10.5	11	11.5	12
b	10	10.5	11	11.5	12
c	11	11.5	12	12.5	13
Calculated Weight with Mercury (pounds)	2222	2566	2943	3356	3805
Dose Point	Dose Rates (r/hr)				
0	0.235	0.112	0.053	0.025	0.012
1	0.277	0.132	0.063	0.030	0.014
2	0.411	0.195	0.093	0.044	0.021
3	0.539	0.256	0.122	0.058	0.028
4	0.531	0.252	0.120	0.057	0.027
5	0.459	0.218	0.104	0.049	0.024
6	0.417	0.198	0.094	0.045	0.021
7	0.419	0.199	0.095	0.045	0.022
8	0.449	0.214	0.102	0.048	0.023
9	0.448	0.213	0.101	0.048	0.023
10	0.343	0.163	0.077	0.037	0.017
11	0.220	0.104	0.050	0.024	0.011
12	0.182	0.087	0.041	0.020	0.0094

Fig. 3. Comparison of Dose Rates for Different Thicknesses of Mercury Surrounding the Boiler

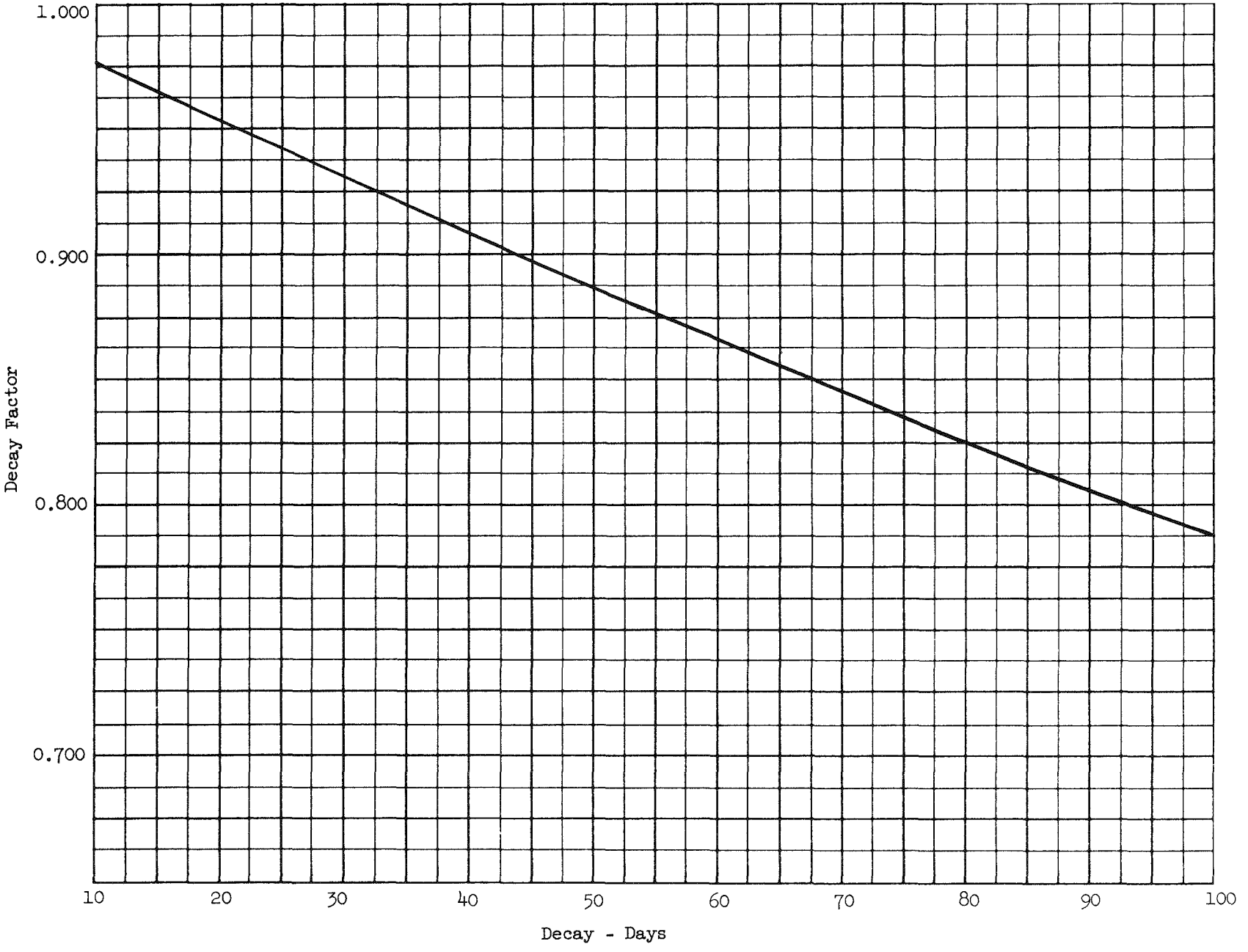

Fig. 4. Decay Factor versus Days Decay of Ce-144

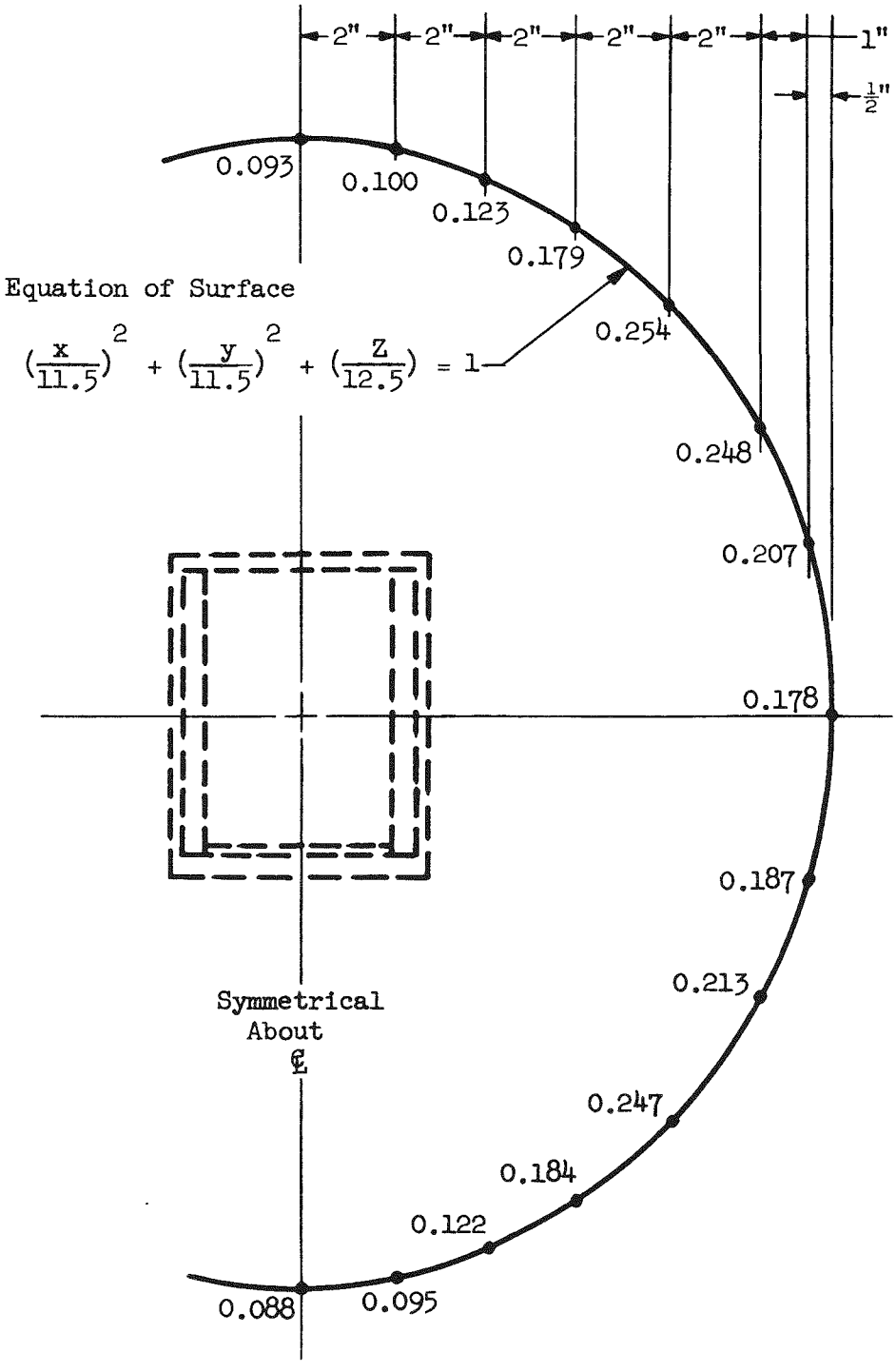

Fig. 5. Dose Rates at Surface of Mercury Shield with Shield Filled

2. Dose Rates from Two-Section Biological Shield

The concept of the two-section biological shield has been presented earlier. The dose rates associated with filling the inner shield alone and for both sections with mercury are shown in Fig. 6. The dose rates for the completely shielded case are somewhat higher than previously calculated due to the replacement of some of the biological mercury by insulation. However, these dose rates are still acceptable. The dose rate at 12 feet from the surface with only the inner shield filled with mercury is analogous to the dose rates of the completely filled shield at one foot from the surface.

D. OPERATIONAL HAZARDS

1. Launch Abort Hazards

Core Integrity Tests Under Missile Failure Forces. - This test program was to determine the integrity of APU fuel core models during simulated missile failures. The adverse forces involved were explosive shock, high transient temperatures and oxidation.

The test procedure consisted of injecting test specimens of 1/6, 1/3, and 1/2 scale cores at operating temperature of 1500°F into a mixture of liquid oxygen and kerosene. This is accomplished by causing seam failures in the 1/18 and 1/10 scale missiles shown in Fig. 7. As a result of the seam failure, the liquid oxygen and fuel forms a puddle on the pad into which the hot specimens are automatically injected by a boom mechanism. The mixture is detonated, generally by the specimen, giving the required effect. The test apparatus and field layout are shown in Fig. 8.

Two types of protective coatings tested were colmonoy and chromalloy. Some specimens were predamaged prior to testing so the effect of the detonation upon a damaged specimen could be determined. The results of the tests are found in Table 1.

The results indicated that the scale model test assemblies were not significantly damaged as a result of being exposed to conditions existing during the failure of the model scale missiles. Specifically, it was found that:

1. There were no visible indications of damage to the test assemblies other than a few small dents and abrasions on the corners. These seemed to be due to the initial impact of the test assembly on the concrete pad;

2. There were no detectable changes in the linear dimensions of the test assemblies, however, this was not an extremely sensitive measure since the unevenness of the surface coating resulted in an uncertainty of about 0.01 inch. Shock wave traces are shown in Fig. 9.

3. Although there were detectable changes in the weights of the test assemblies, these were very small. Test assemblies with undamaged coatings had changes in the order of 0.1 per cent of the total weight and those with the heavily pre-damaged coatings were on the order of one per cent.

It is not possible to guarantee that the full-scale core will withstand a full-scale Atlas missile abort, however, the results of the model tests indicate it will.

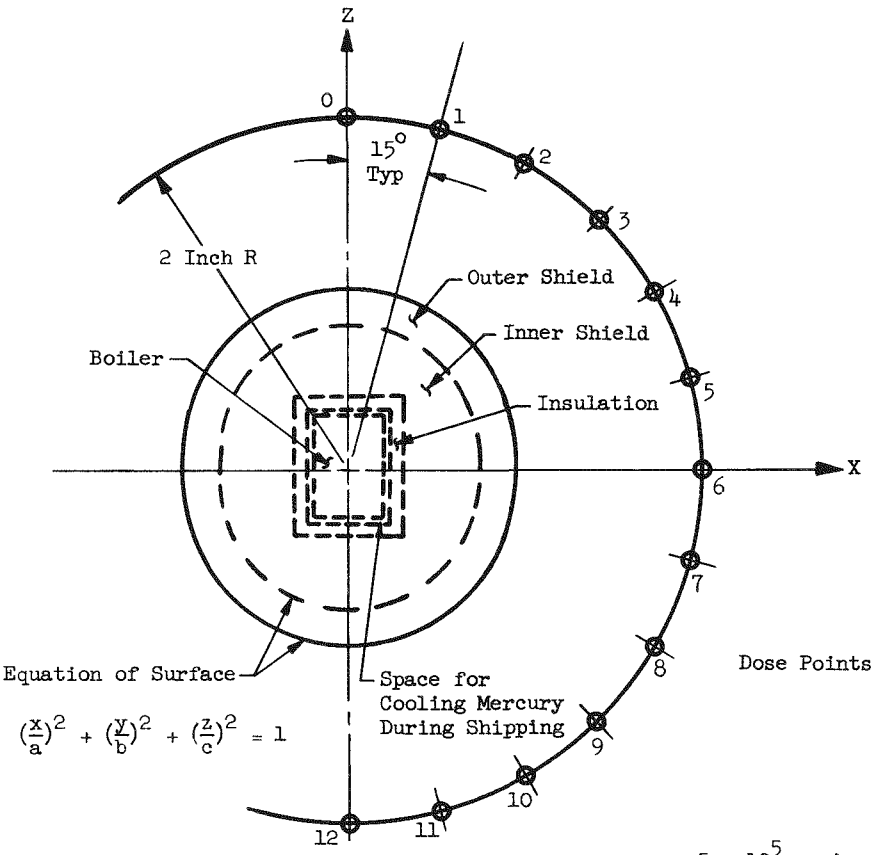

Surface Constants	Shields	
	Inner (inches)	Outer (inches)
a	9	11.5
b	9	11.5
c	10	12.5
Weight of Mercury (pounds)	1420	3150*

Dose Point	Dose Rates r/hr	
0	6.69	0.159
1	8.46	0.200
2	22.0	0.502
3	38.36	0.890
4	23.05	0.541
5	15.05	0.356
6	12.92	0.305
7	13.81	0.327
8	18.83	0.443
9	32.42	0.750
10	19.28	0.437
11	6.72	0.159
12	5.19	0.124

* Includes mercury within inner shield

Based upon one inch of Insulation and $\frac{1}{4}$ inch space for coolant

Fig. 6. Dose Rates from Boiler with Inner and Outer Biological Shield

Scaling Information for Model Missile		
Linear Scale Reduction	1/18	1/10
Propellant Mass Reduction	1/5,800	1/1,000
Nominal Diameter	6-5/8"	12"
Depth of Fuel	13-1/4"	23-1/2"
Air Gap Between Fuel and Liquid Oxygen	1-1/2"	2-3/4"
Depth of Liquid Oxygen	19"	34-1/2"
Air Gap Between Liquid Oxygen and Plug	1/2"	3/4"
Plug Thickness	1/2"	3/4"
Overall Length	35-3/4"	61-3/4"

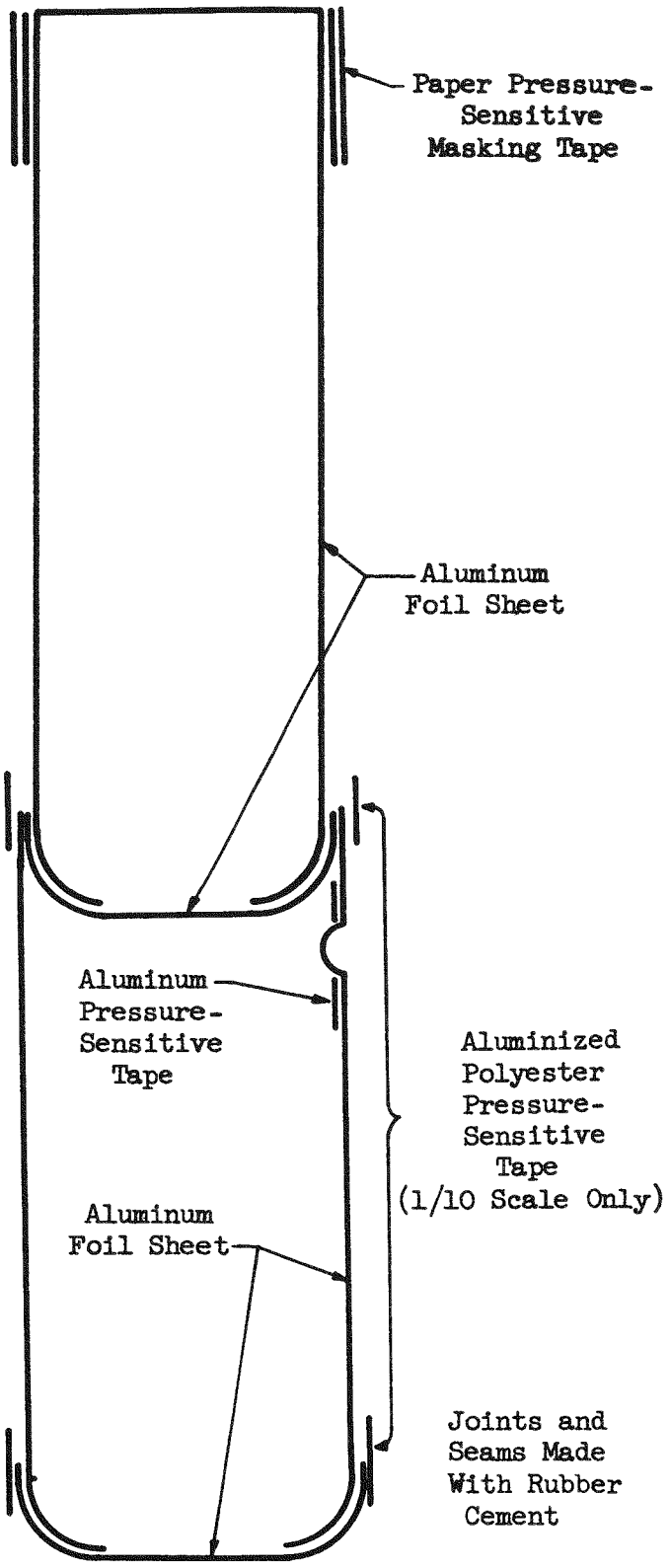

Fig. 7. Scaling Information and Schematic Showing of Missile Construction

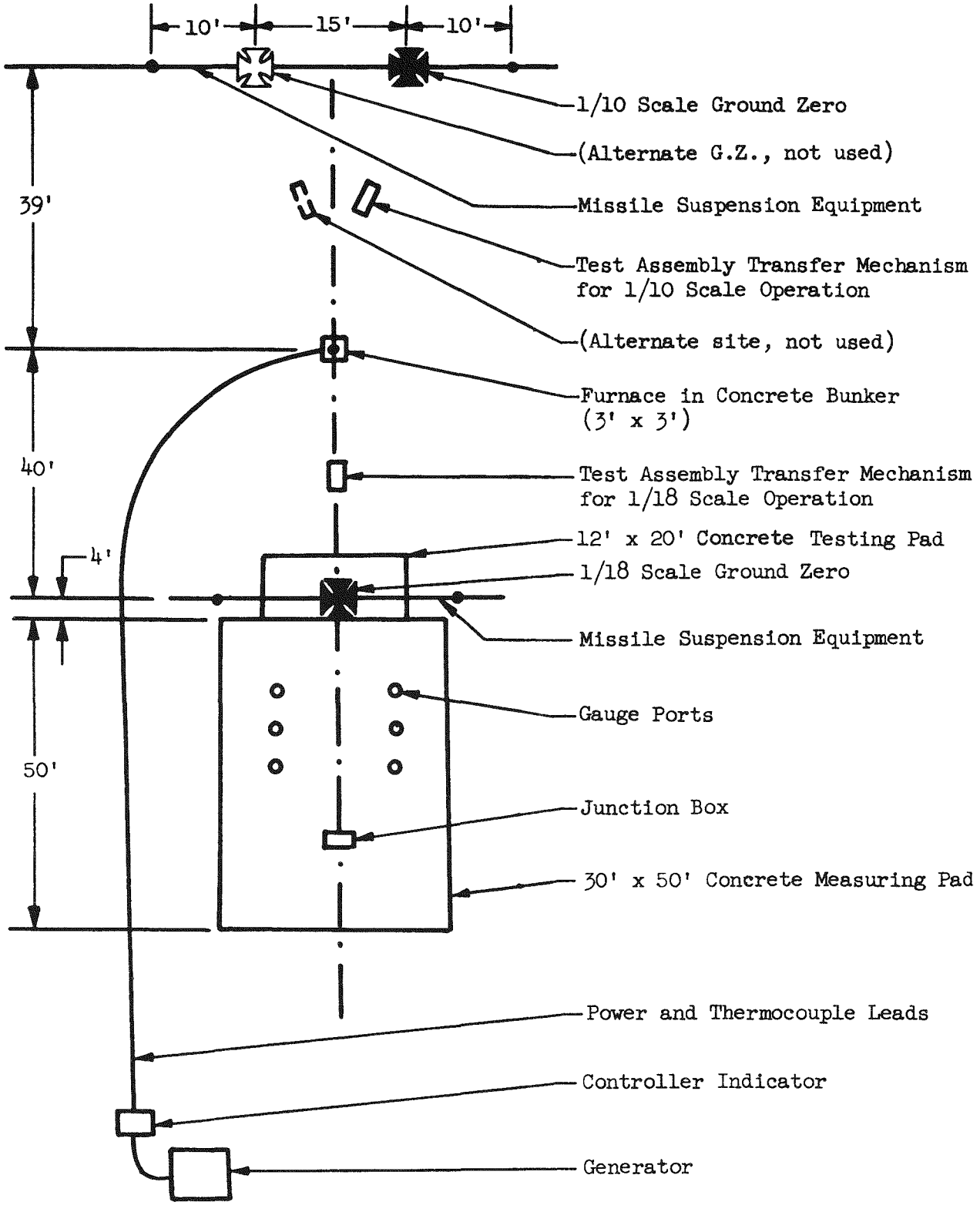

Fig. 8. Pad Area

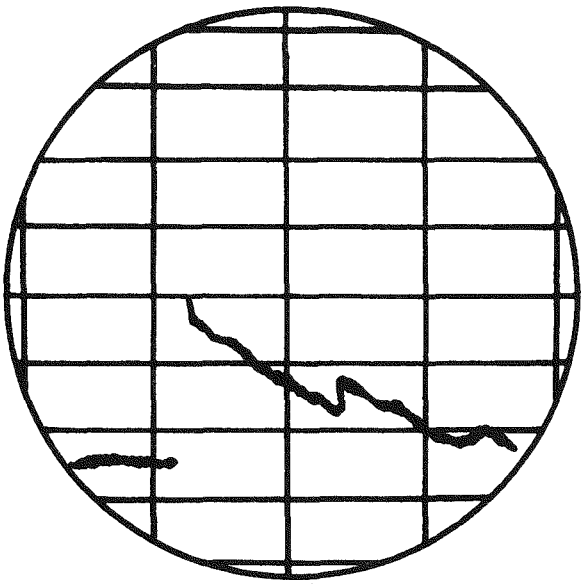

Shot 10 1/18 Scale
Peak Overpressure: 9.2 psi
158 μsec/division
Distance from GZ: d = 205 Inches

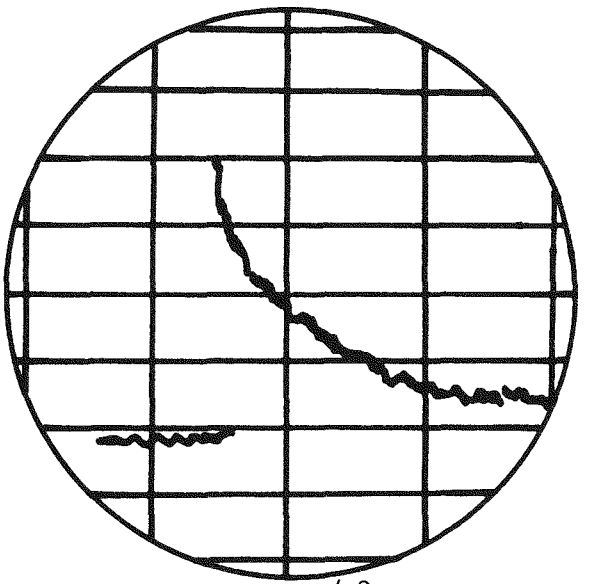

Shot 19 1/18 Scale
Peak Overpressure: 7.2 psi
435 μsec/division
Distance from GZ: d = 311 Inches

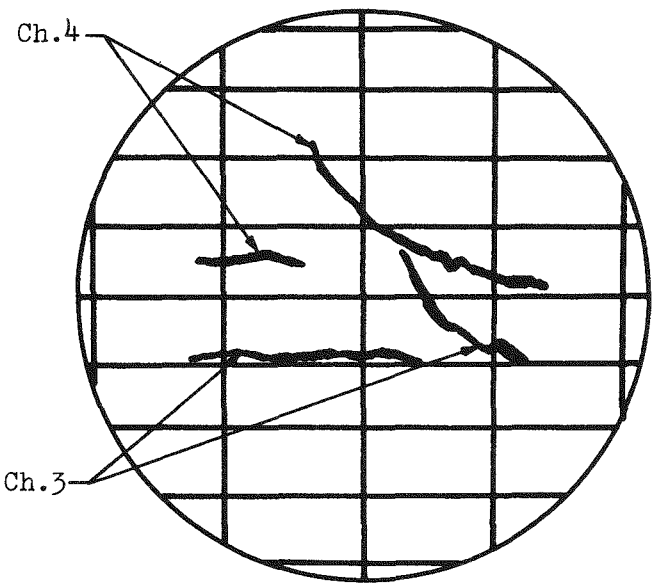

Shot 23 1/10 Scale
Peak Overpressure: Ch.3: 2.9 psi
Ch.4: 3.5 psi
1.30 msec/division
Distance from GZ: Ch.3: d = 1248 Inches
Ch.4: d = 1116 Inches

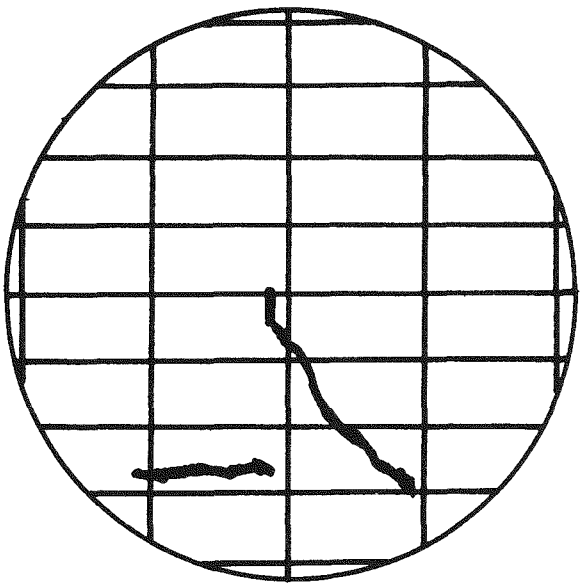

Shot 25 1/10 Scale
Peak Overpressure: 2.6 psi
1.33 msec/division
Distance from GZ: d = 1248 Inches

Fig. 9. Sample Traces

TABLE 1

Test Assembly Exposure Conditions and Resulting Weight Changes

Shot No.	Assembly No. and Scale	Temp (°F) [1]	Delay Time Failure To Detonation Planned (sec)	Delay Time Failure To Detonation Measured (sec)	Exposure Time To LOX [2] (sec)	Initial Condition of Coating [3]	Missile Yield (% TNT)	Weight Change [4] (grams)
				1/18 Scale Missiles				
6	2 - 1/2	1650 ±30°	0.9	1.0	0.0	0+	25	0.0
7	4 - 1/2	1650 ±30°	0.9	1.0	0.0v	0	24	- 0.6
8	3 - 1/2	1500 ±30°	0.9	1.0	0.0	0	>19	- 0.6
13	15 - 1/3	1570 ±20°	0.9	1.0	0.0	0	39	- 0.6
14	16 - 1/3	1630 ±20°	0.9	1.0	0.0	0	--	- 0.6
15	21 - 1/6	1600 ±20°	0.9	1.0	0.0	0	39	Lost
	24 - 1/6							- 0.2
	25 - 1/6							- 0.2
16	22 - 1/6	1380 ±20°	0.9	1.0	0.0	0	34	- 0.4
	23 - 1/6							- 0.2
	26 - 1/6							- 0.2
12	1 - 1/2	1450 ±30°	2.5	>1.7	>0.7	0+	26	- 1.0
10	5 - 1/2	1510 ±30°	2.5	1.0*	0.0	0	37	- 0.6
17	4y - 1/2	1550 ±20°	2.5	1.1*	0.0	0	28	+ 0.5
9	8 - 1/2	1630 ±30°	2.5	1.0*	0.0	I	35	- 1.6
11	7 - 1/2	1510 ±30°	2.5	>1.3	---	I	12	- 0.9
18	9 - 1/2	1550 ±20°	2.5	1.0*	0.0	II	45	-14.3
19	10 - 1/2	1570 ±20°	2.5	1.0*	0.0	II	36	-11.9
20	19 - 1/3	1585c±50°	2.5	---	---	I	36	- 0.0
				1/10 Scale Missiles				
21	11 - 1/2	1460c±50°	1.3	1.4	---	I	--	- 1.0
	12 - 1/2					0		- 0.2
23	6 - 1/2	1600c±50°	3.5	1.7*	0.0	0	77	- 0.4z
	13 - 1/2					Ib		- 1.0z
24	17 - 1/3	1500 ±20°	3.5	1.5*	0.0	0	71	- 0.6
	20 - 1/3					0		- 0.5
25	14 - 1/2	1580 ±20°	3.5	1.8*	0.2	0	59	- 0.3
	18 - 1/3					0		- 0.5

(1) All temperatures monitored by a thermocouple were measured within ten seconds of explosion. Where the thermocouple was inoperative, the controller indicator temperature (c) is listed.

(2) This time is determined as follows: From the high speed films, the time between failure and detonation and between failure and release of the test assembly from the heat sink are measured. Latter time is added to the calculated time of all and subtracted from former time to yield exposure time.

(3) Two test assemblies marked (+) were coated with Chromalloy; remainder had Martin coatings. Test assemblies marked (0) were undamaged, those marked (I) slightly damaged, and those marked (II) were heavily damaged.

(4) Probably error in each observation; 0.3 gram for 1/2 scale test assembly, 0.2 gram for 1/3 test assembly and 0.03 gram for 1/6 scale test assemblies.

\+ See (3).

v High speed films show test assemblies did not reach mixture before the LOX detonator initiated it.

* Indicates test assemblies initiated the propellant mixture.

y Test Assembly No. 4 was used in two tests.

z Test Assembly No. 13 was altered in field.

Core Integrity Tests Under Hot Molybdenum On Liquid Oxygen Reactions. - The preliminary objective of this experiment was to determine whether the reaction between hot molybdenum and liquid oxygen would constitute a special hazard to the integrity of the APU molybdenum core. This is directly related to a launch pad abort condition in which the core would be immersed in or in contact with liquid oxygen.

The test procedure consisted of immersing hot molybdenum wire, rods, and 1/2 scale test assemblies in liquid oxygen and recording the reaction, (See Fig. 10).

Molybdenum wires 0.05 and 0.1 inch in diameter and rods 3/8 inch in diameter exhibited a basically different behavior from that of the 1/2 scale model test assemblies. These samples either ignited and were completely consumed, or were quenched with substantially no reaction. When samples were completely consumed, there was no evidence of any explosive reaction.

Figure 11, shows the results from immersing 1/2 scale test assemblies in liquid oxygen. Both bare and protective coated assemblies damaged in various ways were tested. The outstanding feature of the investigation was the failure of uncoated 1/2 scale test assemblies that were heated to temperatures as high as 2100°F to support combustion when immersed in liquid oxygen.

It was revealed that full-scale cores having intact coatings will be safe from loss of integrity. The cores with damaged coatings will not support combustion or undergo an explosive reaction when immersed in liquid oxygen at temperatures as high as 2100°F.

Low Velocity Impact Tests of Full-Scale Test Assemblies. - Low velocity impact tests will be carried out at Aberdeen Proving Ground, Aberdeen, Maryland, October 1, 8, and 15, 1958. In the tests conducted at operating temperatures, cores and complete boilers will be dropped from a height of about 70 feet simulating their position on the WS-117L Atlas Vehicle. They will impact at pre-determined angles upon concrete which simulates the launch pad.

Test results will be reported in the next quarterly report.

2. Post Orbit Hazards

High Velocity Impact Tests of Full-Scale Test Assemblies. - High velocity impact tests will be performed on the Aberdeen Proving Ground Supersonic Ballistic Sled Track after the low velocity impact tests have been completed. Test parameters, in particular impact velocities and impact media, have been defined by the re-entry evaluation study. At present, it appears that the tests will adequately simulate the impact conditions existing in the post-orbit phase of the APU.

Re-Entry Evaluation Study. - The results of the first phase of The Martin Company re-entry evaluation study for SNAP-I was completed. It provides the theoretical re-entry history for the APU complete body and boiler alone. The following analyses are included:

1. Limits of flight corridor;

2. Altitude time history;

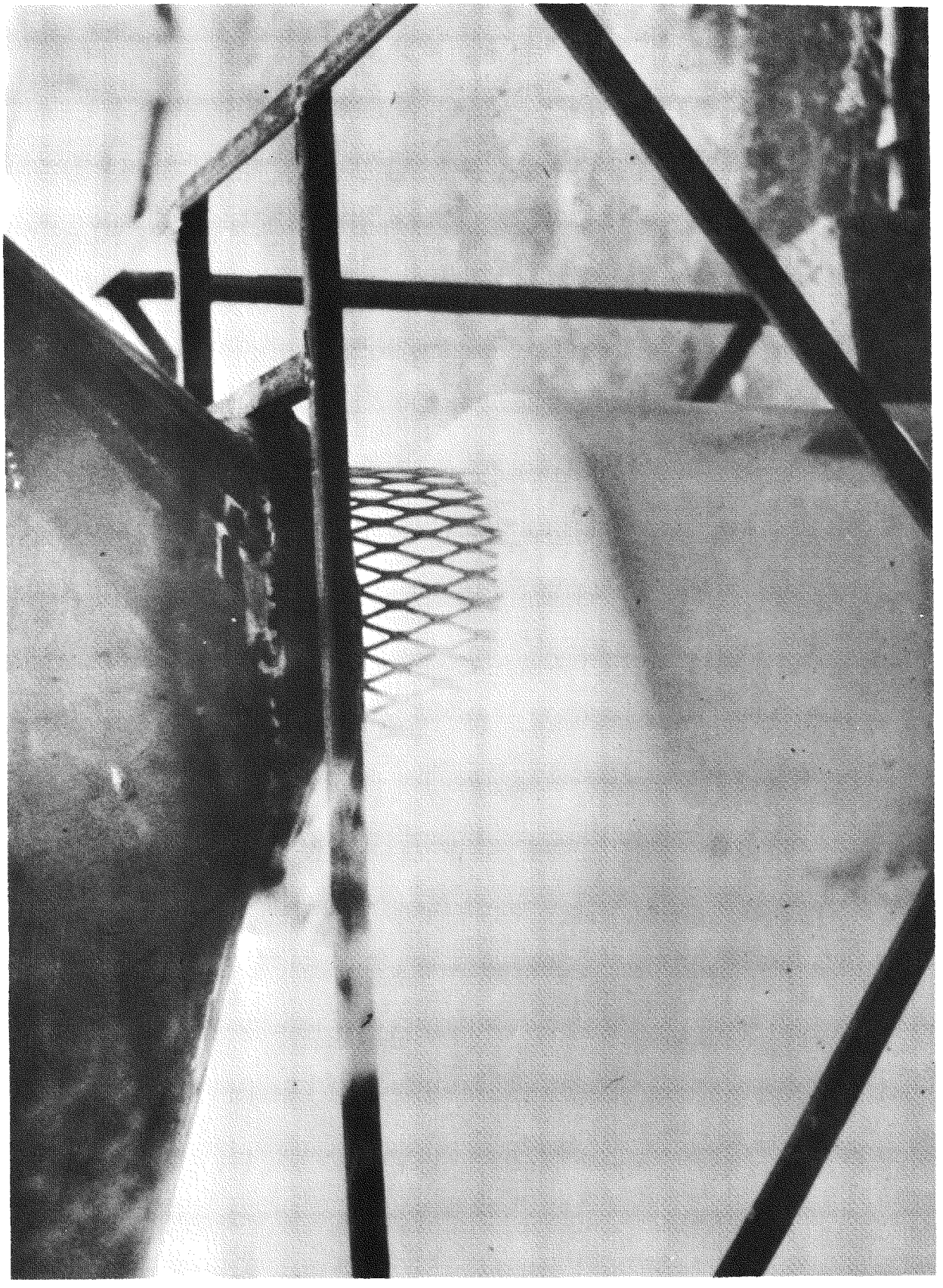

Fig. 10. Test Specimen Immersion in Liquid Oxygen

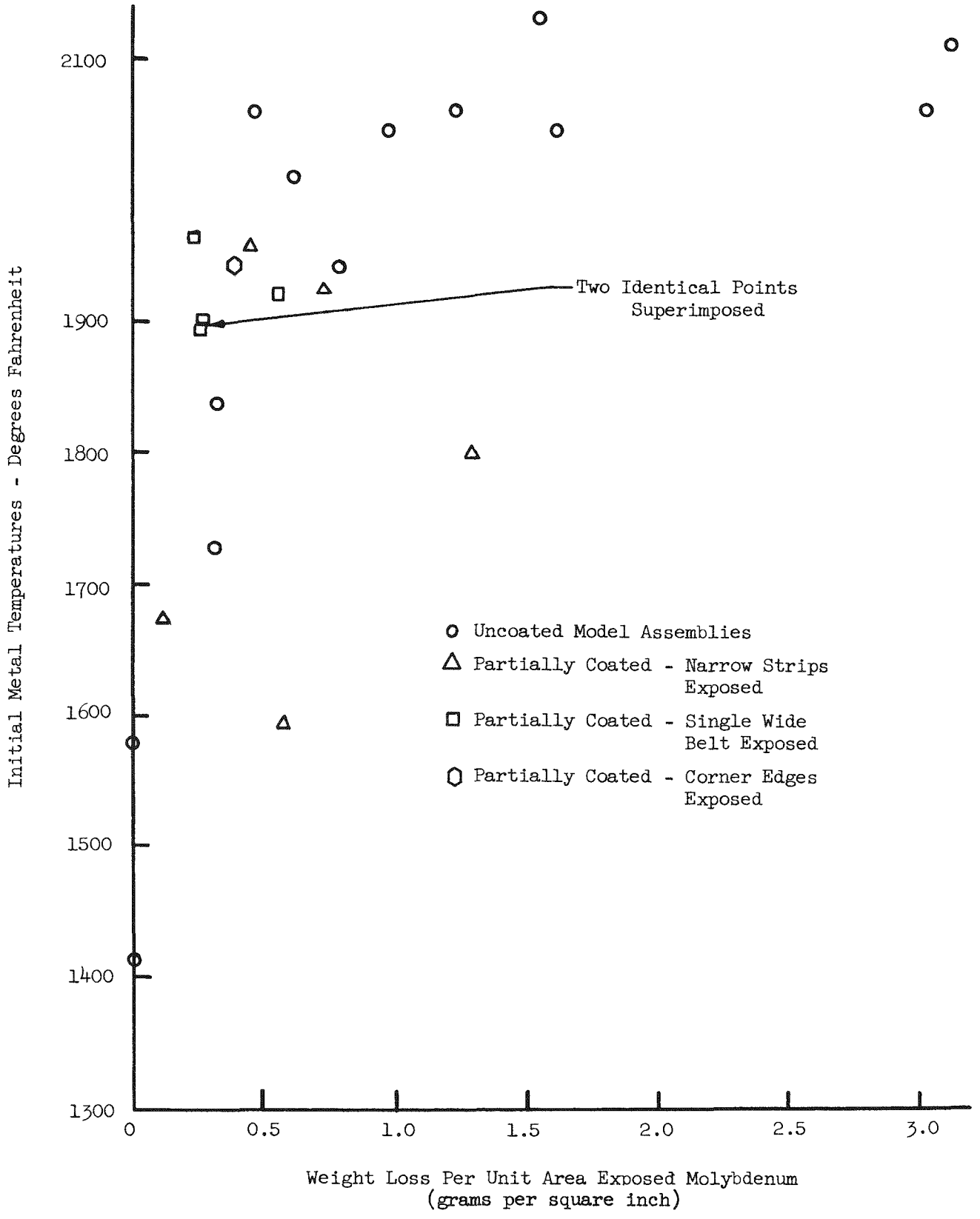

Fig. 11. Weight Loss per Unit Area of Exposed Molybdenum versus Temperature for Both Uncoated and Partially Coated Half-Scale Model Test Assemblies

3. Velocity time history;

4. Altitude time history;

5. Dynamic pressure time history;

6. Heating rate time history;

7. Equilibrium temperature time history.

The re-entry evaluation includes the re-entry velocity impact, and aerodynamic heating. The evaluation for the re-entry velocity shows the differential deceleration between the complete body and boiler. The velocity curves approach one another at impact.

Three analyses were made of impact velocities. The complete body (boiler and biological shield configuration) would impact at 134 feet per second if its integrity was maintained throughout its flight. The boiler would impact at 419 feet per second assuming it re-enters alone.

The mode of impact damage and relative hazard are predicted for the five cases of impact based upon the APU core being intact when it reaches the point of impact.

Case A - Case A predicts the effects of the core impacting on unconsolidated soil. In this case the relative hazard from the APU would decrease markedly with time, since the fuel would be contained, the core would be partially shielded, and natural decay would further reduce the source strength.

Case B - The APU core impacting upon consolidated rock at a velocity of 419 feet per second would probably bury itself about one foot beneath the surface which means that the surface dose rate would be large.

Case C - The APU core impacting upon crystalline rock would probably fragment. This is the most pessimistic case.

Case D - The APU core impacting upon water would present a relatively minor hazard. The core would remain intact, be inaccessible, and would be shielded by water. This is the most probably fate.

Case E - The APU core impacting upon ice would present little or no hazard.

TABLE 2

Impact Probabilities

Impact Media	Probability	Case
Water	1 to 1.4	D
Ice	1 to 15.2	E
Unconsolidated Rocks	1 to 13.9	A
Consolidated Rocks	1 to 12.5	B
Crystalline Rocks	1 to 14.7	C

Combining the re-entry effects upon the complete body and the boiler alone, it is doubtful that the core, based upon the present design, will reach the point of impact intact. However, several designs and materials recommendations are made which would provide survival of the core through the intense aerodynamic heating cycle. The following broad recommendations are made:

1. Use of ablative and heat sink materials such as graphite, ceramics, and plastics on the outer shell;

2. Use of insulating material such as potassium titanate;

3. Design to increase the structural integrity of the biological shield and thermal shutter.

These modifications would not affect the validity of calculated re-entry history, impact velocity, or the validity of present test programs for SNAP-I. It appears that these incorporations in the APU would insure integrity of the APU throughout the aerodynamic heating cycle existing during re-entry.

II. TASK II - BOILER DEVELOPMENT

A. TEST FACILITY DESIGN

1. Isotope Boiler No. 1

Manufacturing drawings of the boiler including the biological shield baffles were complete in July. Need for increased fuel capacity necessitated revisions to the fuel block housing and mercury coil. Revisions to the biological shield cans were necessary and in one case a new can design was required.

The redesigned fuel block, housing and coil were completed. A change was made in the four outer can contours to facilitate manufacturing. An investigation was made into space requirements for the valves and manifolds which ultimately were relocated. Review and checking were resumed on the revised work. An approximate release date is October 15th.

2. Isotope Loading and Assembly

Conceptual design studies for remote fuel loading of the isotope boiler unit and remote welding of the boiler housing and cap were initiated.

Investigation was made of loading the fuel pellets into the block. This will be done by using slave manipulators in the cell and in an inert atmosphere. After investigation, it was determined that ORNL will design a chamber for the loading in an inert atmosphere.

A method for cooling the block, during loading operations, was determined. A heat sink made of two copper plates separated by insulation with a cooling coil imbedded in the lower plate will be used.

Investigation into means of rotating the fuel block to load the holes in the other end after initial loading was made. It was determined that this could be done by the General Mills remote handling manipulator in the cell.

Studies of concepts for remote automatic welding of the housing and cap were initiated.

The boiler housing and cap must be welded while in place in the biological shield. This is necessary since the housing containing the cooling coil is permanently attached to the shield.

Investigation was made as to welding procedure, type of torch drive and control, limitations imposed by hot cell facilities, positioning equipment for the welding fixture, actual welding time and general operating procedure for the entire operation.

B. CONTROLS

The control system is being prepared for installation on the half-power boiler mock-up. Some time has been spent on modification of the amplifier. The following itemizes the progress of this effort.

1. Amplifier

The printed circuit servo amplifier was obtained from the electronics model shop and checked. Gain and voltage output were as designed and plans were made

for reducing the weight of future amplifiers. The holding fixture for vibration testing of the amplifier and a wheatstone bridge were constructed to drive the amplifier during the vibration tests. The amplifier was tested under power using a direct current power supply. These tests lasted three days and the amplifier was vibrated along all three axes. Tests were made in accord with Mil E-5272A and Lockheed detailed specifications. At the last, multiple breakage of component lead wires terminated the test. It was apparent that all parts must be constrained to move in unison with their mounting board.

Repair of damage done during vibration tests has been completed. The amplifier is now panel-mounted, wired to plugs and ready for use. A decade pot has been added for adjustment of gain.

2. Error Detector

This consists of a wheatstone bridge excited with 400-cycle voltage; one leg of the bridge contains a resistance thermometer to sense the working fluid temperature. A minimum power consumption, a maximum of sensitivity to changes in resistance of the thermometer element, and a minimum of signal output at the null point are desirable. The latter two qualities are absolutely necessary for proper operation. Maximum sensitivity was easily obtained by construction of equal arm bridges. The power consumption is negligible (usually less than 0.1 watt) at the level of bridge current (20 milliamperes maximum) involved. A great deal of noise pick-up in the first trial bridges gave an unsatisfactory null point of about five millivolts. Shielding and grounding of the bridge and grounding of all input and output instruments resulted in a null as low as two millivolts which was still too high. Later the input impedance of the bridge was reduced and a transformer used to step down the excitation voltage. Further excitation voltage reduction was obtained by use of a voltage divider at the bridge input. Non-inductive resistors were used except in the sensing element which was wire wound. This combination resulted in a null output as low as 0.02 millivolt which was satisfactory. Several of these bridges are being constructed for panel mounting.

C. HEAT TRANSFER

1. Experimental

Full Power Boiler Mock-Up Test. - Emphasis was placed on the pressure drop realized at design conditions and on the overall stability of the system during boiling. The pressure drop for the 50-foot long, 3/8 inch outside diameter tubing (containing a 0.109 inch outside diameter tube helically wound with a 0.051 inch outside diameter wire) were on the order of 125 psi at design conditions and superheated mercury. About 20 psi pressure drop is expected for the half-power boiler.

Upon completion of the full-power boiler test the loop was extensively renovated to carry out the following half-power boiler prototype tests:

1. Design feasibility test

   a. Pre-flight;

2. Ground handling

   a. Filling and draining mechanism of biological mercury;

b. Thermosyphon cooling;

c. Auxiliary gas-cooling system.

This test program will be initiated early in the next quarter.

Mercury Heat Transfer Test. - The design of the test loop components and necessary design drawings were completed during the last quarter. All instrumentation has been purchased and delivered. The instrumentation section has calibrated all of the instrumentation panel constructed for this particular application.

2. Analytical

IBM 704 Machine Code. - Work on the IBM machine program for the temperature distribution of both the full- and half-power molybdenum blocks has progressed to the point where preliminary answers have been realized. This program includes radial and axial conduction of heat and will eventually include the effects of the thermal shutter. The program is not as yet considered practical due to the slow convergence of the iteration process.

Appendix A contains pertinent information on the use of the program and the mathematical basis of the code.

Efforts in the next quarter will be directed toward improving the convergence factor and incorporating the effect of the thermal shutter into the code.

Thermal Shutter Orbital Performance. - The requirements of the thermal shutter are dictated by two criteria:

1. Excess power needed to make up for isotope decay during the normal operating life of the APU;

2. Excess power above what is needed in 1 resulting from the inaccuracy in the isotope pellet manufacturing.

Thus, the thermal shutter must be capable of dissipating thermal power equal to the sum of 1 and 2. The excess power required to make up for isotope decay during a 95-day APU life (fabrication, transportation, and 60 days operating life) is 636 watts. The quantity, 2, however, is not currently known and a plot depicting the capabilities of the thermal shutter is included. Figure 12 shows the allowable excess power versus shutter area for various emissivities.

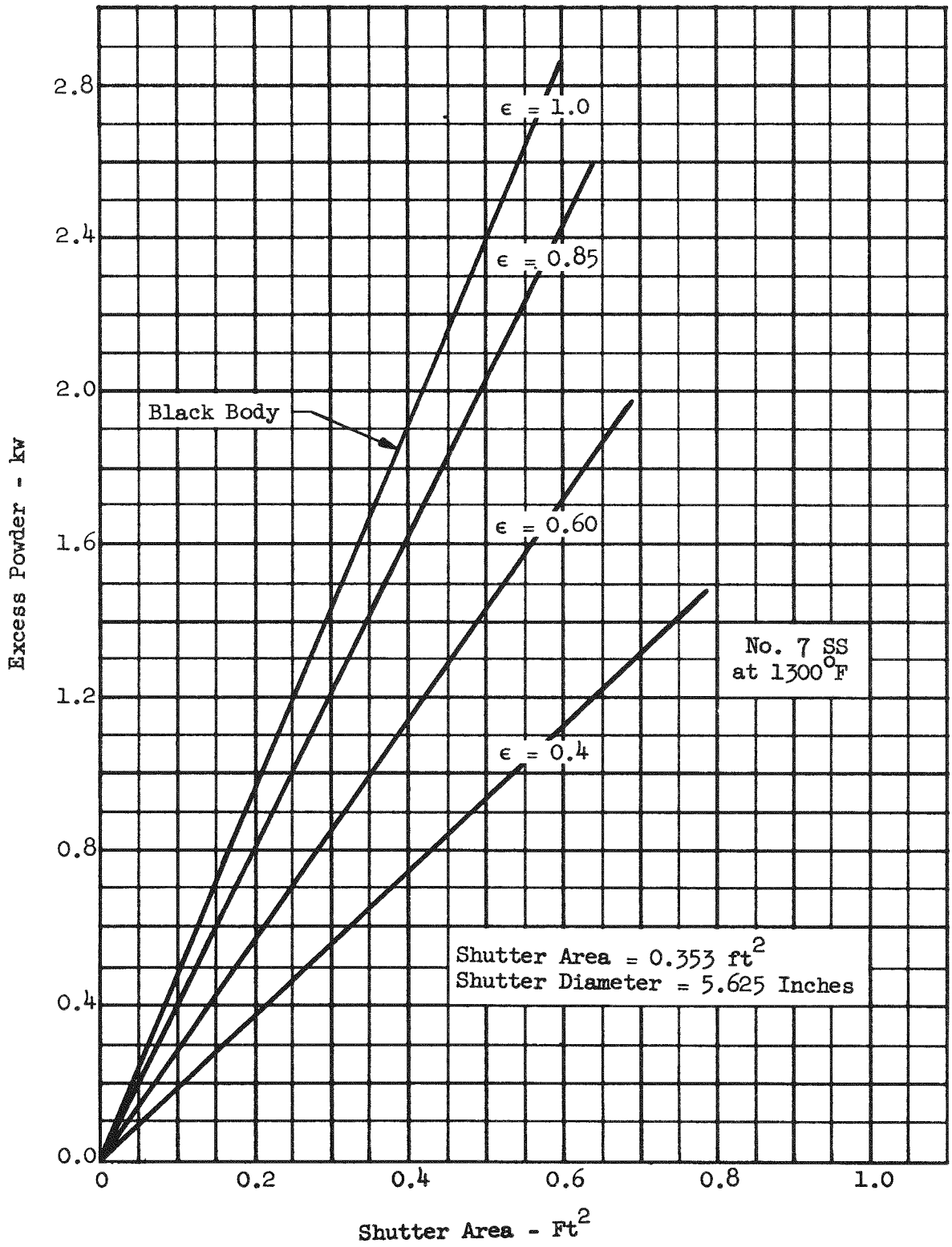

Fig. 12. Thermal Shutter Orbital Performance T_s = 1300°F

III. TASK III - FUEL DEVELOPMENT

A. PROPERTIES STUDY OF CeO_2

A study was conducted by the Ceramic Department at Alfred University on samples of ceric oxide specifically prepared in the laboratory. The tests were:

1. Thermal conductivity of unsintered CeO_2 to 600°C;
2. Thermal diffusivity of unsintered CeO_2 to 670°C;
3. Specific heat of unsintered CeO_2 to 300°C;
4. Thermal expansion of sintered CeO_2 + CaO to 1000°C;
5. Thermal conductivity of sintered blend to 760°C;
6. Thermal diffusivity of sintered blend to 975°C;
7. Specific heat of sintered blend to 1000°C.

The thermal conductivities of the sintered and unsintered bodies were determined by a steady state comparative method. This method consisted of measuring the temperature differences over two known materials and one unknown material with the unknown positioned between the knowns, when a certain thermal gradient is established through all three. Uniaxial heat flow is assured by using "thermal guard-rings" around the sample.

The specimens were heated slowly and allowed to achieve equilibrium temperature conditions before values were recorded. The sintered materials were heated to a maximum mean sample temperature of 760°C. No weight or dimensional changes were noted. The unsintered materials were heated to a maximum mean sample temperature of 600°C. A weight loss of 4.5 per cent and a shrinkage of 0.3 per cent were noted. The complete cycle for one thermal conductivity curve determination required approximately five days. Five curves were run.

The thermal conductivity curve for the sintered material is a straight line with a slight negative slope. The curve for the unsintered material is a straight line with a very slight negative slope up to approximately 300°C. From 300°C to 600°C the curve is positive. Table 3 presents the thermal conductivity data, Fig. 13 the curve.

Both thermal conductivity and thermal diffusivity were measured to cover the entire temperature range desired and to use two independent methods for determining the heat conduction values. Thermal diffusivity relates to thermal conductivity in the following manner:

Thermal conductivity = thermal diffusivity x specific heat x bulk density. Thus it is possible to compare these two heat transfer parameters, if the specific heat and bulk density are known as a function of temperature.

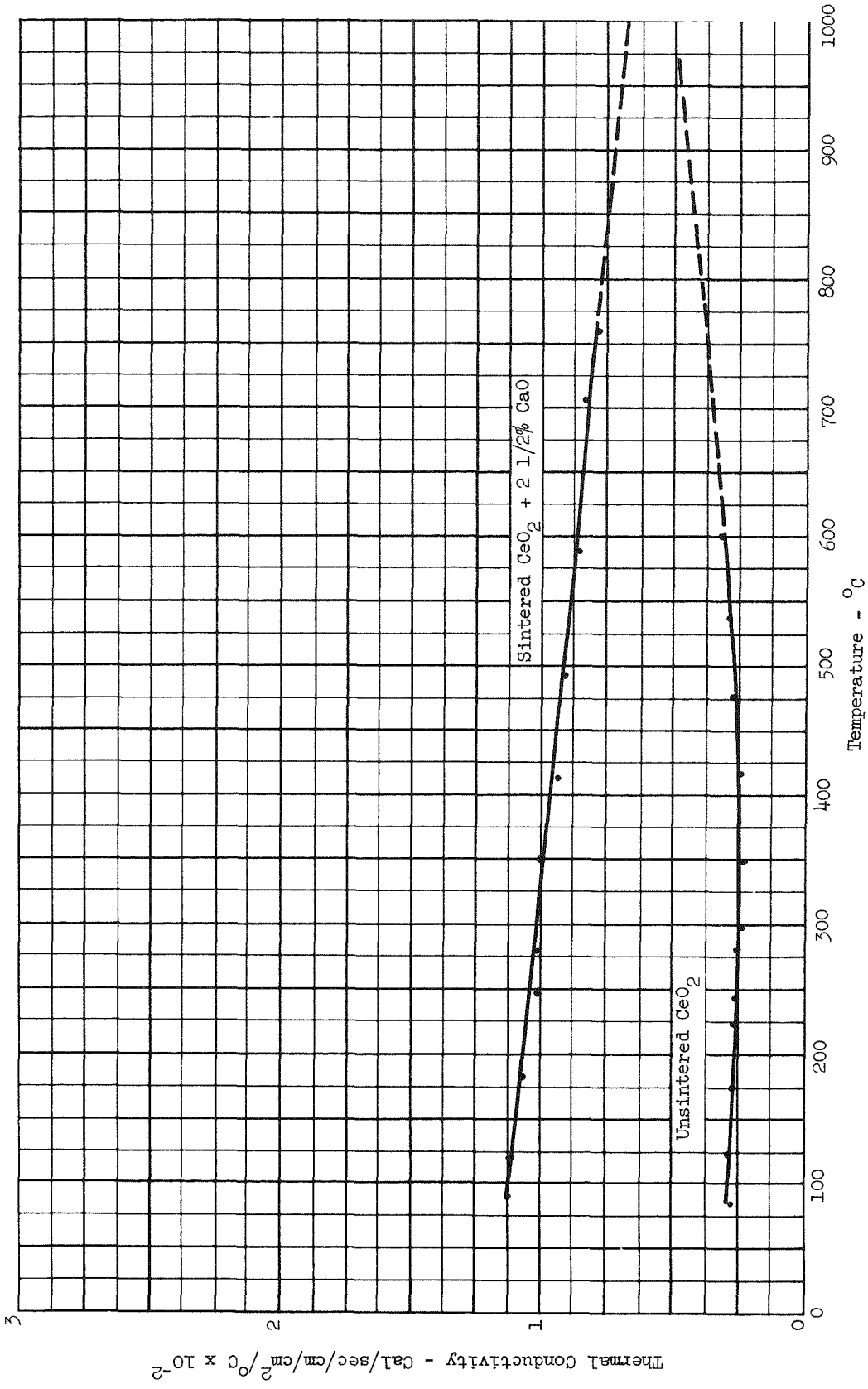

Fig. 13. Thermal Conductivity of Sintered and Unsintered Material

TABLE 3

Thermal Conductivity of Cerium Oxide Mixtures

Sintered CeO_2 + 2.5 Per Cent CaO		Unsintered CeO_2	
Temperature (°C)	K(Cal/sec/cm/cm^2/°C)^x	Temperature (°C)	K(Cal/sec/cm/cm^2/°C)^x
92	0.0112	86	0.0028
122	0.0112	124	0.0030
184	0.0108	176	0.0028
248	0.0102	225	0.0029
280	0.0105	245	0.0028
353	0.0102	282	0.0027
413	0.0096	300	0.0024
392	0.0092	350	0.0025
590	0.0088	417	0.0026
704	0.0085	476	0.0029
757	0.0080	536	0.0030
		600	0.0033

x - Actual experimental values divide cgs units by 0.00413 to convert to BTU/hr/ft/ft^2/°F

Weight loss of 4.5 per cent occurred in unsintered sample when heated to 600°C. A shrinkage of 0.3 per cent also occurred.

A specimen, in the shape of a semi-infinite cylinder with a thermocouple in place at a position along the cylindrical axis, is suddenly moved into a radiation-boundary type hot zone of a furnace, and the temperature rise at stipulated times is recorded. Using several different hole depths in similar specimens it is possible to plot a "nest of heating curves" from which the thermal diffusivity may be calculated.

Table 4 presents the data for the unsteady state diffusivity tests, for both the sintered and the unsintered materials. Table 5 shows the difference between the measured and the calculated thermal conductivities using the thermal diffusivity, specific heat and density.

Only one thermal conductivity curve is shown, that which was measured, because the differences are small between the two methods and are well within the experimental error. The higher temperature values for thermal conductivity may be taken from Table 5.

Values for mean specific heat were determined by an adiabatic-calorimeter. The procedure was to heat the specimen to equilibrium at a desired temperature, drop the specimen into the calorimeter and measure the temperature change under adiabatic conditions. Because the calorimeter was operated without water, there were no losses caused by steam or splashing.

TABLE 4

Thermal Diffusivity of Cerium Oxide Mixture

Material	Temperature (°C)	Thermal Diffusivity (cm^2/sec)	Surface Heat Transfer Factor (cm - 1)	Biot's Modulus Unity
Unsintered	175	0.006	0.22	0.2
CeO_2	275	0.006	0.33	0.3
	430	0.006	0.45	0.4
	670	0.006	0.67	0.6
Sintered	200	0.018	0.06	0.04
CeO_2 mixture	420	0.015	0.12	0.09
	660	0.012	0.27	0.2
	860	0.010	0.55	0.4
	975	0.0095	0.96	0.7

The unsintered specimens were tested from temperatures approximately 100, 200 and 300°C. It was essential to hold the specimens at temperature in the furnace for upwards of five hours before dropping into the calorimeter, because of the large exothermic effect observed in the 100 to 200°C range. The mean specific heat values were plotted in Fig. 14 with the curve indicating the average values listed in Table 5. No shrinkage of specimens was observed in this series and weight loss was less than ten per cent.

The sintered specimens were tested from temperatures of about 100, 300, 575, 750, 1000°C. No significant weight losses or volume changes were observed. The mean specific heat values are plotted in Fig. 14, with the curve representing the average values listed in Table 5.

A sintered specimen 2.907 inches long, 0.532 diameter weighing 67.9108 grams, was heated in a fused quartz dilatometer to 1000°C at the exact rate of 5°C per minute. Change in length was measured to the nearest 0.0001 inch on heating and cooling. The expansion measured at 1000°C was 1.217 per cent and upon cooling to room temperature the specimen showed a slight shrinkage of 0.020 per cent and a loss in weight of 0.0032 gram. Results correlated for the expansion of the fused quartz dilatometer are shown graphically in Fig. 15.

B. CeO_2 FUEL PELLETS

Fabrication studies of CeO_2 based bodies were continued during this period. The studies consisted of use of ORNL prepared cerous oxalate, effects of calcining temperatures on compactibility and sinterability and use of ORNL material with additives.

Three lots of cerous oxalate were received from ORNL containing known amounts of Nd_2O_3 and La_2O_3. The cerous oxalate powders will produce CeO_2 powders of 85, 90 and 95 per cent purity and the remainder will be Nd_2O_3 and La_2O_3 impurities in a ratio of about 2.1 by weight.

TABLE 5

Thermal Data for Comparison

Material	Temperature (°C)	Thermal Diffusivity (cm^2/sec)	Specific Heat Thermal Capacity (cal/gr/°C)	Bulk Density	Calculated Thermal Conductivity	Measured Thermal Conductivity
Unsintered	175	0.006	0.098	4.4	0.0026	0.0028
CeO_2	275	0.006	0.101	4.4	0.0027	0.0027
	430	0.006	0.105*	4.4	0.0028	0.0027
	670	0.006	0.112*	4.4	0.0030	0.0033*
Sintered	200	0.018	0.096	6.5	0.011	0.0105
CeO_2 mixture	420	0.015	0.102	6.5	0.010	0.0095
	660	0.012	0.107	6.5	0.0084	0.0086
	860	0.010	0.112	6.5	0.0073	0.0077*
	975	0.0095	0.115	6.5	0.0071	0.0075*

* Extrapolated Values

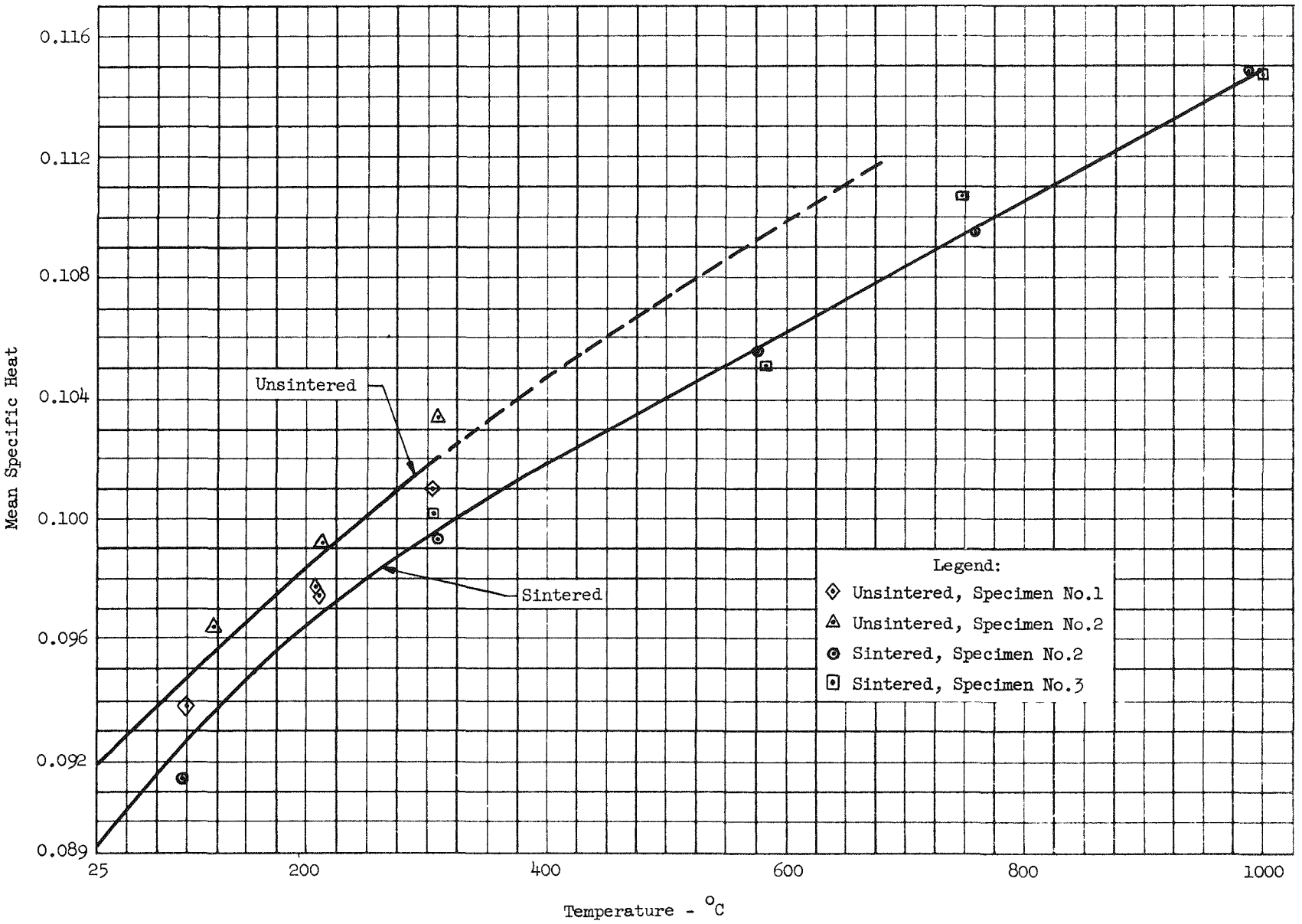

Fig. 14. Mean Specific Heats of Unsintered and Sintered Specimens

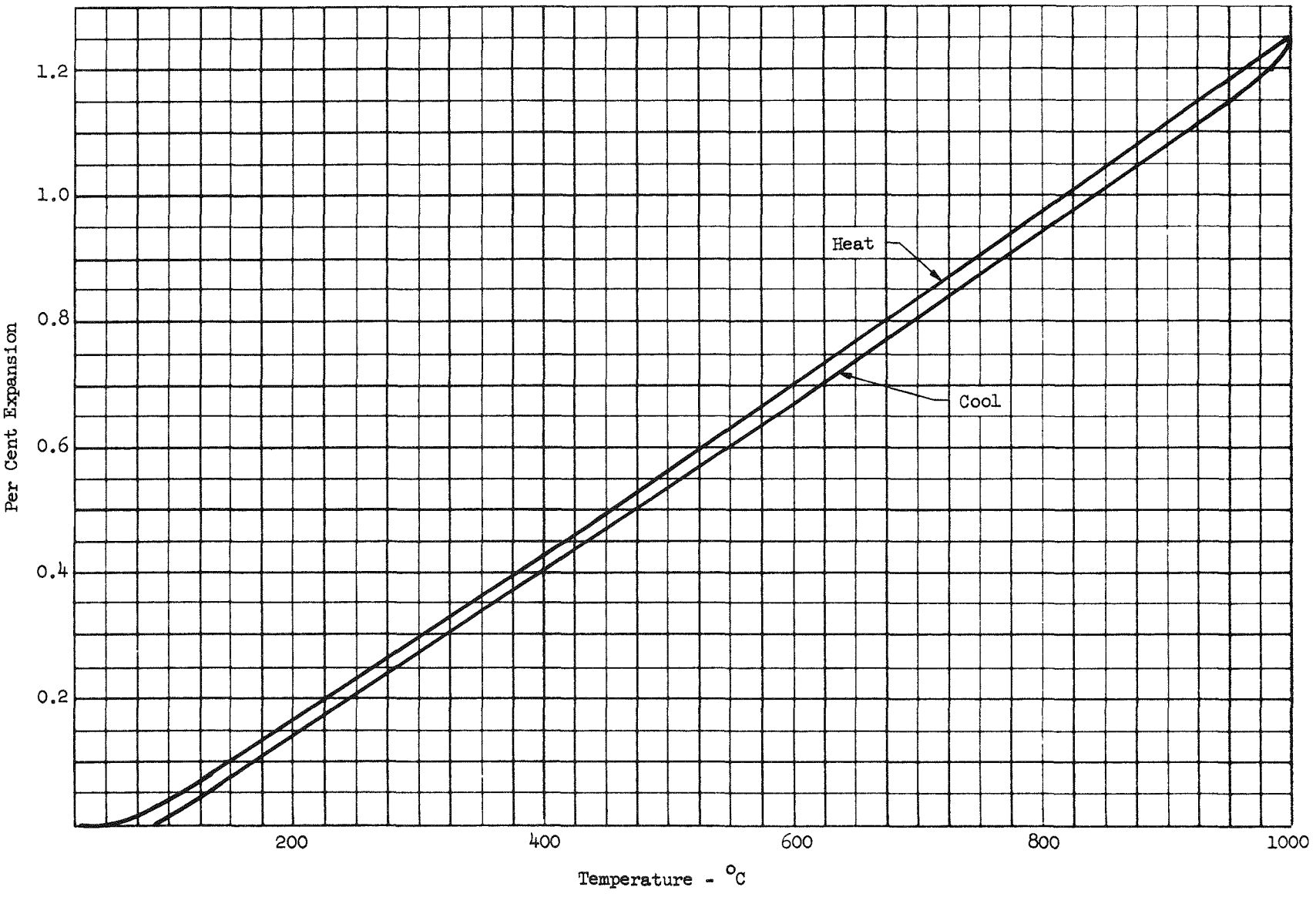

Fig. 15. Thermal Expansion of Cerium Oxide plus CaO Heated at a Rate of of Five Degrees Centigrade per Minute

Preparation of each of the three samples were initially the same. Rare earth oxalates were precipitated from 40 liters of solution of 1.5 N nitric acid and containing the required amount of Ce $(NO_3)_2 .6H_2O$, Nd $(NO_3)_3 .6H_2O$ and La $(NO_3)_3 .6H_2)$ to yield the desired proportions of cerium, niodymium and lathenum oxides. Under microscopic examination Sample 1 appeared to be granular while Samples 2 and 3 were crystalline. However, after calcination all three samples appeared to be a fine fluffy powder.

The batches were calcined at temperatures of 350 to 750°C at 100°C intervals in air for a period of 12 hours. A study is being conducted to see if the calcination temperature will have any effect on the particle size of the material, compacting behavior of the powders and sintered density. Pellets prepared from material calcined were compacted at 10, 25, 37.5 and 50 tsi and indicate an increase in density with an increase in calcining temperature. However, due to the fine particle size of the powder produced, it was difficult to form pieces at high pressures (37.5 tsi up) that were free from laminations. The sintered results showed that densities of 90 per cent of theoretical could easily be obtained. Higher compacting pressures yielded higher densities after sintering. Table 6 below lists results of variations in pressure and calcining temperature.

TABLE 6

Results of Variations in Calcining Temperature

Sample No.	Calcining Temperature (°C)	Green Density (per cent theoretical)	Sintered Density (per cent theoretical)	Compacting Press (tsi)
1	350	53	Laminated	50
1	450	55	Laminated	50
1	550	60	Laminated	50
1	650	62	Laminated	50
1	750	66	85	50
2	350	51	85	50
2	450	54	96	50
2	550	57	95	50
2	650	59	95	50
2	750	63	95	50
3	350	Pellets laminated while ejecting from die		
3	450	51	94	50
3	550	Pellets laminated while ejecting from die		

TABLE 6 (Cont'd)

Sample No.	Calcining Temperature (°C)	Green Density (per cent theoretical)	Sintered Density (per cent theoretical)	Compacting Press (tsi)
3	650	56	97	50
3	750	62	98	50

Because of difficulty in ejecting pellets from the die when compacting at 50 tsi, the same batches were repeated at 25 tsi. Table 7 show the resulting data.

TABLE 7

Results of Variations in Calcining Temperature

Sample No.	Calcining Temperature (°C)	Green Density (per cent theoretical)	Sintered Density (per cent theoretical)	Compacting Press (tsi)
1	350	47	Laminated	25
1	450	51	93	
1	550	54	Bloated surface	
1	650	52	92	
1	750	64	94	
2	350	47	Laminated	
2	450	49	98	
2	550	53	95	
2	650	57	96	
2	750	60	96	
3	350		Laminated while ejecting from die	
3	450	45	86	
3	550	50	94	
3	650	53	95	
3	750	59	96	

A study is being made with the ORNL powders of the effects of adding two per cent TiO_2 - 0.5 per cent $CaCo_3$. Compacts pressed at 25 tsi were sintered in air at 1500°C for four hours. Table 8 lists the results of sintering with additives.

TABLE 8

Sintering With Additives

Sample No.	Calcining Temperature (°C)	Green Density (per cent theoretical)	Sintered Density (per cent theoretical)	Compacting Press (tsi)
1	750	61	94	25
3	350	44	95	25
3	450	47	95	25
3	550	51	95	25
3	650	53	94	25
3	750	58	94	25

C. PREPARATION OF MOLYBDENUM TEST BLOCKS

Three molybdenum blocks 3.5 inches in diameter by six inches high were prepared for test, (Fig. 16).

The steps in preparing the blocks were:

1. Blast surface with a steel grit to insure a good mechanical bond between coating and molybdenum;

2. Flame spray a coating of colmonoy of approximately 0.012 to 0.015 inch in thickness on the sides of the molybdenum block, (Fig. 17);

3. Heat treat the block in a high purity hydrogen atmosphere at a temperature of 2000 to 2200°F for two hours;

4. Insert a lead filler and pellets in one end, after fusing sides and placing molybdenum caps, (Fig. 18);

5. Braze the molybdenum caps in vertical position in argon atmosphere at 2000°F, (Fig. 19 and 20);

6. Invert the molybdenum block and insert lead and pellets in other end and braze;

7. Flame spray both brazed ends and fuse, (Fig. 21 and 22).

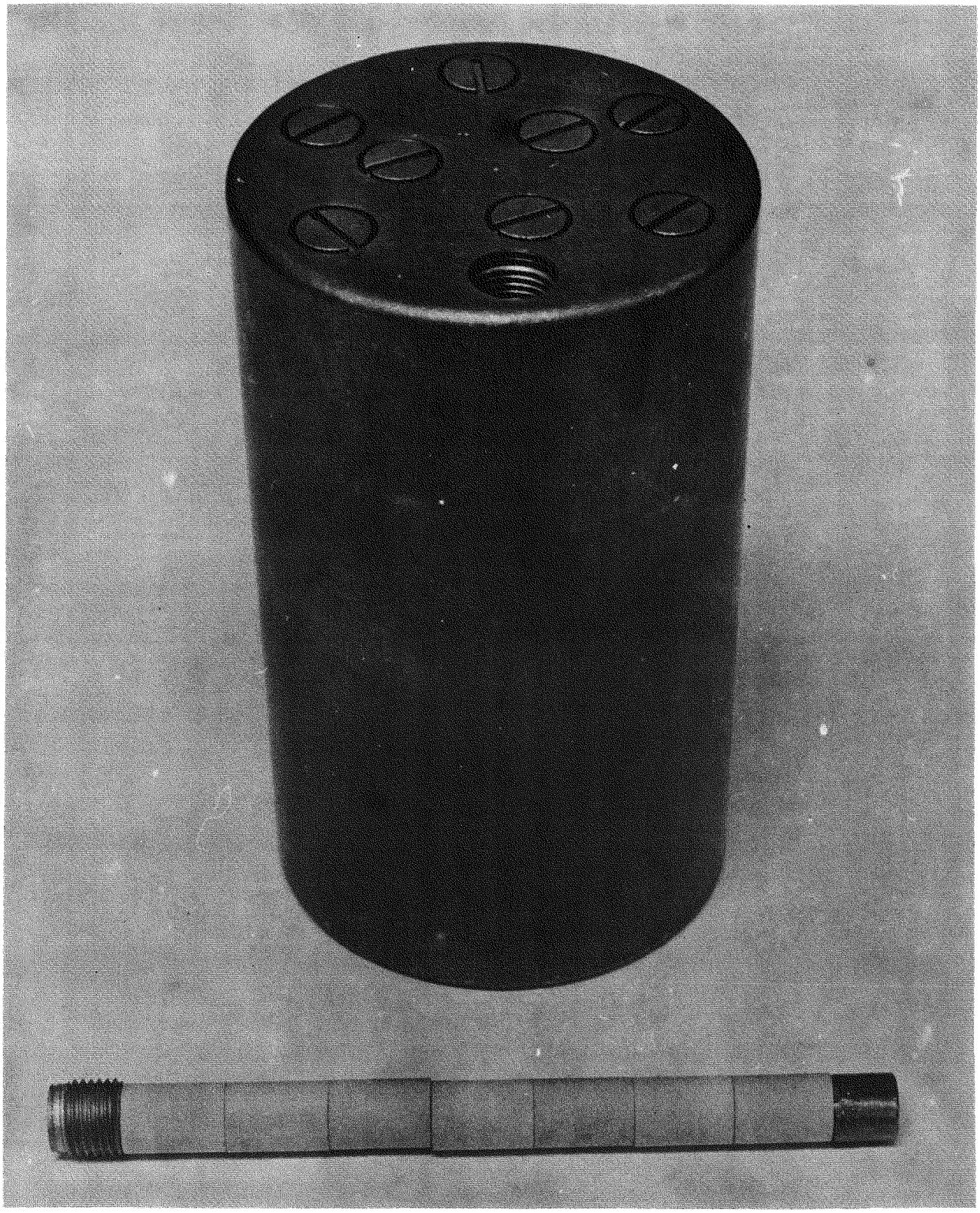

Fig. 16. Molybdenum Block Showing Contents of A Single Section

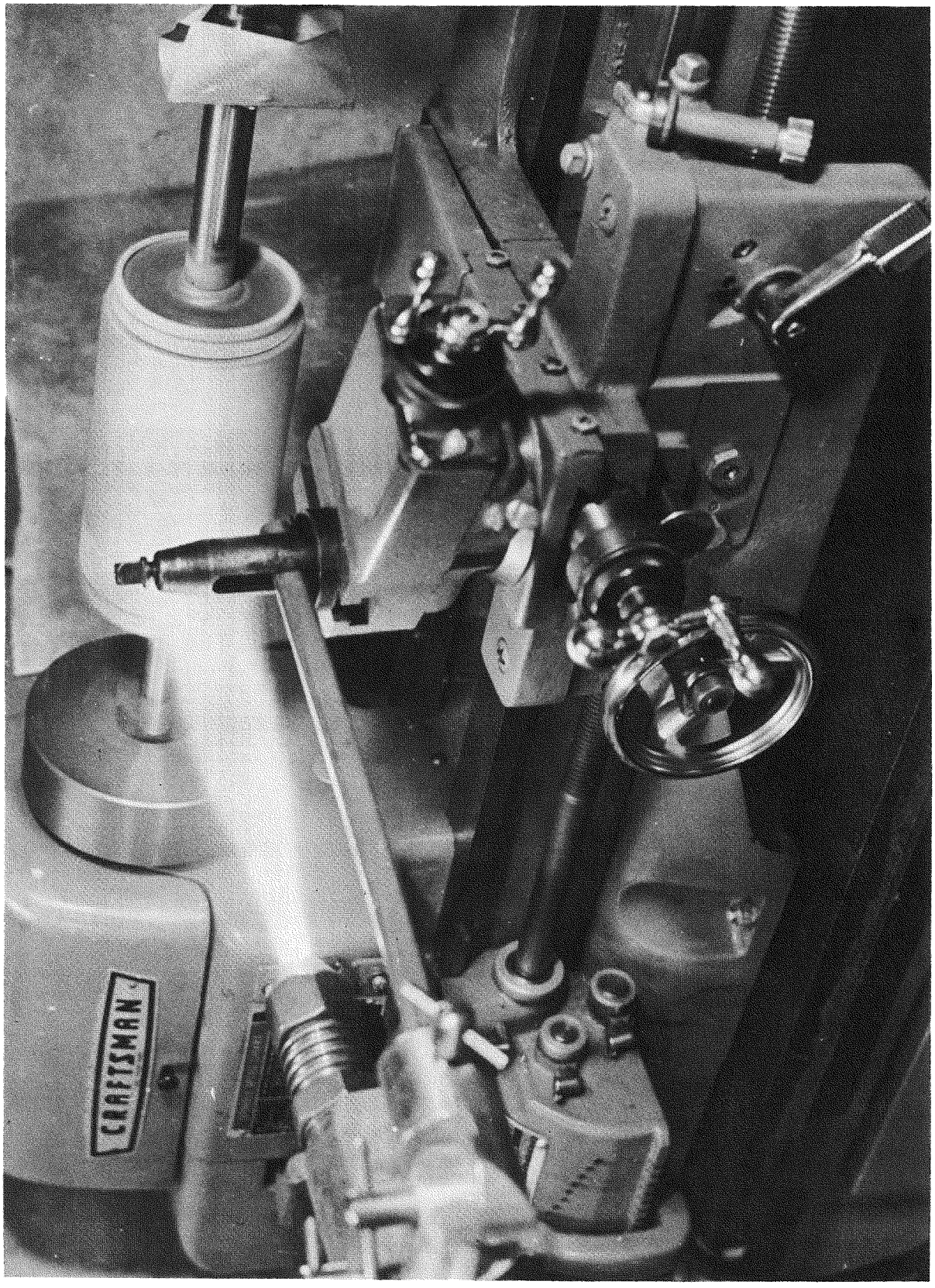

Fig. 17. Flame Spraying of Molybdenum Block with Oxidation Resistant Coating

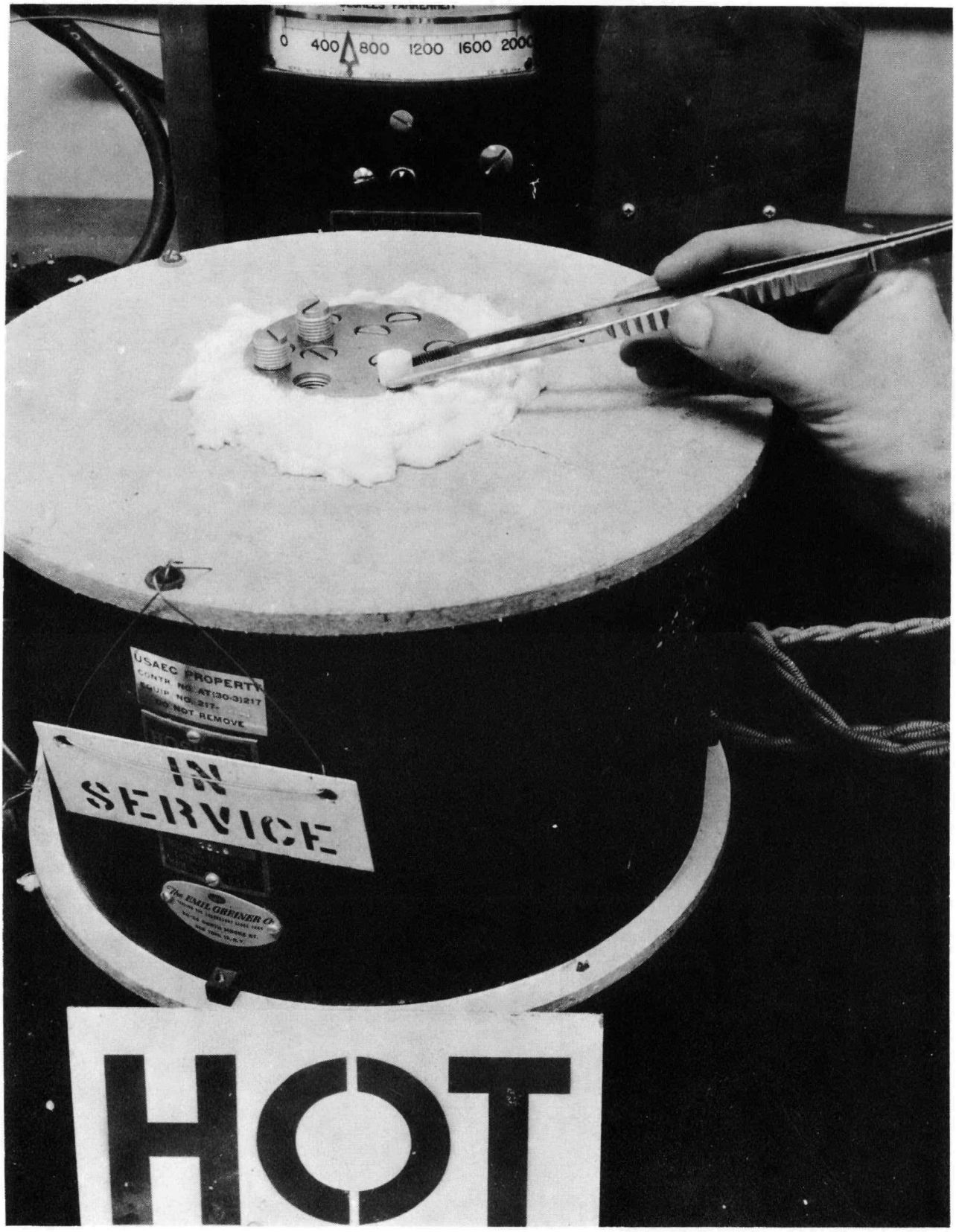

Fig. 18. Heating of Molybdenum Block and Inserting of Simulated Pellets Into Liquid Lead Filler

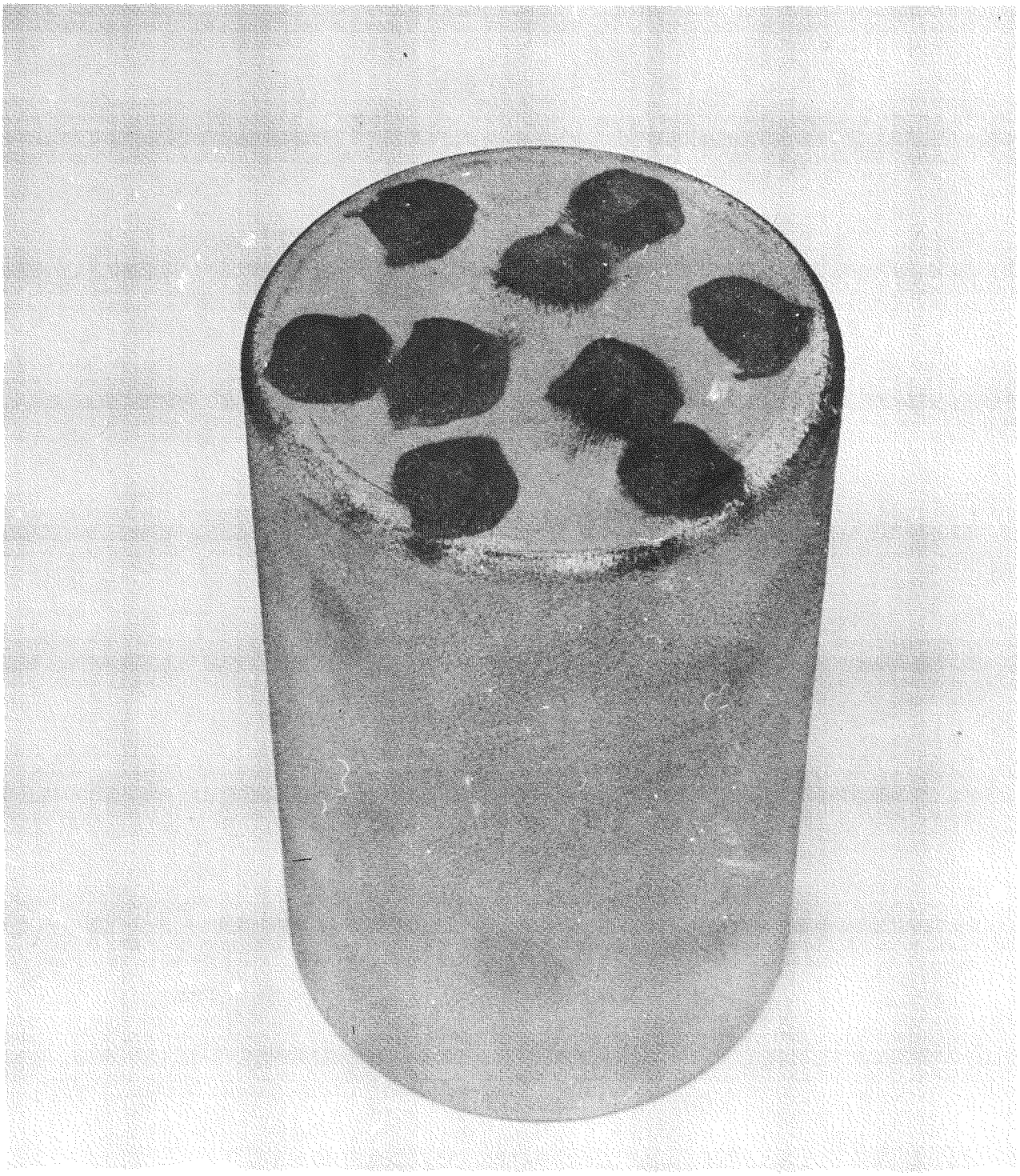

Fig. 19. Top View of Molybdenum Block Showing Application of Brazing Powder

Fig. 20. View of Brazing Furnace

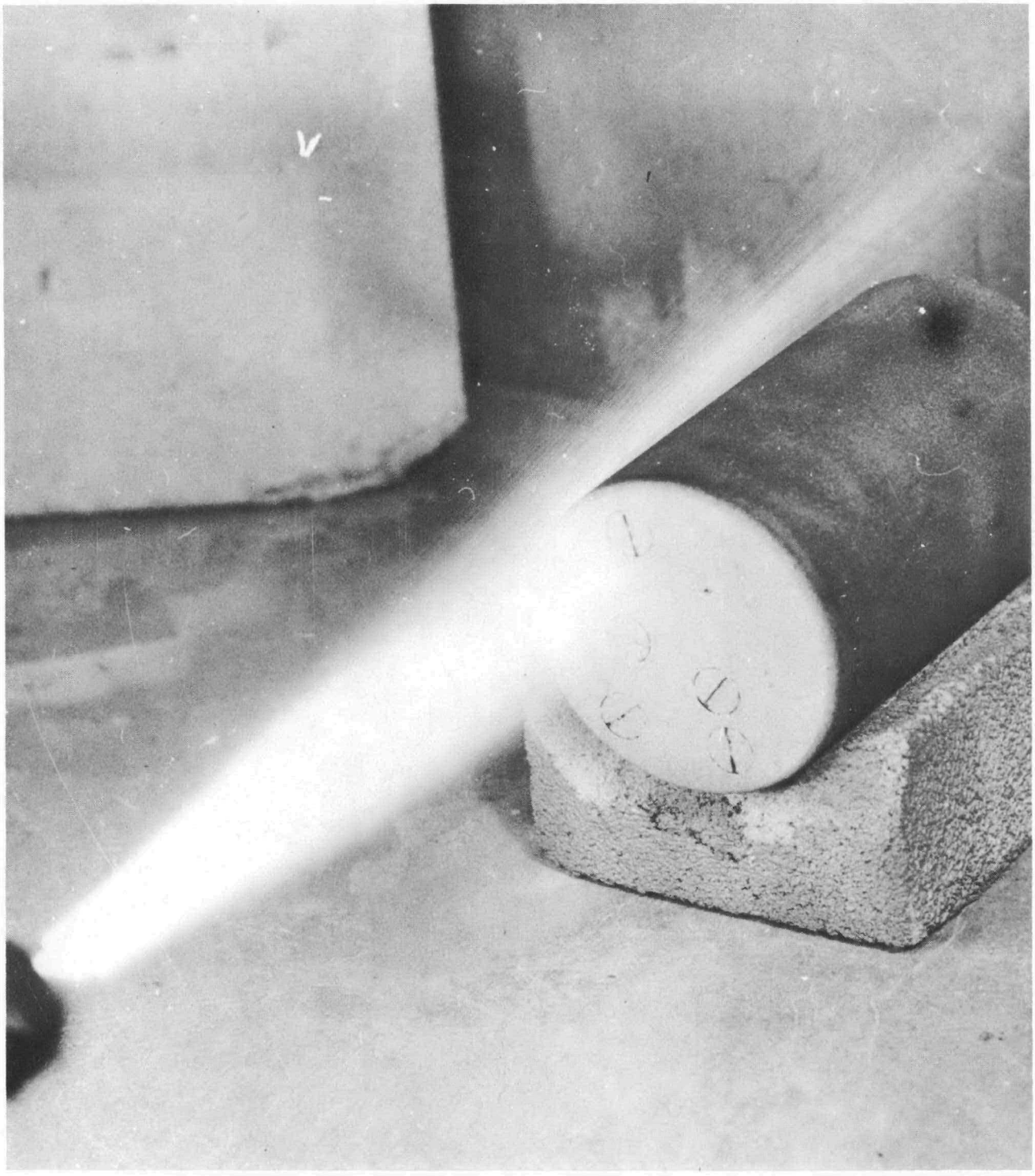

Fig. 21. Flame Spraying of Molybdenum Block with Oxidation Resistant Coating

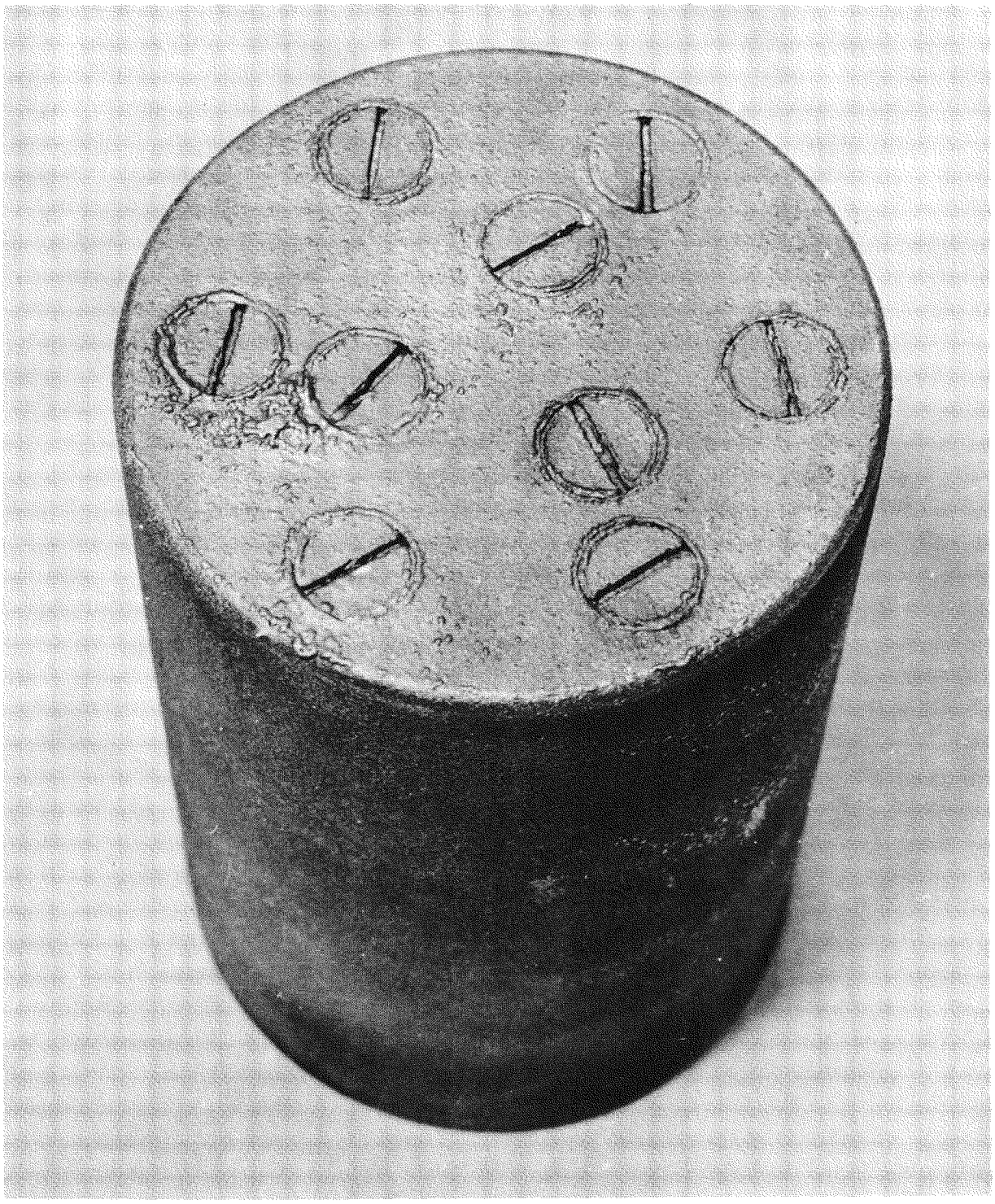

Fig. 22. Completed Molybdenum Assembly

The best brazing results were obtained by piling loose nicrobraz powder around the area to be brazed. When using nicrobraz bushings it appeared that the braze did not melt completely. Additional studies are being conducted to determine the best method of applying the braze material. Additional pellets are being prepared in order to make up three more molybdenum blocks for testing.

During the brazing of the molybdenum caps, lead beads formed on the top of the block. Although the lead content was calculated so as to have a 1/8 inch void within the hole containing the fuel, it appears that the lead is being forced out by entrapped gases. Brazing will continue in an effort to get a sound seal around the threads.

D. OXIDATION PROTECTIVE COATINGS

The development of oxidation protective-lead resistant coatings is continuing. Those under consideration are two-layer coatings consisting of a Colmonoy No.5 alloy base coat and an Al + Cr - Si overcoat. In addition, improvement of a Colmonoy alloy coating by molybdenum, tantalum, niobium and tungsten additions is being studied. Table 9 shows results of coatings that have been investigated.

TABLE 9

Results of Coating

Coatings	Composition	Oxidation Before Lead Corrosion (hours)	After Lead Corrosion Test	Oxidation Test Following Lead Corrosion	Remarks
Colmonoy (b) No.5 (No.300)	No.5 + 10% Mo (79 Ni, 12 Gr, 4 Si, 2 B)	Good - 8	No defects after 500 hours(a) Weight gained + 0.2793 gram	No good	Oxidized within $1\frac{1}{4}$ hours (Rupture on bottom)
Colmonoy (b) No.5 (No.301)	No.5 + 20% Mo	Good - 8	No defects after 500 hours(a) Weight gained + 0.3642 gram	No good	Oxidized within $\frac{1}{2}$ hour (Rupture on bottom)
Colmonoy (b) No.5 (No.302)	No.5 + 30% Mo	Good - 8	No defects after 500 (a) hours Weight gained + 0.4938 gram	No good	Oxidized within $\frac{1}{2}$ hour (Rupture on side)
Al + Cr - Si (No.600) (No.604) (d)	20 Al, 45 Cr 32 Si	Good - 8	No defects after 500 (a) hours Weight gained + 0.5836 gram	Fair	Oxidized within 6 hours (Rupture on edge)
Al Si + Cr-Si	20 Al 80 Cr-Si	Did not test	-----	-----	Blend did not bond
Chromalloy (No.2)		Good - 8	No defects after 500 (a) hours Weight gained + 0.0162 gram	Poor	Oxidized within $\frac{1}{4}$ hour (Rupture on bottom and edge)
Chromalloy + Colmonoy No.5 (No.5)		Good - 8	Cracked Surface	Poor	Oxidized within 3/4 hour
Chromalloy W-2 (No.8)		Good - 8	No defects	No good	Oxidized within 2 hours (Rupture on edge)
Chromalloy + Colmonoy No.6 (No.12)		Did not test	-----	-----	Fused surface end-up with cracks
Colmonoy No.6	72 Ni, 15 Cr, 4 Si, 3B	Good - 4	No defects after 500 (a) hours Weight gained + 0.4497 gram	Fair	Oxidized within 4 hours (Centerless and end ground before testing)
Colmonoy No.6 + SS No.420	85% Colmonoy 15% SS	-----	-----	-----	Melting temperature too high, over 1325°C
Colmonoy No.6 + SS No.420 (No.317)	60% Colmonoy 40% SS	-----	-----	-----	Surface cracked during bonding
Colmonoy No.5 + Cr-Si-Al (No.614)	79 Ni, 12 Cr, 4 Si, 2B 20% Al + 80 Cr-Si	Good	No defects after 500 hours	In test	Surface hard, coatings hot bonded (c)

(a) Weight gained caused by lead coating the piece

(b) Molybdenum powder was sintered with the Colmonoy

(c) Difficulty in reproduction of good sprayed coats because of apparent cracks, peeling off of Al-Cr-Si coat and soft surface which touches the boat

(d) Difficulties in reproduction of good sprayed coats

IV. TASK IV - MATERIALS CORROSION PROGRAM

The materials evaluation in lead and dynamic mercury was continued. From this evaluation it was ascertained that:

1. Croloys are unsatisfactory in dynamic mercury without the use of inhibitors;

2. Cerium oxide fuel pellets of the V series prepared from a 95 per cent mixture (CeO-95 per cent with Nd_2O_3-five per cent) and five per cent TiO_2 gave consistently good lead test results;

3. Screening of the molybdenum coated samples by oxidation tests yielded more consistent lead test results;

4. Use of inhibitors to prevent lead corrosion is not as effective when carbon is not present in the testing area, (See Table 10);

5. The 22 per cent chromium, four per cent nickel and nine per cent manganese Armco alloy shows good resistance to lead corrosion.

A. DYNAMIC MERCURY TESTING

1. Croloy 5 Si and 5 Ti Thermal Harp Units

Dynamic mercury tests have been completed on the Croloy 5 Ti and 5 Si loops. The loops were sectioned and examined metallographically.

The Croloy 5 Si and 5 Ti thermal harp units exhibited similar corrosion in dynamic mercury at 1025-1350°F and 210 psi. The greatest amount of corrosion occurred in the superheater area. The attack was a general solution-type which resulted in precipitation of finely divided black powder in cooler areas of the loop. This was mainly ferrous oxide with traces of nickel and chromium. This precipitate inhibited heat transfer of the loops and the 5 Si heaters burned out after seventy hours and the 5 Si tests were discontinued. The boiler tubing of the Croloy 5 Ti loop ruptured after 150 hours and tests were stopped.

2. Carpenter 20 Cb Thermal Harp Unit

The fabrication of the Carpenter 20 Cb loop required more time than originally anticipated. An attempt was made to speed fabrication by quickly filling the boiler with purified lead and wiring and insulating the loop. The Lewis wire used for heating the loop proved unsatisfactory at high temperatures when bent over a small diameter. The insulation powdered at high temperatures and the short circuits which resulted burned the wire in five places. The loop was then rewired with nichrome and insulated with ceramic. Four separate temperature controllers were installed in the superheater area and the Carpenter 20 Cb loop is now in operation.

3. Lead Corrosion Tests

One hundred and twenty-two lead corrosion tests were completed. Molybdenum crucibles were used for testing the cerium dioxide fuel pellets. All other materials were tested in Type 316 SS crucibles.

Thirty-eight lead corrosion tests were completed on cerium dioxide fuel pellets. The V series of samples were not visibly changed during the tests. The AB and T series gave good results of the tests. The AB series is prepared from a 97.5 per cent mixture (CeO_2-98.75 per cent with 1.25 per cent Nd_2O_3) and 2.5 per cent TiO_2. The T series is prepared from a 95 per cent mixture of CeO_2-95 per cent with Nd_2O_3 five per cent, one per cent $CaCO_3$ and four per cent TiO_2.

Seven molybdenum screw samples were also tested. The lead was removed and the samples carefully checked at the completion of the tests.

The remaining sixteen tests were on Type 347 SS, Carpenter 20, Carpenter 20 Cb, and an Armco alloy 22-4-9 (22 per cent chromium, four per cent nickel and nine per cent manganese). The results are as follows:

TABLE 10

Lead Corrosion Tests

Sample	Inhibitor	Weight Change
Type 347 SS	Zr + Ni	1.0557 1.0220 0.0337
		3.2 per cent weight loss
Type 347 SS	Zr + Ni	1.0494 1.0339 0.0155
		1.5 per cent weight loss
Type 347 SS	None	1.0957 1.0603 0.0354
		3.2 per cent weight loss
Type 347 SS	None	1.0492 0.9412 0.1080
		-10.3 per cent weight loss
Carpenter 20	Zr + Ni	5.3808 5.2259 0.1549
		2.9 per cent weight loss
Carpenter 20	Zr + Ni	4.6361 4.4643 0.1718
		-3.7 per cent weight loss
Carpenter 20	None	4.3415 4.2004 0.1411
		3.2 per cent weight loss

TABLE 10 (Cont'd)

Sample	Inhibitor	Weight Change
Carpenter 20	None	5.0877 4.8650 0.2227
		4.4 per cent weight loss
Carpenter 20 Cb	Zr + Ni	3.8136 3.6621 0.1515
		4 per cent weight loss
Carpenter 20 Cb	None	3.7623 3.4823 0.2800
		7.4 per cent weight loss
Carpenter 20 Cb	None	3.6141 3.3471 0.2670
		7.3 per cent weight loss
Armco 22-4-9	Zr + Ni	13.8155 13.8038 0.0117
		0.08 per cent weight loss
22-4-9	Zr + Ni	12.1195 12.1055 +0.0140
		0.1 per cent weight gain
22-4-9	None	10.9088 10.9033 0.0055
		0.05 per cent weight loss
22-4-9	None	13.3496 13.2591 0.0905
		0.7 per cent weight loss

V. TASK V - POWER CONVERSION SYSTEM

Power conversion equipment is being developed by Thompson Products, Inc., under a subcontract to The Martin Company.

Component development has continued during the period and in addition test runs have been made on rotating assemblies of the turbine, alternator and bearings (TATP). Feasibility has been demonstrated but component performance must now be improved.

Two system arrangements were prepared. One arrangement considered the effects of system fluid momentum on vehicle attitude stability, and the other was based on the concept of minimum piping complexity and system pressure drop. As a result of a program concept change, future effort will be restricted to establishing a system configuration which will be acceptable for testing GEPS 1 and GEPS 3. Studies on turbine exhaust pressure drop and moisture carry over, the effects of package rotor unbalance, and the effects of package alignment and system fluid momentum on vehicle attitude stability, formed the basis for the vehicle systems arrangement effort. In addition, the prelaunch procedure was reviewed relative to the proposed vehicle system arrangement.

The "SNAP I Systems Test Enclosure Design and Operation Philosophy," was prepared. This defines the testing capability and general design of the systems test enclosure. A design layout was completed and an overall cost estimate was prepared. These systems test plans were also organized to assure expeditious completion of this test facility. Definition of instrumentation is a major item which will continue in the coming quarter.

A definitive document, "SNAP I Qualification Test Program Philosophy and Recommendations," was prepared. It defines the testing required throughout the program to prove the design adequacy of the system. A procedure for recording all package and system malfunctions was initiated to provide a means of predicting system reliability.

In conjunction with the design of the systems test enclosure, a versatile start-stop system was selected. This consists of the equipment required to provide several means for pressurizing the bearings and providing mercury to the boilers. The object of this start-up program was to select the simplest most reliable, start system that could be easily integrated into the satellite vehicle. However, due to changes in program concept, a single start-stop technique was selected for the initial systems testing. This will consist of pressurizing the bearings with an auxiliary pump and initiating system start by motoring the alternator.

At the request of the USAEC, the feasibility of using magnetic bearings in the package was briefly reviewed. It was concluded that an extensive development program would be required but with no assurance that success could be achieved.

A brief study was initiated to evaluate the desirability of adding turbine reheat to the system to improve overall cycle efficiency. This study is in its preliminary phase.

An SPTP package specification was completed. However, the change in program concept requires that it be revised. Using it as a guide, a set of component specifications are in process which will allow each component group to work independently with assurance that overall system requirements will be met.

An analog computer study was conducted to determine the modifications required to sustain system operation during the application of excessive transient loads as might be experienced during launch. It indicated that by proper use of devices to reduce alternator load during launch, system operation can be maintained.

A. TESTING PROGRAM

1. Breadboard Test Program

During the reporting period, TATP-I and II were operated in the breadboard test rig. Both operated satisfactory over a range of loads and speeds. The major purpose of TATP-I tests was to demonstrate the operational capabilities of the rotating unit. Seven test runs with hot mercury vapor, lasting up to five hours each and at speeds up to 48,000 rpm, were accomplished with TATP-I. In addition, six hours operating time were accumulated using nitrogen as the working fluid.

A greater effort was expended on obtaining performance data from TATP-II than TATP-I. For this particular unit, spindown tests have provided a consistent accumulation of turbine performance information. Several modifications to the test rig were required to obtain meaningful spindown test results. These are described.

The flat plate quarter scale condenser was tested in August. It was necessary to install additional air lines and ducting to provide cooling air for the mercury heat transfer coefficients and low pressure drops. However, non-condensibles leaking into the system somewhat impaired the results.

The TATP-II unit was removed from the breadboard during late September and modifications started to accommodate the preliminary prototype, which will be installed early in October.

2. Environmental and Systems Test Program

Design of the systems test enclosure was initiated in July. A schematic has been completed. The general philosophy governing the design is that the system to be tested will duplicate the final configuration wherever possible. This involved using similar line sizes, inventories, and thermal capacities and the elimination of any instrumentation that would provide a disturbing influence on the system.

The boiler will be an electrically heated prototype.

3. Start-up and Checkout Console

Effort in this area has been expended to monitor the start-up and instrumentation systems of the STE.

4. Prototype Design

A major effort has been concentrated on completing the assembly and installation of TATP-II so that testing could be initiated. This package was operated 7 hours and 14 minutes assuring that TATP-II was operationally sound.

After the successfully testing of TATP-II, TATP-I was disassembled and modified to form the preliminary prototype. The general condition of the package was good after exposure to mercury vapor for a total of 28.25 hours.

TATP-II was exposed to mercury vapor for 23 hours and 9 minutes. A total of 20 hours and 32 minutes of this testing was accomplished at 40,000 rpm. The prime objective was to determine turbine performance by obtaining full- and no-load speed decay curves. These data agreed closely with previously obtained alternator power data. Additional tests were conducted to obtain data relative to the effects of seal drain pressure on package performance. At completion, the package was delivered to the inspection area where it is being disassembled, cleaned and photographed. Testing was terminated so that the breadboard rig could be modified to include a loop for testing the pump section of the preliminary prototype.

The necessary modifications to the TATP-I housing to form the preliminary prototype have been completed and fabricated. A preliminary assembly of the unit was completed so that a static calibration of the pump-bearing combination could be completed. The parts which will be added to TATP-I to form the preliminary prototype are illustrated in Fig. 23 through 28. Testing in the breadboard rig is scheduled for October. The prime objective will be to prove the functional soundness of the pump-bearing combination and to evaluate the performance of the pump when operating within the package.

A continuous design effort was maintained on the layout of the SPTP package. A design freeze date of October 15, 1958 was set for the SPTP package layout. The package design will utilize the design features of the TATP wherever practical so that assembly and test experience gained can be used to best advantage.

Some of the major problem areas encountered during the initial phase of SPTP layout have been resolved as follows:

1. The critical speed of the shaft was increased to 52,800 rpm by increasing shaft diameter and decreasing shaft length. This length decrease was accomplished by using dished turbine wheels and shortening the alternator labyrinth seal. The calculated tangential stress of the dished turbine wheels is 12,800 psi maximum;

2. The pump end bearing will employ a bearing socket which is shrunk fit into the end plate. This will reduce heat loss to the bearing fluid. The pump impeller will be threaded and pinned to the bearing shaft extension. External plumbing will be used for supplying the bearings and jet pump.

3. An area of major importance is the heat loss from the turbine nozzle and stators. Immediate plans include the use of Synthamica 606 for insulating the interior (as required) and potassium titanate for insulating the exterior of the package.

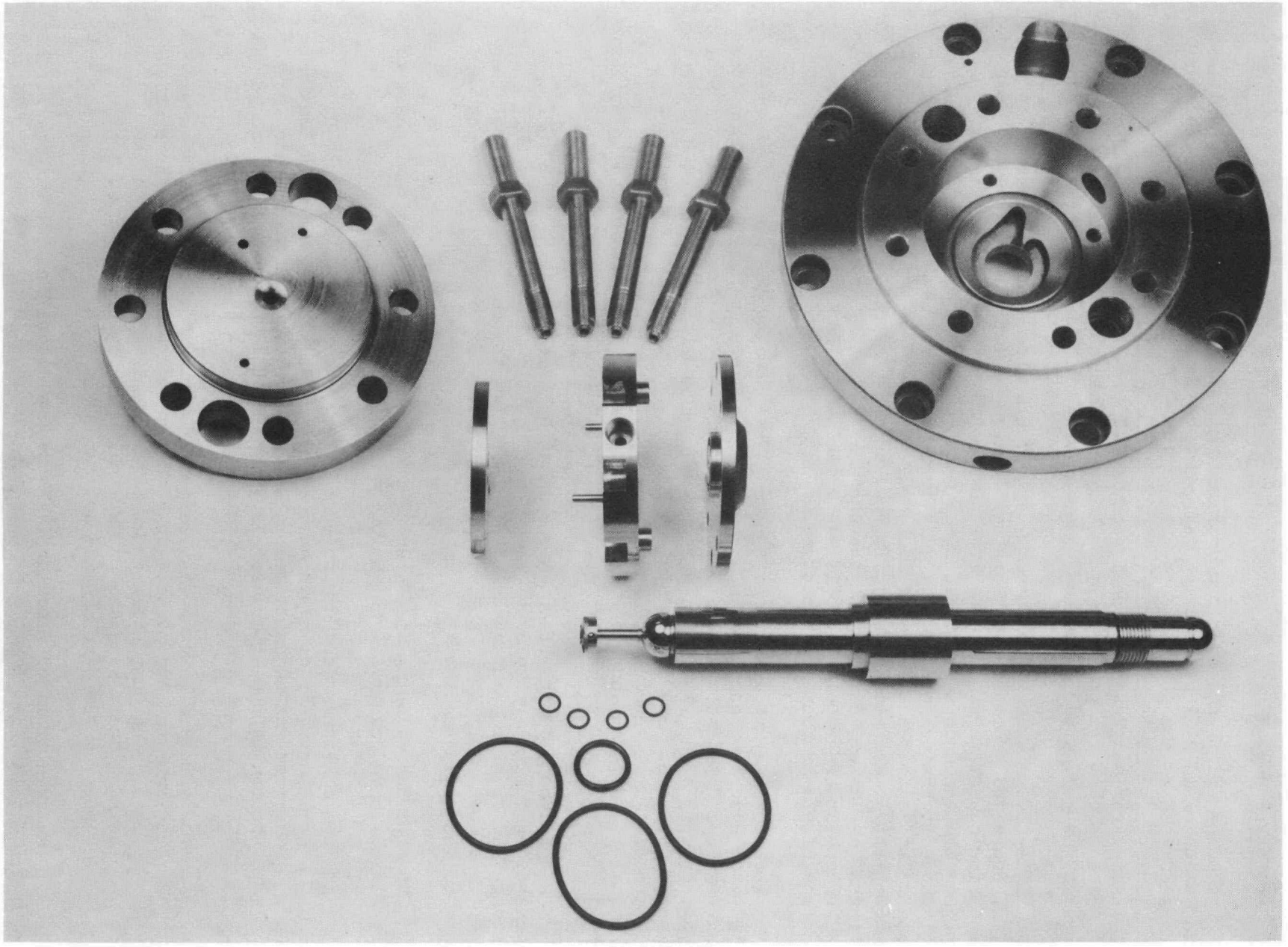

Fig. 23. Preliminary Prototype Parts

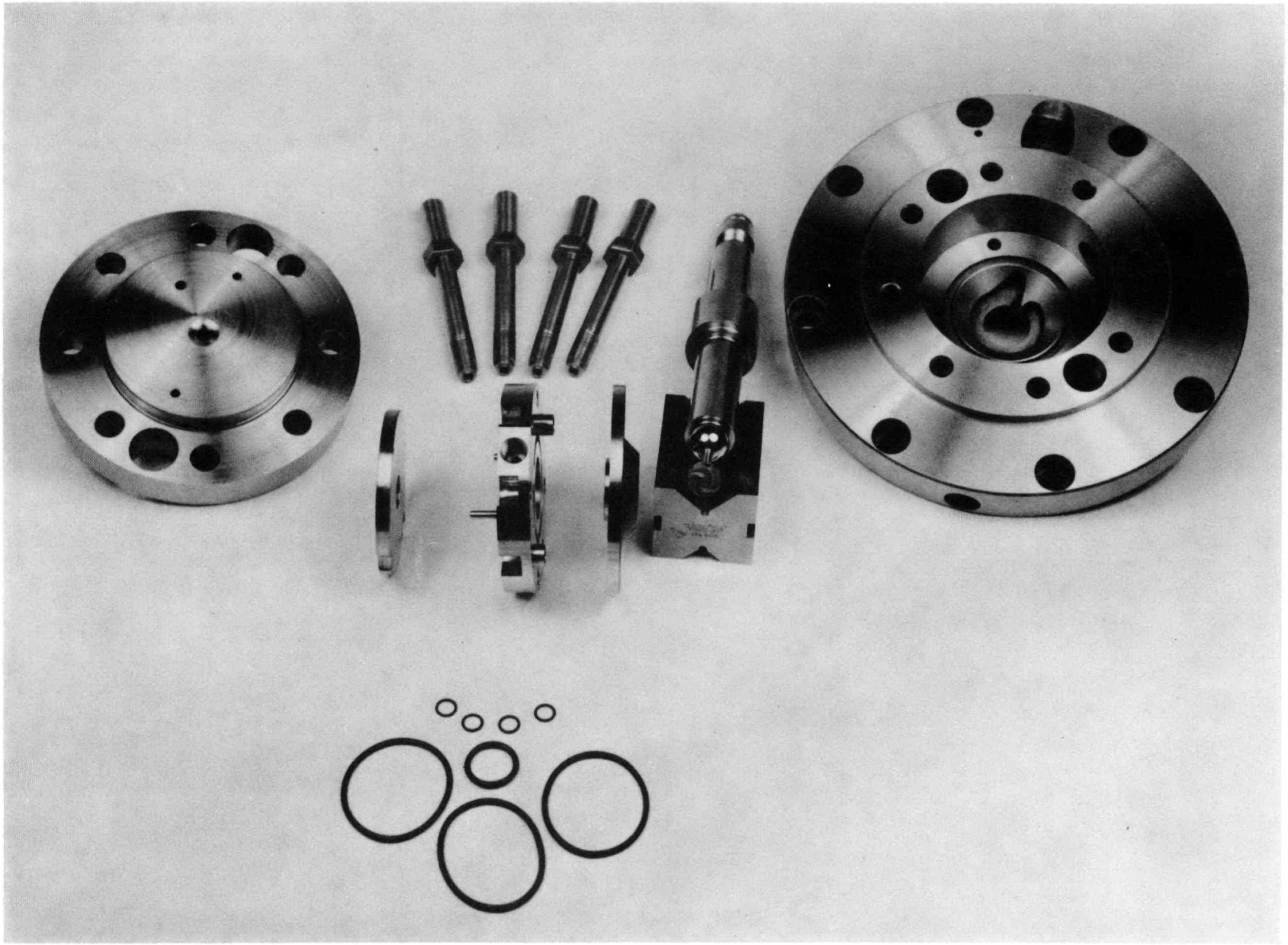

Fig. 24. Preliminary Prototype Parts

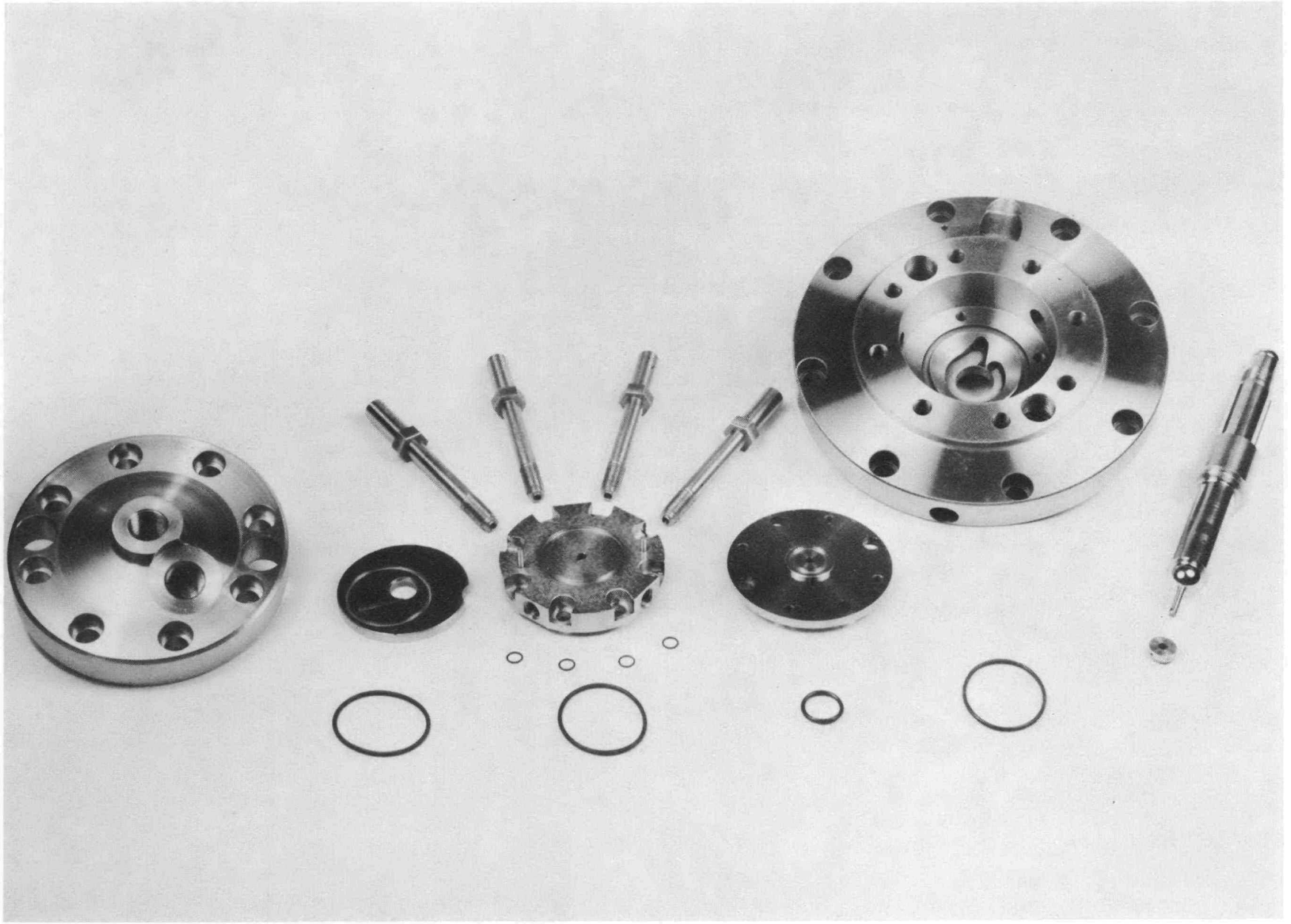

Fig. 25. Preliminary Prototype Parts

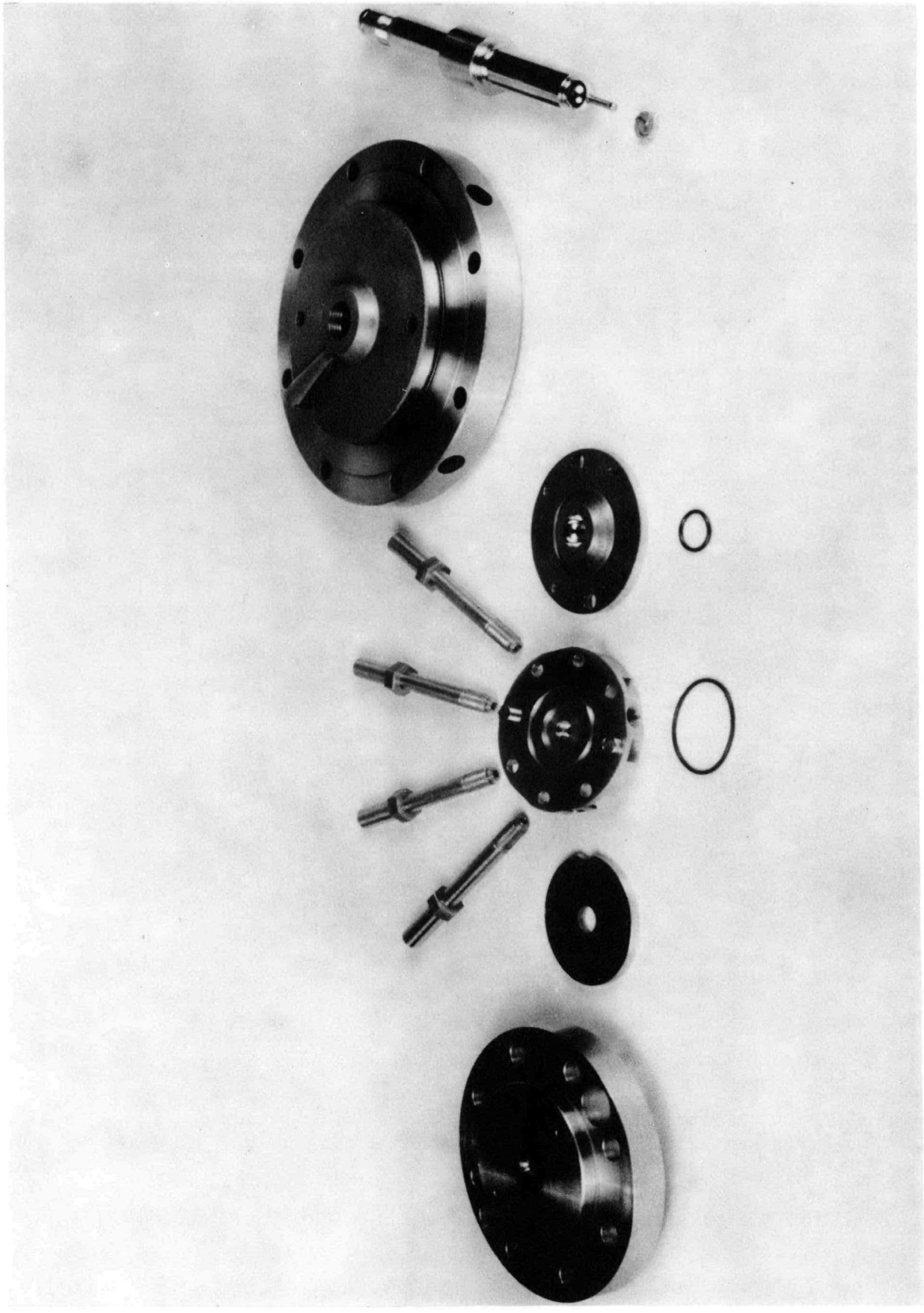

Fig. 26. Preliminary Prototype Parts

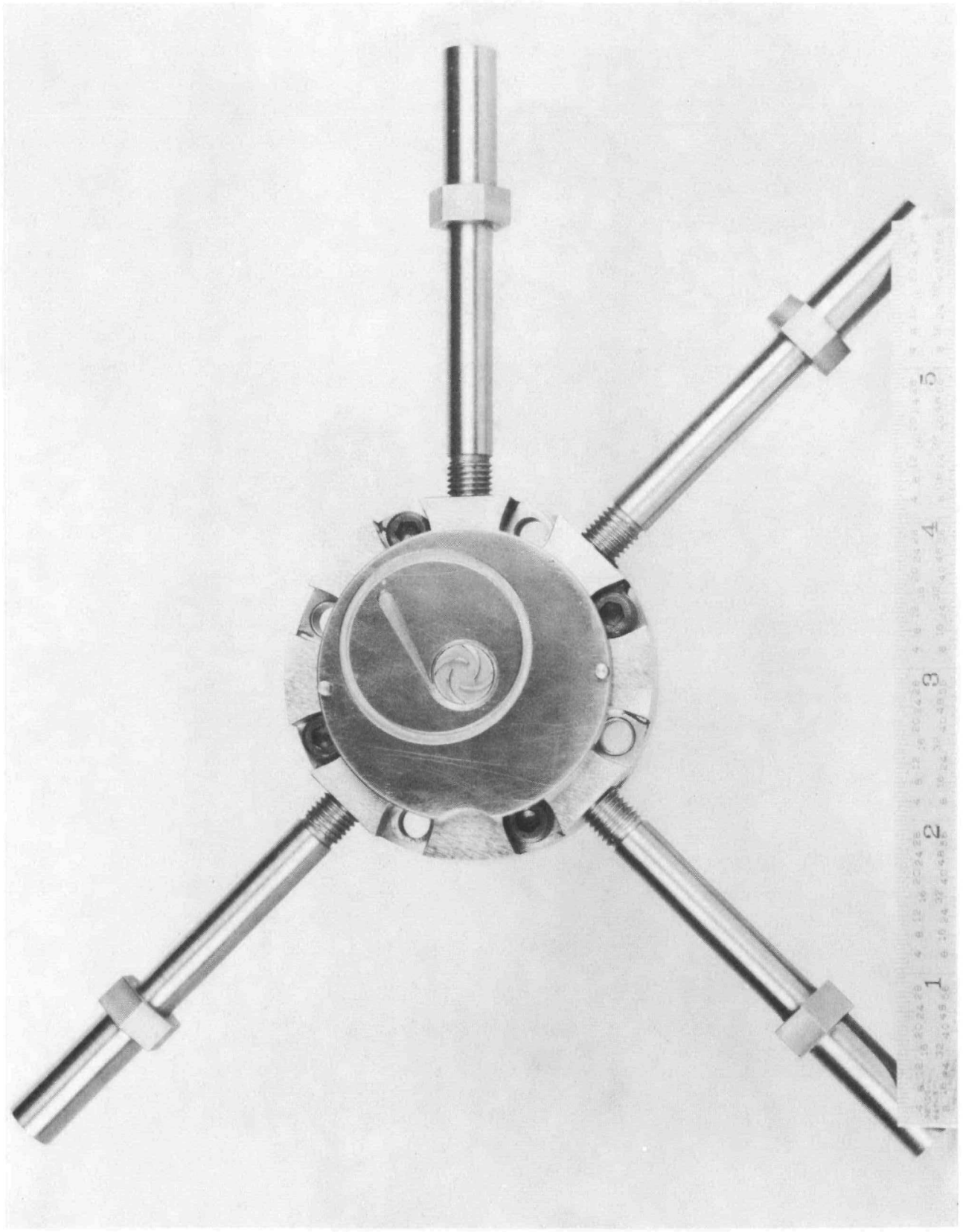

Fig. 27. Preliminary Prototype Parts of Pump Scroll and Impeller

Fig. 28. Preliminary Prototype Pump Impeller

5. Materials Evaluation

Several materials program proposals were prepared by the Materials Group. Pending approval of a specific program, the Group has been engaged in general activities in the areas of corrosion studies, potting-compound development, component parts evaluation, and material application.

Bi-Metallic Capsule Tests. - As a means of generating some information concerning the stability of multi-metallic systems in mercury environments, techniques are being established for conducting exposure tests in glass capsules. Samples of various metallic, cermet, and non-metallic materials are being procured. Tests at 650°F will be started as soon as encapsulating procedures are found to be satisfactory.

Loop Testing. - The loop-testing program was reappraised by the Materials Group and several modifications were made of the test loop design to improve temperature control and to insure a single-material loop (no fittings). A pilot loop of Type 316 stainless steel was placed in operation to evaluate the design and changes of the system were made where necessary.

A test loop, of welded design, was fabricated from Type 347 SS. This loop has been leak tested and the available insulation has been altered to provide a proper fit. The loop will be cleaned by approved procedures, filled, and evaluated. Heaters and thermocouples will be installed and testing will start about October 2, 1958.

A similar loop is being fabricated from Carpenter 20 Cb. However, there is a delay in obtaining small lots of one-quarter inch tubing of this material needed for the inlet and outlet filling and purging ports.

Orders have been placed for pressure controllers and for a centrifugal pump to circulate cleaning fluid.

Insulation and Potting Compound Development. - Two pyroceram glass coils and two pyroceram crystalline coils (all impregnated and coated) were suspended in the one-liter autoclave on a stainless steel wire. Conditions of exposure were 550°F and two psia mercury vapor. Total run time was 100.5 hours. Spectrographic analysis of the mercury reclaimed from the autoclave after the test revealed that the major contaminant picked up was silver with traces of silicon, copper and iron.

Examination at 40X of the potted coils after sectioning revealed no mercury within the pyroceram. Chemical analysis of successive surface layers of one of the pyroceram glass coils revealed only trace quantities of mercury. However, cracking of the pyroceram was quite evident and occasional mercury droplets were found on the copper wire surface.

Two pyroceram glass coils and two pyroceram crystalline coils (all impregnated and coated) were placed in the one-liter autoclave half filled with mercury.

The coils floated on the surface of mercury. The autoclave was operated on a cycling basis. A cycle consisted of eight hours at 600°F followed by 16 hours at 75°F. Atmospheric pressure was maintained throughout the test.

Examination of the coils by sectioning indicated the presence of radial cracks in the pyroceram, each crack terminating or originating at the surface of a copper wire. Internal presence of mercury in the coil was attributed to leakage through the cracks generated either during the coil processing or during the cyclic temperature exposure test. Further work will consist of investigating processing methods and potting configurations to accommodate the differential expansion coefficients of the glass and copper coils.

Two pyroceram glass coils (impregnated and coated) were subjected to resistance cycling tests in air. This consisted of temperature cycling at a frequency of one cycle per hour for 100 cycles. The amplitude was 600°F for one-half hour to 75°F for one-half hour. Resistance measurements were taken at a maximum and minimum temperature every half hour. No deterioration in resistance was noted.

Voltage breakdown tests were conducted using steel plates (2 x 2 x 0.05 inches) coated with glass and pyroceram finish of various coating thicknesses. Tests were conducted at 75°F and 600°F. A hi-pot was used to apply the voltage potential which was maintained for one minute. These data are being evaluated.

Copper coils coated with 100 per cent silicone solids with varying amounts of zirconium orthosilicate filler have been fabricated and tested in the autoclave for compatibility with mercury. The specimens have been subjected to cracking. Further investigation of potting and curing techniques is being continued.

Discs of Supramica 555 and 560 are currently being exposed to both liquid and vapor mercury at 600°F in the one-liter autoclave. Permeability and compatibility with mercury will be checked by dimensional and weight changes.

6. Turbine

Operational and data evaluation assistance was provided by the Turbine Group for testing TATP-I and II. TATP-I operated successfully for a total of 28 hours on mercury vapor and 8-1/2 hours on nitrogen. Disassembly and inspection of the TATP-I turbine parts revealed a possible erosion problem. Damage was observed on the exit surfaces of both interstage nozzle assemblies and on the leading edges of the second stage rotar blades. Since the turbine was operated at other than design conditions, with mercury vapor for all but 8 3/4 hours of the total time, an accurate conclusion of the severity of this problem could not be established.

TATP-II was installed in the breadboard rig and operated a total of 23 hours and 9 minutes on mercury vapor, 20 hours and 32 minutes of which were at 40,000. The major objective was to evaluate turbine performance and determine turbine efficiency. Breadboard rig limitations made it difficult to obtain good spindown data during initial testing. Installation of a modified high temperature valve in close proximity to the turbine nozzle and the elimination of a long instrument line from the turbine nozzle to a pressure transducer reduced the system capacitance so that good full- and no-load speed decay curves at the design point were finally achieved. In addition, tests of TATP-II indicated that the performance of the alternator when installed in the package agreed closely with its test rig calibration performance.

By using the two techniques of speed decay and steady state power output, it was found that the turbine produced a shaft power of 512 watts average at 40,000 rpm. The brake turbine efficiency was calculated to be 33 per cent. This value is probably low because an accurate means of determining the decay of the turbine inlet pressure did not exist and it is probably that some energy existed at the turbine nozzle during spindown. Turbine efficiency was not expected to approach the 40 per cent specification value because of the excessive heat and seal losses in the TATP. It is the general conclusion that the results obtained have verified the applicability of the turbine design procedures and the mercury vapor performance predictions.

An IBM optimization study of the SPTP turbine has been completed and with assumed heat losses an overall turbine efficiency of 45 per cent is indicated. The turbine will include the following: all wheels will have pitch diameters of 1.85 inches, the first stage rotor will contain supersonic blading, and the third stage will have partial reaction. The remainder of the turbine will be similar to the TATP turbine. The 45 efficiency will include: estimated heat, collector, seal (both interstage and end seals), and turbine windage losses. The first two stages will employ straight back subsonic converging nozzles. Design of the SPTP turbine has been initiated.

Preliminary analysis was performed on the SPTP package heat transfer study and initial results were incorporated in the SPTP turbine optimization study. This is currently being refined. Some of the major areas to be studied are: turbine nozzle heat losses; turbine exterior insulation requirement; and determination of the heat lost to the bearing fluid.

7. Pump

Performance tests were completed on the Edwards screw-type pump. The performance attained was inferior to that attained with the jet-centrifugal pump.

A pump system for installation in the free running bearing rig was designed. Fabrication of the system has begun and machined pump parts have been inspected and approved.

A test was conducted which simulated the pump-bearing seal configuration. Pump back-face pressure was found to be approximately as calculated. An evident loss of pump output was noted when seal leakage was introduced. However, because of shaft runout and the test pieces not being square, it was not possible to accurately evaluate this loss. A further evaluation of this problem will be made when the pump configuration for the SPTP is tested.

The pump test rig was modified to permit vacuum starts and accurate power measurements. To permit vacuum starts, a vacuum was pulled on the pump drains and one of the test pumps was used to transfer drain flow to the main reservoir. To permit more accurate power measurements, a dynamometer was designed, fabricated and tested and later modified to balance the effects of pump radial thrust.

Two basic impeller types have been designed and fabricated for testing in the pump test rig. The configurations are adaptable to either breadboard testing or testing in the free running bearing rig.

The design of a screw seal to prevent the leakage of bearing lubricant into the pump was completed.

A redesign of the jet pump was made to enable it to accept full pump discharge pressure rather than regulator discharge pressure.

Assistance in the design of the test pump installation was provided the Systems Test Group as required.

8. Control and Start-up System

Development of control system components was continued. The prototype pressure regulator was tested statically and dynamically, and proved to have a satisfactory response time and pressure modulation range.

Since the control may be required to operate over a range of temperatures, the electronic equipment must be designed to be relatively unaffected by temperature change. A frequency discriminator has been tested from -25 to +100°C with a null shift of only 1.5 cps. Curve A in Fig. 29 demonstrates the temperature stability of this particular design. The resistance of the torque motor increases slightly with temperature but not sufficiently to cause a deterioration of control system performance.

Consideration has been given to start-stop systems and three methods were found to be practical.

Early concepts of the systems test enclosure included provisions for utilizing any of the three methods. The change in program scope, required that only one method be incorporated into the STE. A typical check valve required by the start-stop system is shown in Fig. 30, and a diverter valve which will not be required by the STE, due to concept change, is shown in Fig. 31. This valve would permit a rapid turbine shutdown to be achieved if a small volume pressurizing accumulator is used. The design will be retained for later use, if required.

A refined analysis of the complete system taking into account system thermodynamics and inventory was affected. Emphasis was placed on boiler and condenser operations. A mathematical model of the system incorporating latest information and test data was prepared. A computer study based on this is being programmed.

9. Alternator

Two radial gap alternator designs were evaluated, the open slot stator and the closed slot stator. The results of the tests and analyses show the open slot design to be the more feasible because of the high distortion and regulation inherent in closed slot designs. Sealing considerations which make the use of the closed slot design advantageous have been minimized. This was done by reducing the sealing problems encountered on the open slot unit to the extent that only a few minor trouble areas exist. The test results on sample coils sealed with pyroceram show the seal is effective and the material is compatible with mercury. Another sealing method, the use of a thin ceramic sleeve between rotor and stator is being considered and a unit is being fabricated to evaluate this method.

A detailed stress analysis of the rotor design was made and results indicate that no serious stress problems exist. Tests to check rotor strength at operating temperature have been undertaken.

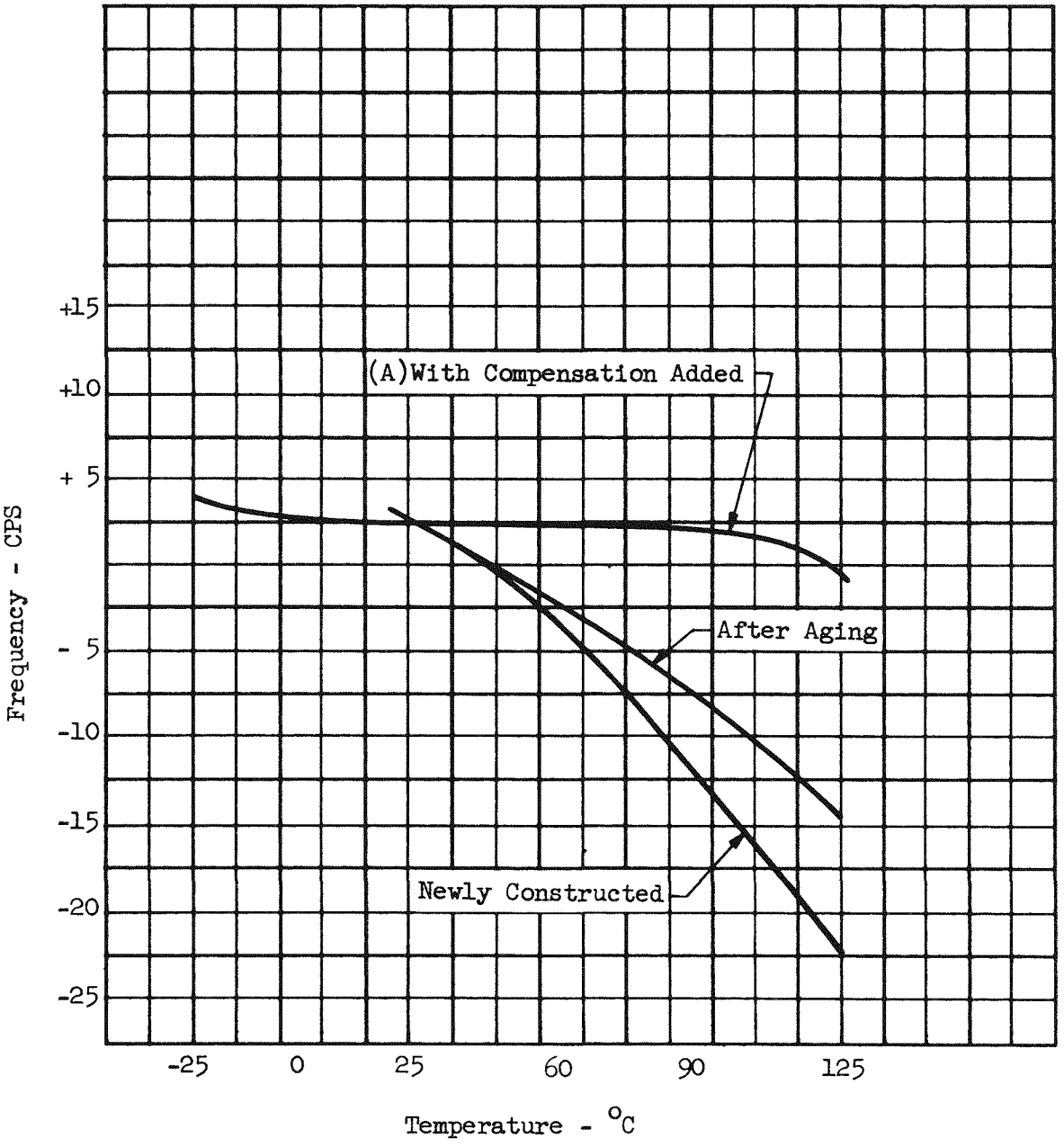

Fig. 29. Null Shift versus Temperature

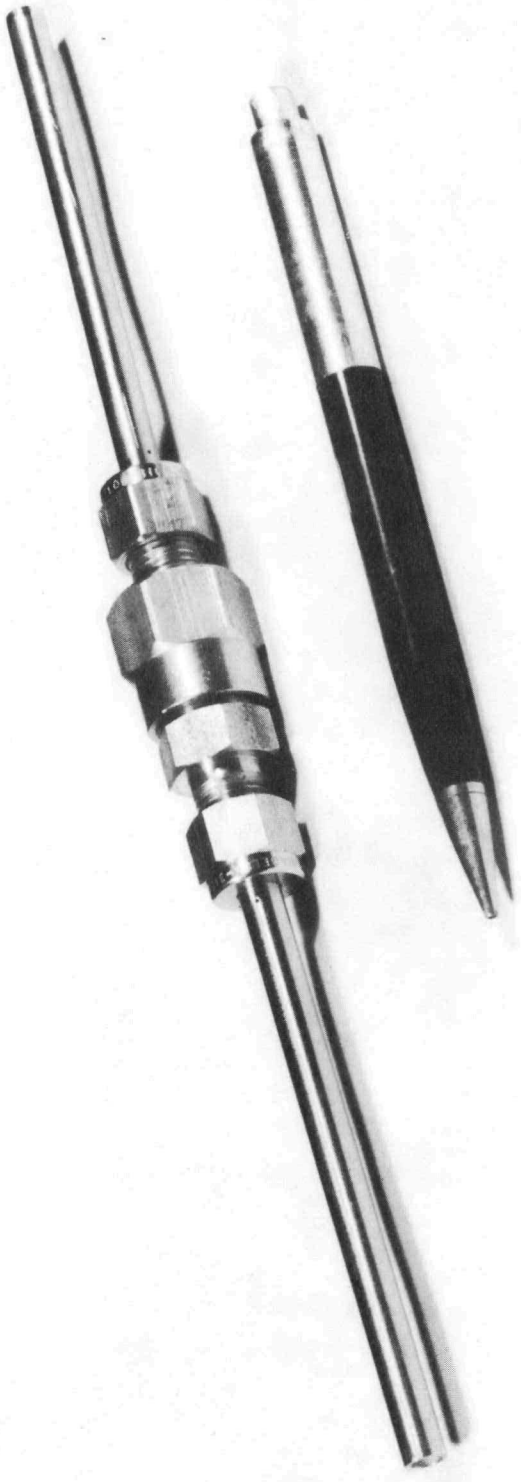

Fig. 30. Check Valve

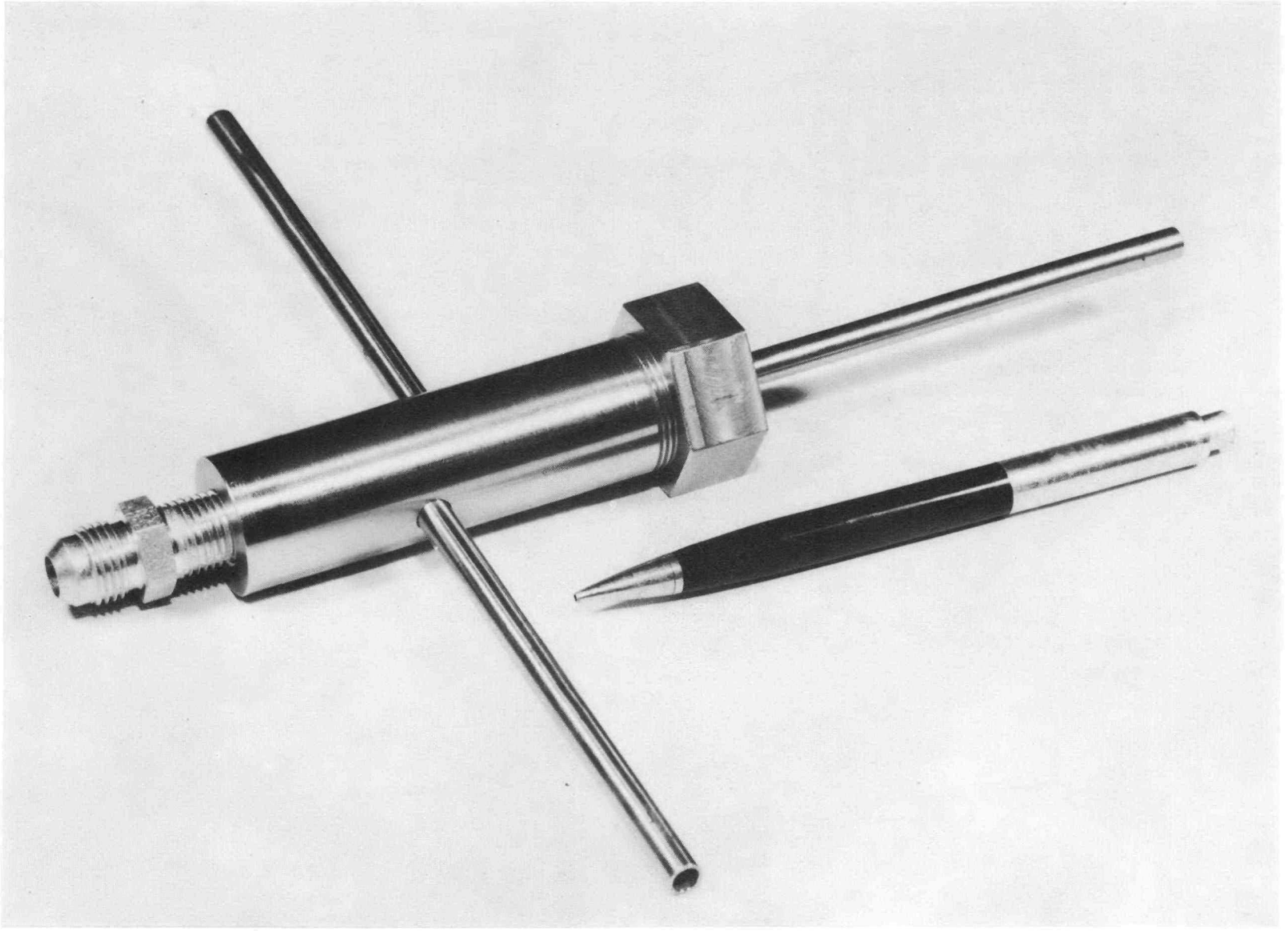

Fig. 31. Diverter Valve

The prime development objective during this period was to design and construct a unit capable of operating in a 550°F ambient without external coolant. The results of the development effort show the objective is feasible.

Five alternator development units were fabricated. They were variations of the radial gap permanent magnet design.

The two designs, open-slot and closed slot, were tested for voltage regulation, distortion, short and open circuit, and stability at several air gap dimensions. These results are tabulated in Table 11.

The motor start-up test rig was designed and many of the parts have been fabricated. The variable frequency supply contains a specially wound stator driven by a high speed universal motor. Several tests on a breadboard of the variable frequency supply show that the start-up technique is feasible.

The fabrication of the motor start-up facility parts has been partially completed.

Two TATP alternators, TATP-II and a spare, were fabricated and spot tested.

Detail drafting for the SPTP alternator was completed.

The dynamometer was designed and the ordering of parts completed. As a result of procurement delays, this part of the program is approximately six weeks behind schedule.

The fabrication of dynamometer parts has been started and some of the parts have been completed.

10. Bearing Design and Development

In July, effort was concentrated on evaluating the performance of the hydrosphere bearings in TATP-I and similar bearings in TATP-I and similar bearings which were tested in the free running rig. The bearings operated satisfactorily for more than 26 hours at speeds up to 48,000 rpm when supplied with 330° mercury. The bearings used consisted of a flame-plated tungsten carbide surfaced ball and a blue chip socket.

Tests of similar bearings in the free running bearing rig were conducted with axial loads to 20 pounds and radial loads to five pounds at 40,000 rpm. However, a failure occurred which indicated a possible ball growth due to mercury attack of the bond between the plate and parent metal. During testing, water from a manometer was introduced into the system, causing rusting of the bearings which resulted in increased power consumption. These incidents indicate disadvantages connected with the use of plated-bearing surfaces and blue chip steel for bearing construction.

A bearing with an extended shaft was fabricated for test early in the quarter. However, during installation a crack in the socket at the pump seal was discovered. New parts have been fabricated and extended shaft testing will start. The principles of extended shaft bearing operation will also be demonstrated in the testing of preliminary prototype.

TABLE 11

Radial Gap Alternator Voltage
Regulation and Distortion
For Air Gaps of 0.011 to 0.018 Inch

Alternator	Regulation		Distortion	
	Power Factor			
Open Slot	Unit (per cent)	0.8 (per cent)	No Load (per cent)	Rated Load (per cent)
4 Turns/Coil	7.5	24	1.3	5.5
5 Turns/Coil	10.	35	1.3	6.2
Closed Slot				
4 Turns/Coil	13.9	47.0	3.5	17.5
After Capacitor Compensation	1.0	2.0	-	16.1
Specified Limit		25.		7.

This testing confirmed the fact that one-half inch hydrosphere bearings can support a radial load of 25 pounds at speeds up to 50,000 rpm. Testing also indicated that no reduction in the radial load carrying capacity occurs as a result of increasing the bearing socket inlet diameter. It is estimated that bearing power consumption will decrease as bearing socket inlet diameter increases.

Analysis of TATP-II spindown data substantiated the bearing test rig data. Bearing power losses of approximately 100-120 watts were noted. Analysis of rotating shaft capillaries indicates that they will probably be more sensitive to clearance changes between ball and socket than fixed capillaries. Tests will be required to establish the actual degree of sensitivity.

Preliminary testing was conducted which indicated that it may be possible to accelerate the bearings to design speed without damage when no mercury pressurization is applied prior to start. This capability would greatly reduce the complexity of the proposed system start-stop technique. It will be studied further.

A photoelastic analysis was performed to optimize socket configuration. By extending the equator of the socket 1/32 of an inch, the Hertz contact pressures should be reduced by at least 45 per cent of the present value. The results of this study will be employed in future bearing design.

A materials anti-score capability program was initiated for the purpose of increasing bearing overload capability and also providing greater assurance of achieving an unpressurized start capability. Materials were selected and procurement was initiated. Two of the selected materials, boron carbide and silicon carbide, are unavailable and substitution materials will be selected. Testing has not begun because materials were not available, but it is expected they will be completed by the end of November.

A mercury lubricated journal bearing was analyzed, designed and tested. The test parts consisted of two one-half inch diameter by one-half long bearings. Tests were run to 34,000 rpm with zero radial load. Thrust bearing instability prevented test completion.

Power losses were 150 per cent that of the present hydrosphere. This value was not considered unreasonable because no attempt was made to optimize the design. Work on journal bearings will be discontinued due to program funding limitations.

A Gishold high speed balancing machine which is capable of balancing rotating assemblies on the hydrosphere bearings was put in operation. Balancing accuracy has been improved.

Substantial effort was concentrated on completing the design of a dual bearing test rig and automating the free running rig for endurance testing. Change of program concept has caused termination of this effort. All items procured for these rigs will be used where ever possible to supplement other work in the bearing program or other component areas.

11. Condenser and Subcooler

Fabrication of the quarter scale flat plate test condenser was completed, and tested in the breadboard test rig. Test data are being analyzed, and a report covering data reduction, calculation of results, and accuracy analysis will be issued.

Several results of extreme importance have been ascertained from the data obtained. A maximum pressure drop of 0.2 psi across the condenser was noted, and no substantial pressure fluctuations occurred. Also, the simulated radiation heat transfer coefficient on the outside of the condenser controlled the heat transfer. This indicates that the condensing coefficient is high enough to be virtually insignificant.

The condenser test amplified another important point, the need for absolute system leak tightness. Non-condensibles collecting in the test condenser lowered the partial pressure of mercury, giving a lower condensing temperature than that which corresponds to the condenser total pressure.

Detail design of the compact air-cooled condenser was completed during the reporting period. Figure 32 is a photograph of the condenser-subcooler unit without air ducts.

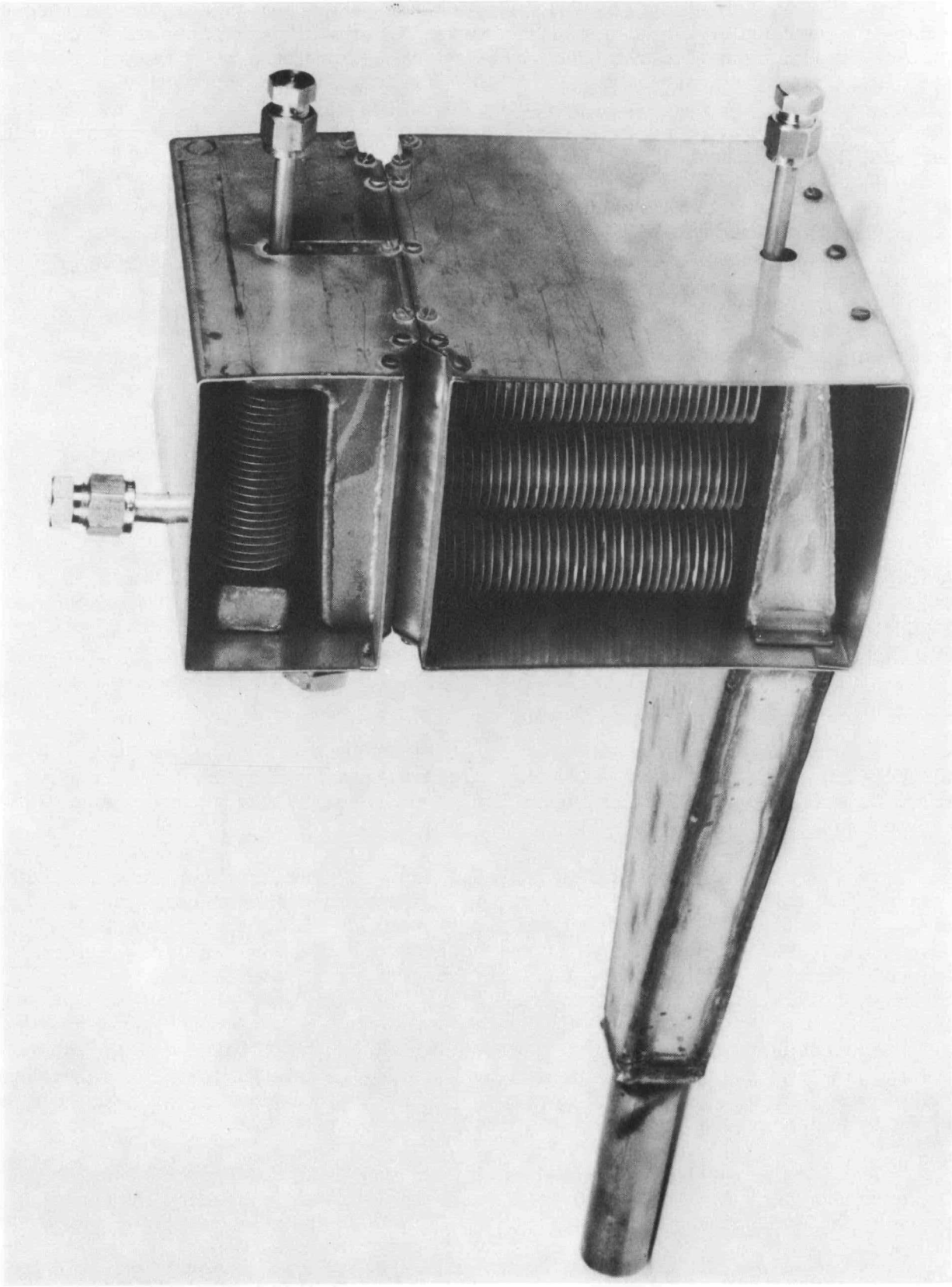

Fig. 32. Compact Air-Cooled Condenser

Steam tests for the air-cooled compact condenser are scheduled prior to mercury vapor tests. The purpose of the steam tests will be to aid in location of instrumentation and to determine any weaknesses in test procedure.

A steam condenser rig which will be used to investigate vapor-liquid interface instabilities has been partially fabricated. Completion of this rig is being held up by several parts which were not delivered.

Preliminary design for a prototype condenser internal geometry has been completed. The geometry incorporates flat plates with spacing dimensions in the capillary range, and depends on the assumption that the condensate film is insensitive to body forces for Reynolds numbers below one. A condenser test rig will be built in the near future to evaluate prototype condenser core designs. Small scale sections will be tested in this rig.

[redacted]

B. SHIELDING

1. Shielding of Test Cell

Several hypothetical cases were investigated to check out the test cell under different situations. One was to find the dose rates at several points around the edge of the pit, assuming it was filled with water to shield the boilers. This situation would be considered only as a last resort and would occur only if the biological shield were not filled with mercury. Should this situation occur, the boilers would have to be disassembled, packed into shielded casks and returned to ORNL for disposal. Flooding the pit would provide shielding and a means of cooling the boilers while they were being disassembled. Calculations indicated a maximum dose rate of six mr/hr at points above the test cell when the cover was removed.

Calculations were made to show dose rates to be expected during ground testing, at a ground test facility similar to a hot cell. For the purpose of calculation the inside dimensions used were the same as those of the pit at the Martin Critical Experiment Facility. This is an area 8 by 12 feet high with ordinary concrete walls five feet thick. A water tank some nine feet deep was proposed as a cover for this pit.

Calculations showed that with two unshielded boilers containing 5×10^5 curies each positioned in the pit, a maximum dose rate of 12 mr/hr occurred in the adjacent control room. Nine feet of water reduced the dose rates directly above the tank to 29 mr/hr. The tank, however, proved unacceptable as a cover because of the excessive dose rates around the bottom edges. To enlarge the tank to overcome this leakage would make it too large and unwieldy, and any flexibility would be lost. For purposes of safety, the thicknesses of the test cell walls of a test facility were increased to six feet of ordinary concrete or three feet of ferrophosphorus concrete.

Figures 33 and 34 are preliminary designs of the proposed test facility. The water cover tank shown in Fig. 34 will be replaced by a ferrophosphorus reinforced concrete cover. The steel work frame shown above the test pit will support a ten-ton crane intended for lifting the components into the test pit. Provisions for slave parts, L-camera parts and a viewing window are also shown on Fig. 34. An instrument shed for housing radiation spectrum equipment is shown located approximately 100 feet from the test pit.

2. Shielding of Transportation Skid

A skid is being designed to transport two assembled boilers and the associated power conversion equipment. Dose rates at various distances from this skid have been calculated.

An extreme case of exposure to radiation during transportation would occur if all the mercury were to leak from the biological shield. The possibility of an occurrence of this kind is remote since provisions to prevent this are included in the design of the skid.

Dose rates at various radii from a power unit assembly which has lost all its biological shield mercury are given in Table 12. The locations of the points at which the dose rates were determined are shown in Fig. 34.

As can be seen from this Table the dose rates close to the source are excessive.

Dose rates for the case in which the biological shields are filled with mercury are given in Table 13. Locations of the dose points are as shown in Fig. 35.

It should be noted that relatively close to the sources, the dose rate depends upon the position of the dose point with respect to the sources. The dose rates at some points are four to five times higher than for other positions. The difference between dose rates becomes less as the distance from the sources becomes greater.

C. TRANSPORTATION COOLING OF THE APU

Calculations were made on cooling of the APU during transport by means of natural and forced circulation of the working fluid through the boiler coil. Pressure drops through the coil in both cases precluded these methods.

Natural circulation of the biological shield mercury is one possibility which was not investigated analytically because of the inherent complexity of the biological shield. Due to its foolproof nature, this method of cooling is attractive and will be investigated in the half-power boiler testing program.

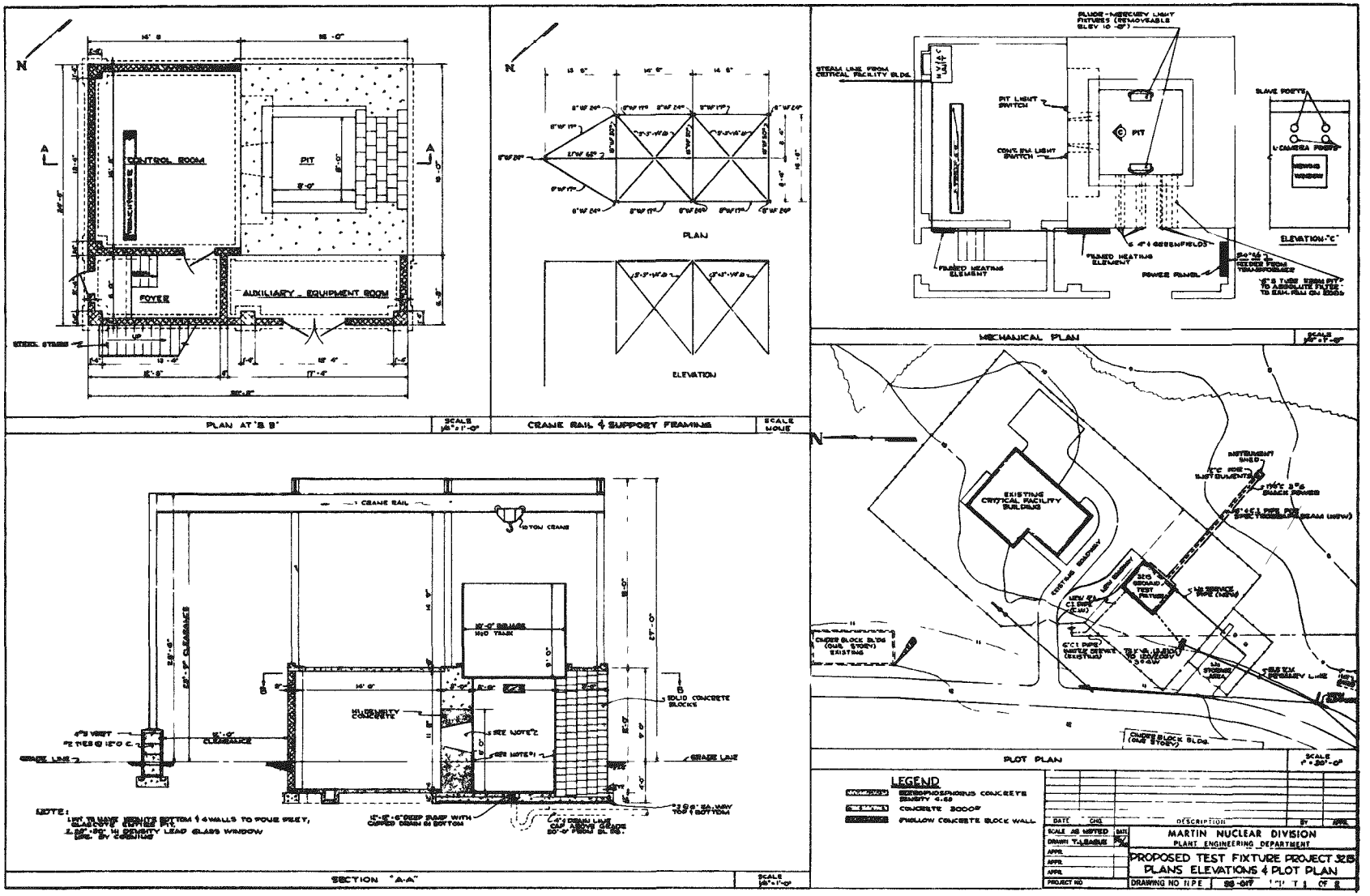

Fig. 33. Proposed Test Fixture - Plans Elevation and Plot Plan

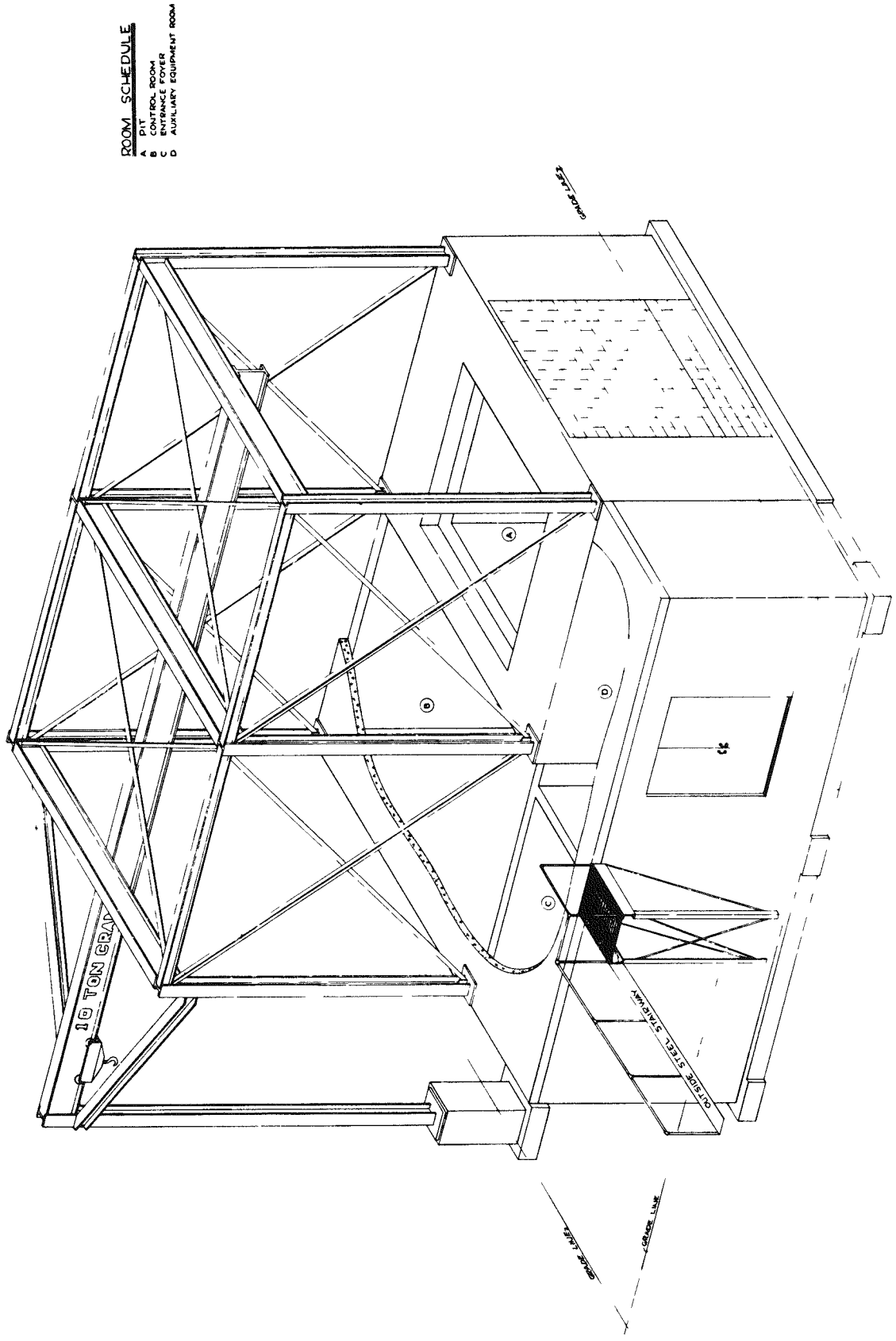

Fig. 34. Proposed Test Fixture - Isometric View

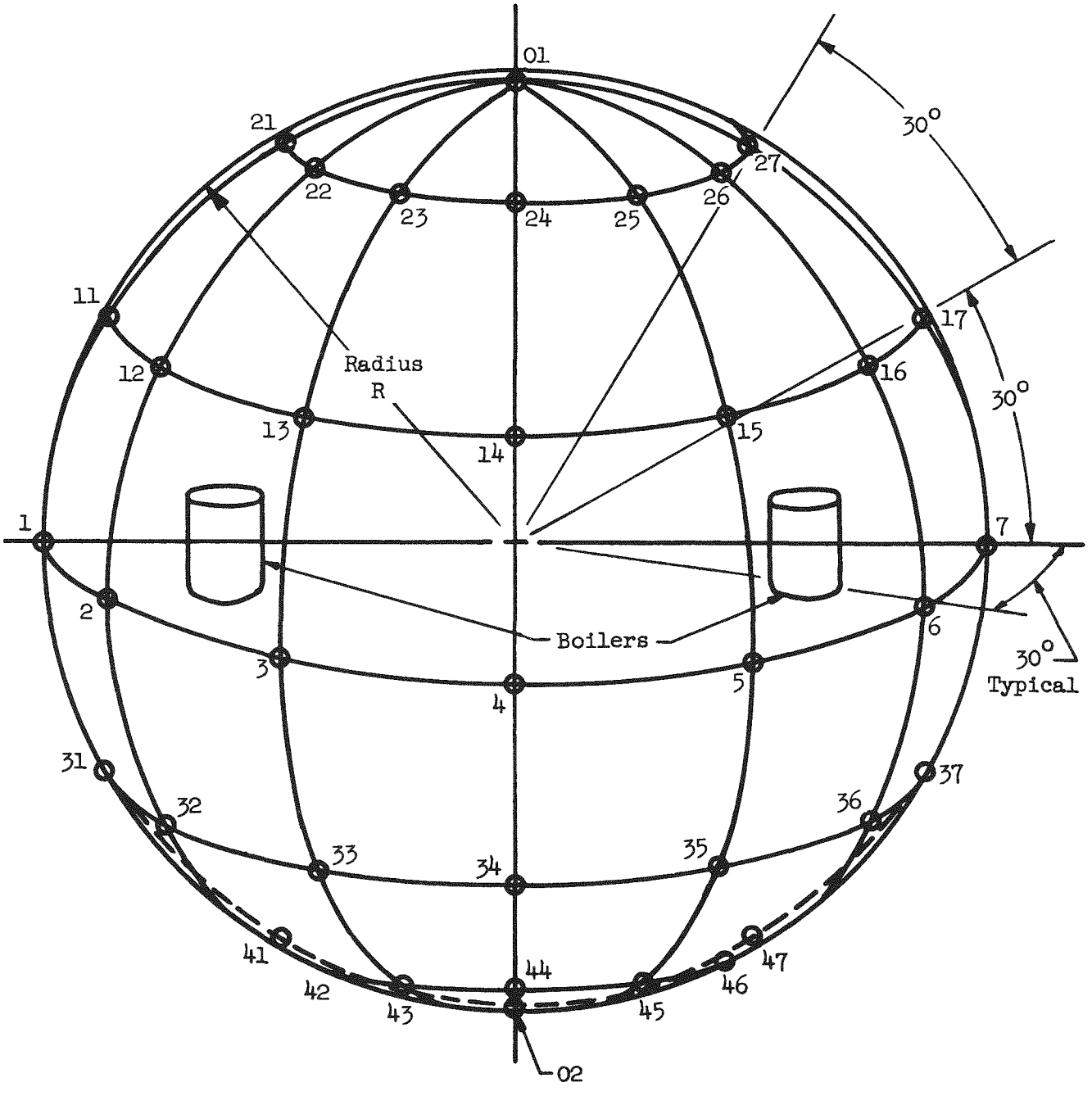

Fig. 35. Location of Dose Points in Space Surrounding Transportation Skid

TABLE 12

Dose Rates Without Mercury in Biological Shield

Radius	Feet 3	5	10	20	40
Point No.	Dose Rates (Roentgens/Hour)				
01	9930	4420	1270	326	80.6
02	8010	3410	983	253	62.6
1	85500	12200	2170	493	118.6
2	40700	10200	2090	489	118.3
3	19800	7710	1990	480	117.8
4	15700	6860	1880	476	117.5
5	19800	7710	1940	480	117.8
6	40700	10200	2090	489	118.3
7	85500	12200	2170	493	118.6
11	27400	7480	1650	396	96.4
12	19900	6860	1620	394	96.3
13	15000	6010	1560	391	96.1
14	13400	5680	1530	389	95.9
15	15000	6010	1560	391	96.1
16	19900	6860	1620	394	96.3
17	27400	7480	1650	396	96.4
21	14300	5400	1260	308	75.9
22	12600	5030	1230	307	75.1
23	11000	4560	1210	305	75.0
24	10500	4440	1200	304	76.0
25	11000	4560	1210	305	75.0
26	12600	5030	1230	307	75.1
27	14300	5400	1260	308	75.9
31	21700	6730	1580	384	86.9
32	17700	6410	1560	383	89.0
33	14600	5830	1520	380	104.7
34	13200	5560	1500	379	109.4
35	14600	5830	1520	380	104.7
36	17700	6410	1560	383	89.0
37	21700	6730	1580	384	86.9
41	11600	4380	1020	250	61.3
42	10300	4100	1010	250	62.1
43	9330	3770	988	249	60.2
44	9180	3690	985	249	61.2
45	9330	3770	988	249	60.2
46	10300	4100	1010	250	62.1
47	11600	4380	1020	250	61.3

Calculations made for each boiler containing 5×10^5 curies assuming all mercury drained from biological shield.

See Fig. 35 for location of points.

TABLE 13

Dose Rates with Mercury In Biological Shield

Radius	Feet 3	5	10
Point No.	Doses Rates (Roentgens/Hour)		
01	0.029	0.0096	0.00214
02	0.030	0.0099	0.00214
1	0.143	0.0231	0.0042
2	0.072	0.0194	0.0041
3	0.037	0.0148	0.0038
4	0.030	0.0132	0.0037
5	0.037	0.0148	0.0038
6	0.072	0.0194	0.0041
7	0.143	0.0231	0.0042
11	0.067	0.0230	0.0048
12	0.066	0.0208	0.0047
13	0.042	0.0173	0.0045
14	0.035	0.0157	0.0044
15	0.042	0.0173	0.0045
16	0.066	0.0208	0.0047
17	0.067	0.0230	0.0048
21	0.028	0.0113	0.0032
22	0.031	0.0121	0.0033
23	0.034	0.0132	0.0033
24	0.035	0.0135	0.0033
25	0.034	0.0132	0.0033
26	0.031	0.0121	0.0033
27	0.028	0.0113	0.0032
31	0.067	0.0222	0.0045
32	0.064	0.0203	0.0044
33	0.039	0.0157	0.0031
34	0.031	0.0144	0.0040
35	0.039	0.0157	0.0031
36	0.064	0.0203	0.0044
37	0.067	0.0222	0.0045
41	0.027	0.0111	0.0033
42	0.030	0.0119	0.0034
43	0.035	0.0132	0.0035
44	0.034	0.0146	0.0036
45	0.035	0.0132	0.0035
46	0.030	0.0119	0.0034
47	0.027	0.0111	0.0033

Calculations made for each boiler containing 5×10^5 curies assuming biological shields filled with mercury.

See Fig. 35 for location of points.

VII. TASK VII - SNAP-III

A. SYSTEM ANALYSIS

As a result of the low material efficiencies achieved by Westinghouse Corporation during the last quarter, The Martin Company has arranged for the purchase of a thermoelectric generator with a minimum efficiency of five per cent under space conditions, from another source.

Constant power and voltage outputs are generally desirable in secondary power systems. In order to achieve this with radioisotope fueled units, it is necessary to discard heat early in life (see Appendix B). The SNAP-I technique has been described and that for SNAP-III is in this report. A completely static heat dump would be compatable with the inherent reliability of the static auxiliary power system of radioisotope heat source and thermoelectric conversion. To achieve this end, materials whose thermal conductivity varies inversely with temperature have been investigated. Figure 36 shows this variation for two promising materials, BeO and Thermistor 735. The temperature range of measurements will be extended during the next period.

The effect of incident solar energy on the heat-dissipating radiator of a SNAP-III type of device and in an earth satellite application has been investigated. The following assumptions were made in the calculations:

1. Circular orbit;
2. Emissivity in infra-red - 0.8;
3. Absorptivity of solar energy - 0.4;
4. Uniform emitting cylinder;
5. No tumbling (worst condition).

In order to find the maximum temperature of the radiator, it was necessary to determine the orbit which gives rise to the maximum incident energy from the sun and the earth's albido. After this had been done by a digital computer program, parametric studies were performed on emissivities and absorptivities of the radiator and the altitude of the orbit. Figure 37 shows the variation in radiator temperature depending on heat generating rate for two altitudes and two sets of emission and absorption constants. A change in the direction of the axis of the cylinder produces no significant changes in the radiator temperature. As can be seen from this Figure, the variation in temperature is small for the range of SNAP-III heat generation - 500 BTU/hr/ft of radiator.

To assist in determining the shielding requirements for polonium-fueled heat sources, Fig. 38 was prepared. This gives the dose rates per watt from an unshielded source at distances up to six feet from a point source and attenuation factors for iron, molybdenum, tungsten and uranium shields.

To use this, the dose rate at the required distance from an unshielded source is read, and multiplied by the power level in watts. This product is then divided into the required dose rate to find the attenuation factor. The thickness of shield corresponding to the attenuation factor is then read.

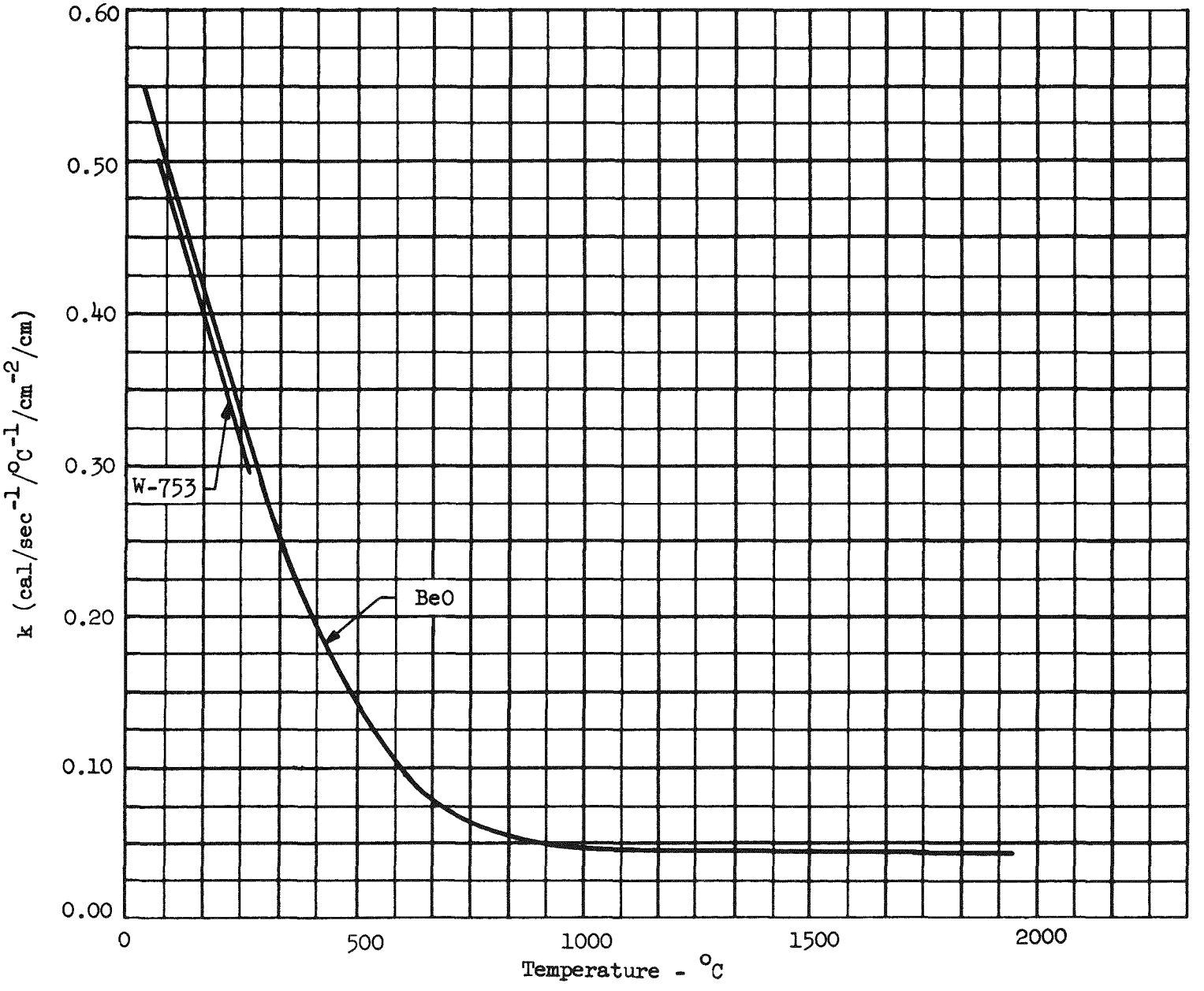

Fig. 36. Thermal Conductivity of BeO and Thermistor W-753

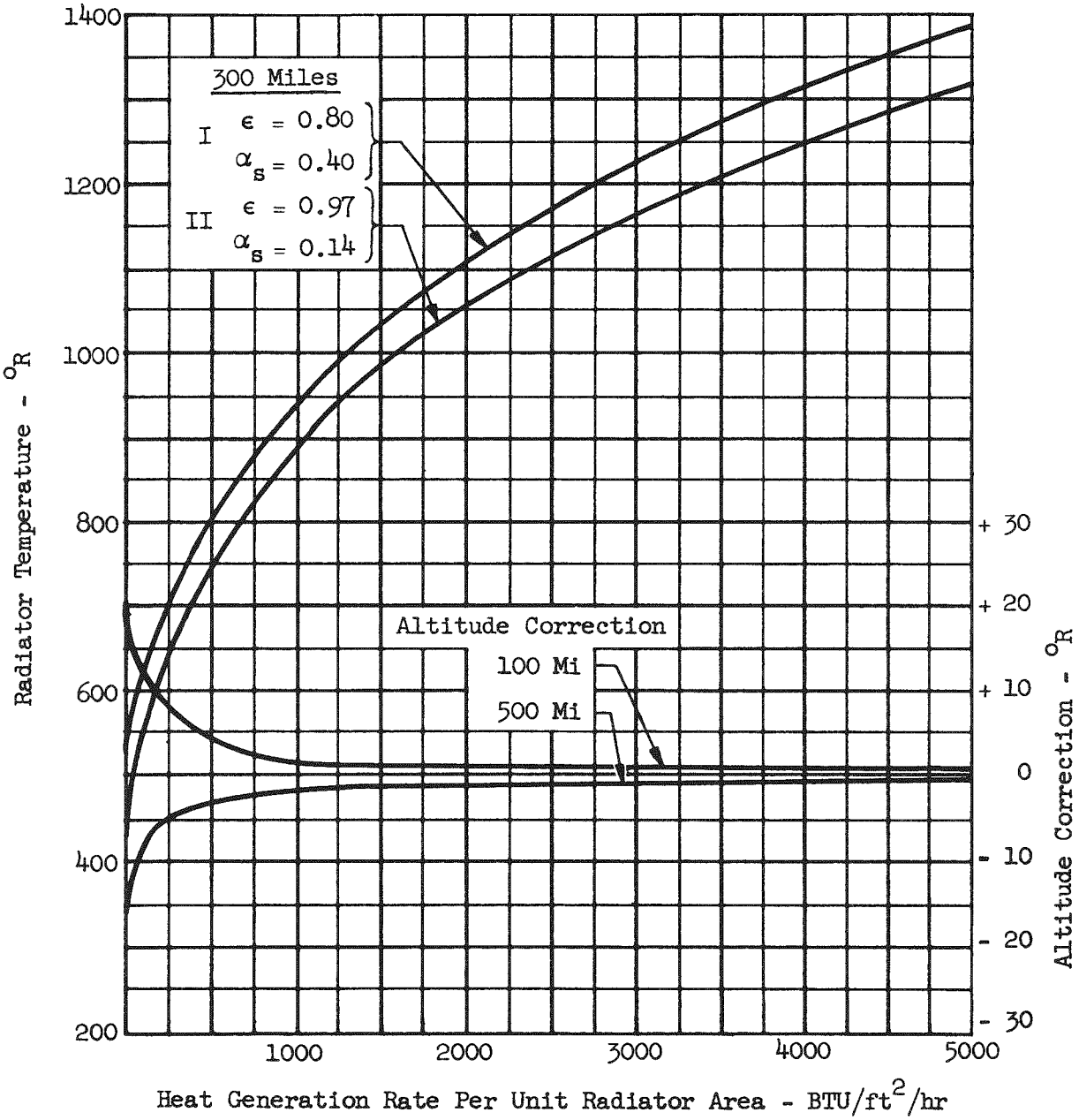

Fig. 37. Radiator Temperature at Most Critical Point in Orbit

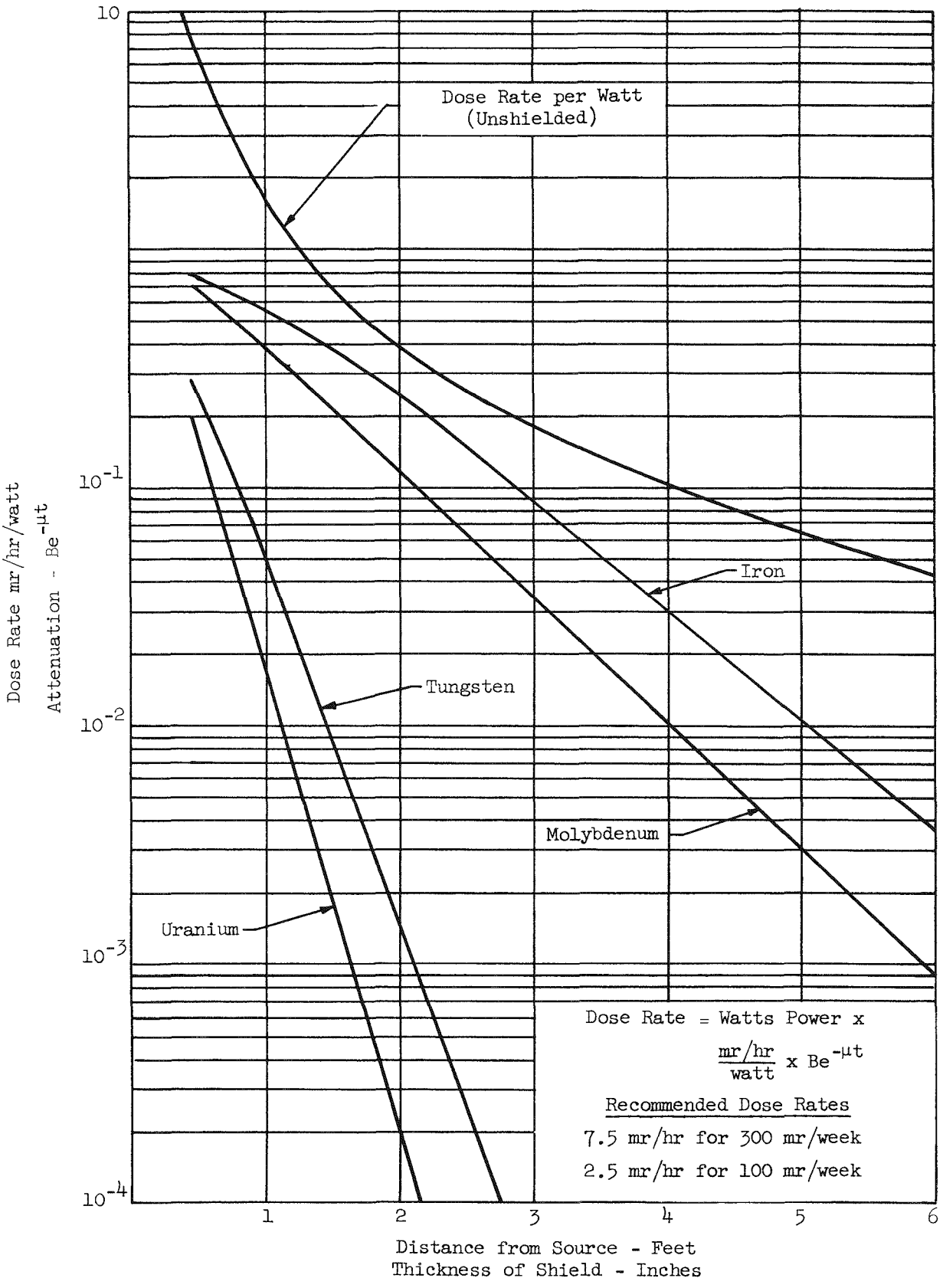

Fig. 38. First Approximation to Dose Rates versus Distance per Watt and Attenuation versus Material Thickness for Po^{210}

B. FUEL ELEMENT DEVELOPMENT

The last report described the results of investigation and tests on various types of compound oxidation resistant and electrical insulation coatings. The flame-sprayed Rokide aluminum oxide coating showed greatest promise, and work in this quarter centered on developing the techniques of application and further testing.

The flame sprayed Rokide alumina coatings were subjected to various tests during this period to determine:

1. Fabricability;
2. Machinability;
3. Stability of coating during extended exposure to elevated temperatures and inert atmosphere;
4. Stability of coating when in contact with the thermoelectric element during long-term exposure to elevated temperatures and inert atmospheres.

The following test results were noted:

1. Rokide alumina coating may be applied with relative ease on cylindrical specimens by rotating the piece in either a horizontal or vertical plane. Coatings deposited show good uniformity and adherence;
2. Cylindrical specimens with Rokide alumina coating may be ground by a centerless grinding operation to a close tolerance (approximately ± 0001 inch);
3. A coated rod, when exposed to argon atmosphere at 800°C (~ 1500°F) for one week, showed no change in color, adherence, and electrical insulating properties;
4. A coated plate, in contact with an indium-arsenic thermoelectric element at 700°C (~ 1300°F) for one week in hydrogen, showed no reaction or reduction appeared to place at the area of contact.

Additional testing of the coating stability against other thermoelectric materials is underway. The thermoelectric materials, ZnSb and InSb, are to be evaluated for stability with the Rokide alumina.

A small prototype of the SNAP-III element was fabricated. A molybdenum tube six inches long with a one inch outside diameter and a 0.545 inch inside diameter was made and stainless steel slugs (0.500 inch diameter by 0.500 inch long) were prepared to simulate fuel pellets. The molybdenum rod was coated with an oxidation resistant Colmonoy No. 5 coating and after grinding and sandblasting a Rokide alumina coating was applied. The alumina coating was then centerless ground to dimension. The stainless steel slugs were loaded into the molybdenum tube with a lead heat transfer medium and the threaded molybdenum end plug was brazed to completely seal the fuel and liquid metal in the tube. An oxidation protective coating was then applied to the plug end of the tube to complete the unit.

Figure 39 shows an enlarged section (100 X) of the molybdenum tube with the oxidation resistant and the Rokide alumina coating.

C. GENERATOR DESIGN

During this quarter the excess heat dump technique has been developed and the thermoelectric generator has been redesigned as a new thermoelectric material is available.

1. Thermoelectric Generator

The newly available thermoelectric material is germanium telluride. Its parameters are listed in Table 14.

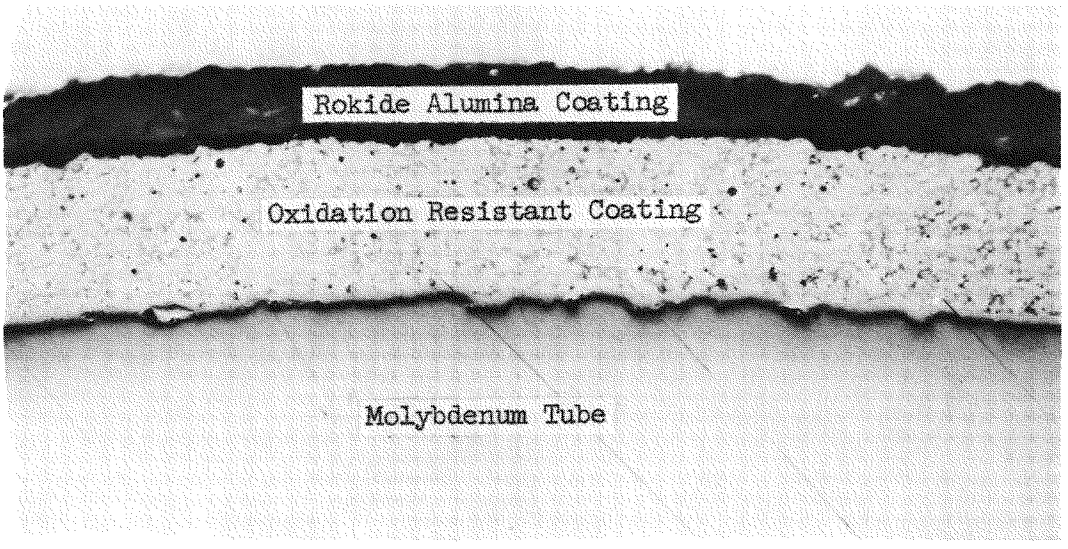

Fig. 39. Molybdenum Rod Coated with Colmonoy No. 5 plus Rokide "A"

TABLE 14

Parameters of InAs (Leg No. 1)

$T^{\circ}C$	$T^{\circ}K$	Ohm Cm ρ	Watts/Cm $^{\circ}C$ k	μ v/$^{\circ}C$ α
650	923	5.3×10^{-4}	8.0×10^{-2}	-140
550	823	6.2×10^{-4}	8.5×10^{-2}	-160
450	723	7.2×10^{-4}	1×10^{-1}	-170
350	623	7.8×10^{-4}	1.2×10^{-1}	-160

When coupled with indium arsenide, whose parameters are listed in Table 15, material efficiencies of three per cent can be achieved at a hot junction temperature of 650°C and a cold junction of 350°C. Figure 40 shows the variation of the index of efficiency, Mw, of the couple as a function of temperature where,

$$Mw = \frac{T}{4} \frac{(\alpha_1 - \alpha_2)^2}{(\sqrt{\rho_1 K_1} + \sqrt{\rho_2 K_2})^2}$$

From this Σ_{tc}, the thermoelectric efficiency is calculated by means of the formula:

$$\Sigma_{tc} = \frac{\sqrt{1 + 2\,Mw \left(\frac{T_h + T_c}{T_h}\right)} - 1}{\sqrt{1 + 2\,Mw \left(\frac{T_h + T_c}{T_h}\right)} + \frac{T_c}{T_h}}$$

The overall efficiency, Σ, is plotted in Fig. 41 as a function of ΔT, assuming a hot junction, T_h, of 650°C.

$$\Sigma = \Sigma_{tc}\, \Sigma_c$$

where Σ_c is the Carnot efficiency;

$$\Sigma_c = \frac{\Delta T}{T_h}$$

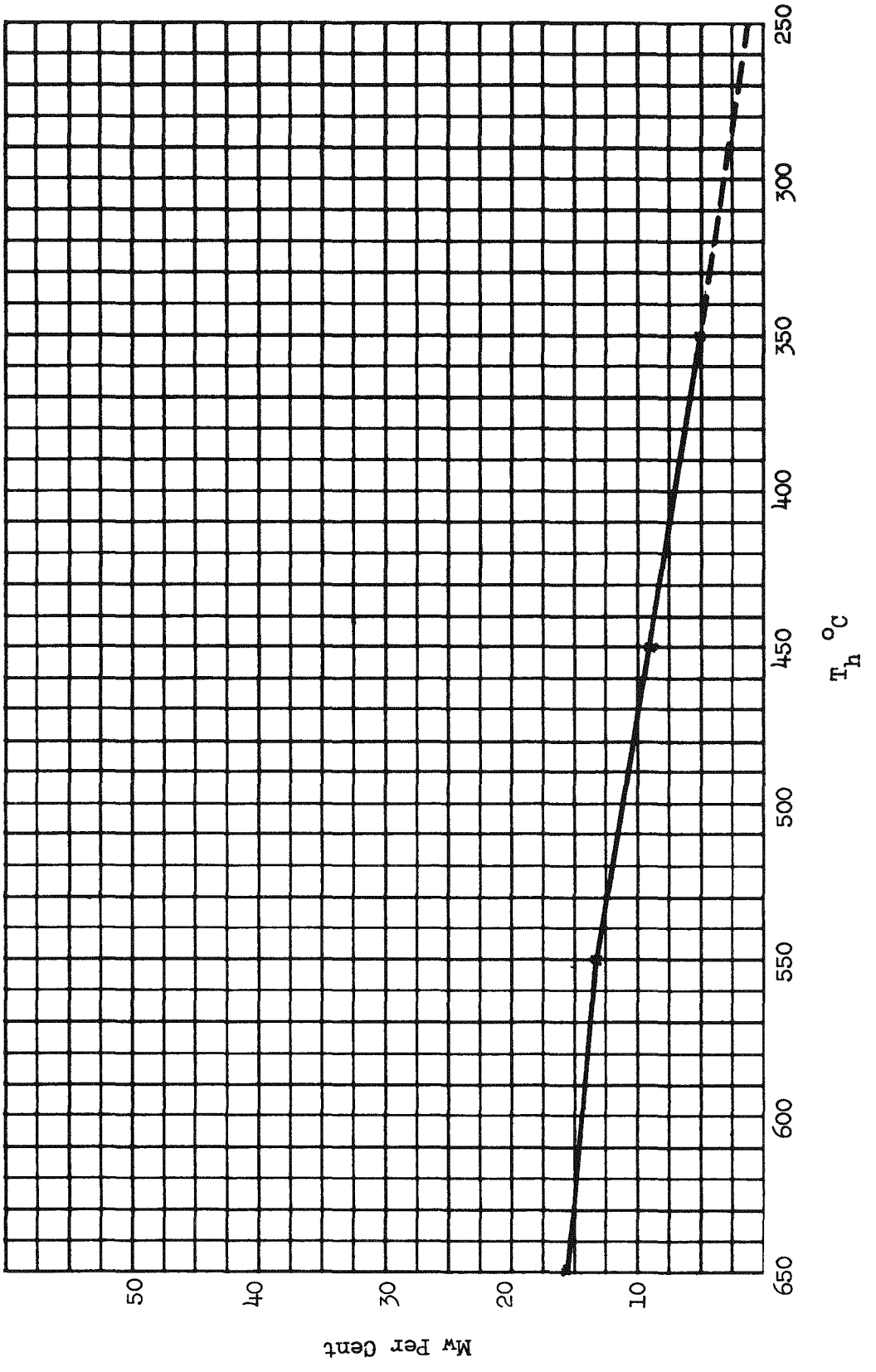

Fig. 40. Mw versus T°C

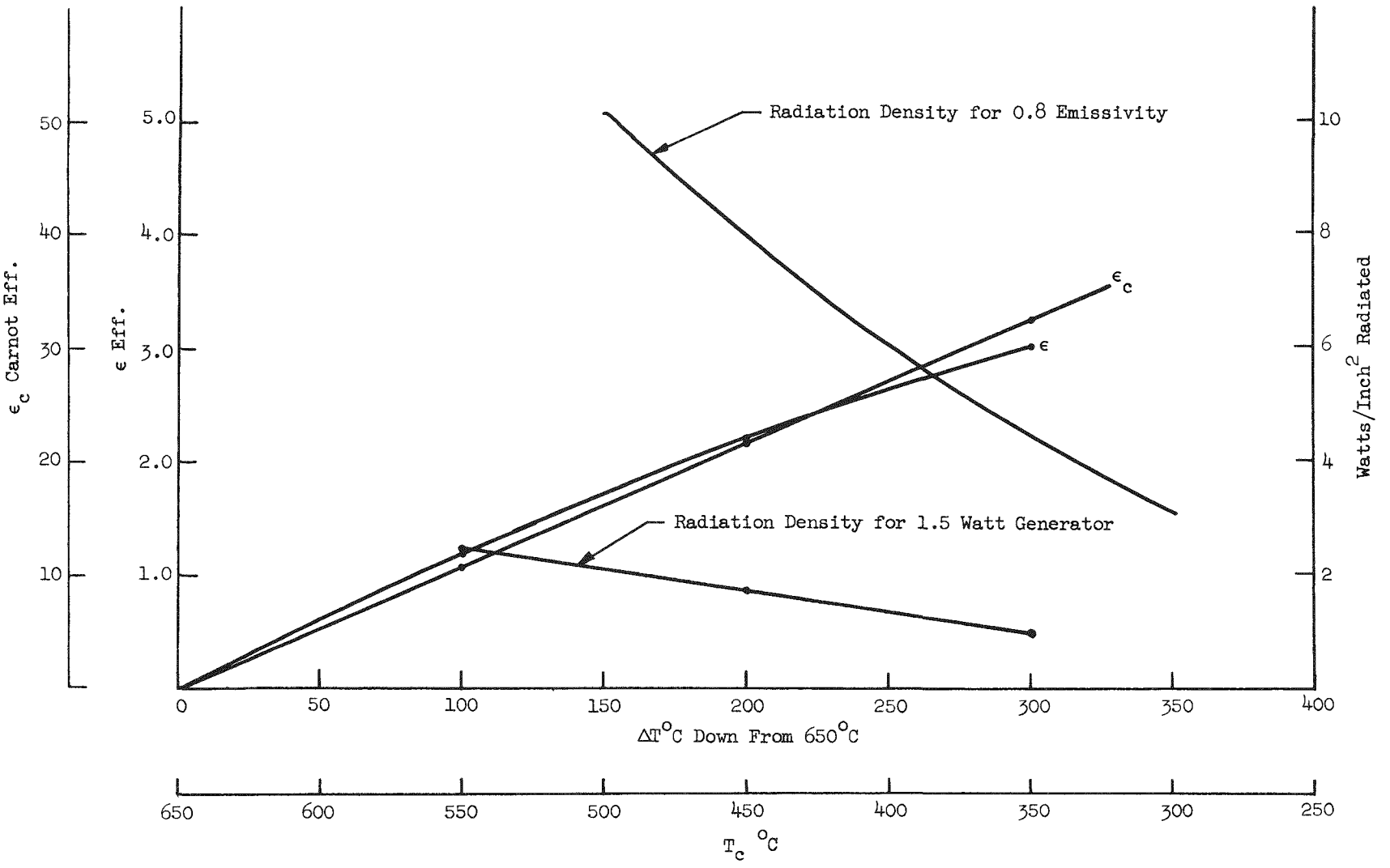

Fig. 41. Radiation Density for 0.8 Emissivity

TABLE 15

Parameters of GeTe (Leg No.2)

$T^{\circ}C$	$T^{\circ}K$	Ohm Cm ρ	Watts/Cm $^{\circ}C$ k	μ v/$^{\circ}C$ α
560	923	6.2×10^{-4}	4.4×10^{-2}	165
550	823	6.0×10^{-4}	4.6×10^{-2}	158
450	723	5.6×10^{-4}	4.8×10^{-2}	140
350	623	4.2×10^{-4}	5.6×10^{-2}	102

TABLE 16

Summary of Mw

$T^{\circ}K$	$T^{\circ}C$	Mw (per cent)
923	650	15.5
823	550	13.3
723	450	9.3
623	350	5.0

Employing the GeTe - InAs couple, 24 couples, four pairs per module, will be used to obtain a two-volt open circuit. Each of the legs will be two centimeters long and about 0.1 cm^2 in area.

2. Heat Dump Regulator

The control system considered is for a power supply consisting of a thermoelectric generator and a heat source which decays in time. Since the heat power available decreases with time, it is necessary to regulate the heat delivered to the generator to maintain the output constant. (The reasons for this are discussed in Appendix B). The principle or regulation is to provide a heat dump for diverting part of the heat supply away from the generator by controlling the efficacy of the heat dump according to the temperature of some part of the generator. In SNAP III the control temperature will be closely related to the cold junction temperature. Since heat rejection is by radiation only, this control will fix the heat flux through the generator and thereby determine ΔT between hot and cold junction temperatures.

The efficacy of the heat dump is varied by varying the pressure of helium gas in the heat dump enclosure. The amount of heat diverted away from the generator is decreased by lowering the helium gas pressure, which in turn causes

a decrease in the thermal conductivity of the medium around the heat dump. As the intensity of the heat source decreases, the pressure of helium is lowered by means of two thermostatic valves each having a sensing bulb adjacent to the control point on the thermoelectric generator. These are arranged to bleed a fixed volume of helium out of the heat dump housing when the cold junction temperature drops a preassigned amount.

Each thermostatic valve is provided with a hydraulic thermal element charged with Dow Corning DC 550 fluid which is stable in a closed system at 700°F. The thermal element (a modified Robertshaw oven Diastat) consists of a 10-3/8 inch by 3/16 inch outside diameter steel bulb, a 3 foot by 3/32 inch outside diameter copper capillary, and a 1-1/4 inch outside diameter stainless steel diaphragm. The element is charged with the thermal fluid under vacuum and sealed at 450°F. The bulb is the sensing member and the effect of the bulb fluid volume change with temperature is transmitted through the capillary to the diaphragm which in turn actuates the valve at temperatures above 450°F. The valve disks are faced with Teflon and close with a force of about six pounds.

The manner of operation may be described with the aid of Fig. 42, which shows the control system located in a portion of the generator housing, with the sensing bulbs near the generator cold junctions and the two valves connected with a storage chamber between them so that gas may be extracted from around the heat dump to the outside of the generator. Assuming that for normal operation the temperature of the generator cold junctions is 700°F, Valve 1 is closed, thus sealing the generator housing and Valve 2 is opened to the outside, thus establishing low pressure conditions in the storage chamber.

When the intensity of the heat source decreases, Valve 2 will close at a bulb temperature of 695°F and Valve 1 will open at a temperature 680°F. At this lower temperature, gas from around the heat dump is admitted to the storage chamber where it is retained since Valve 2 is closed at temperatures below 695°F. The effective increase in volume around the heat dump lowers the gas pressure and causes an increased heating of the generator. As the bulb temperature increases, Valve 1 closes at a bulb temperature of 680°F, thus trapping a volume of gas at housing pressure in the storage tank. Valve 2 opens at a bulb temperature of 695°F, thus exhausting the trapped gas to outside space and again establishing low pressure conditions in the storage chamber.

The thermoelectric power supply is designed to operate initially at a cold junction temperature of about 700°F, and the storage chamber is designed to bleed sufficient gas so as to maintain the operating temperature between 680 and about 700°F. If the intensity of the heat source decreases so that the operating temperature drops below 680°F, Valve 1 will seal the system from the outside.

Tests were successfully conducted that established the feasibility of controlling pressure in a chamber by such thermostat pump as illustrated in Fig. 42. One test was of the pumping action with two valves, and one was of the performance and sealing properties of thermostatic valves, similar to those to be used.

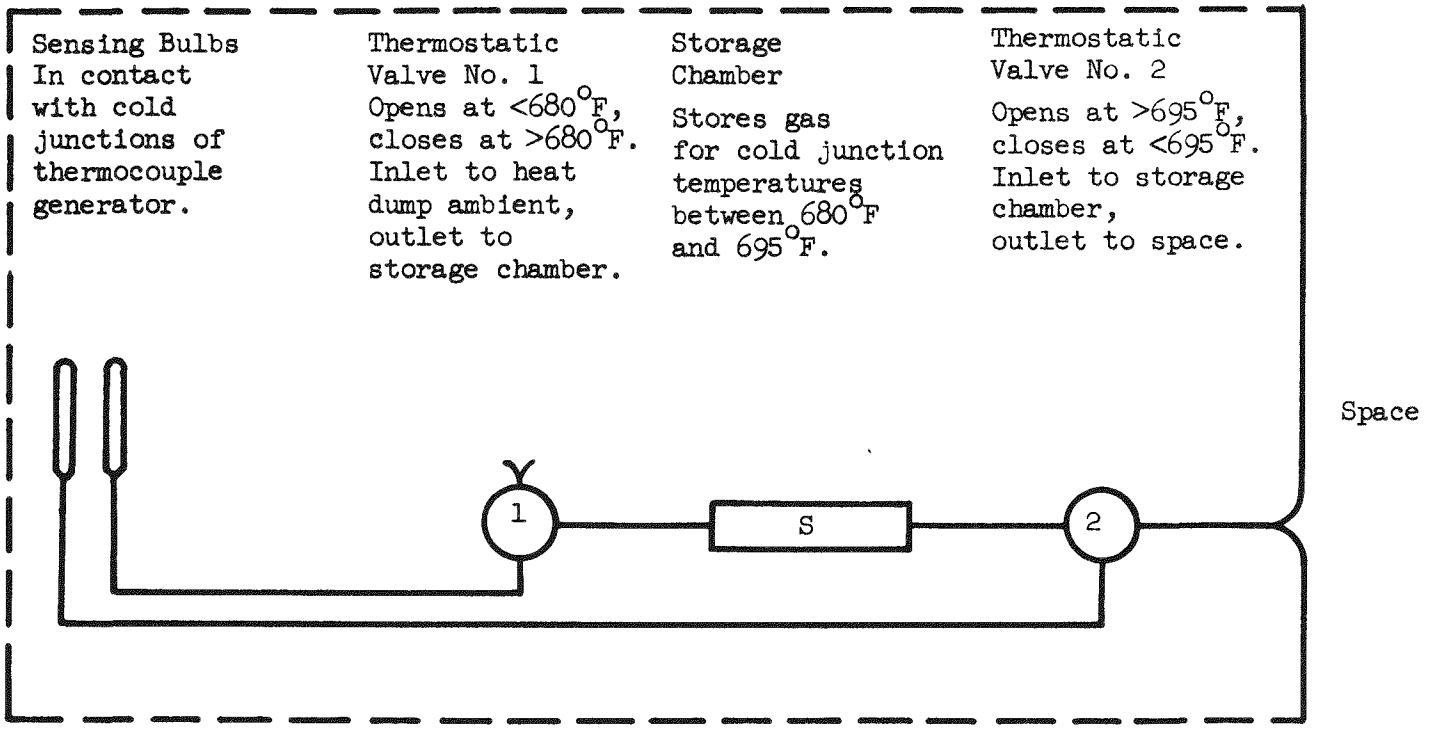

Fig. 42. Schematic Arrangement of Control System

VIII. TASK VIII - HANDLING AND TRANSPORTATION EQUIPMENT

Conceptual studies of equipment, systems and techniques for transporting, handling, servicing and installing the SNAP I Unit, were initiated in this quarter. The work was divided into two phases, the assembly phase which will be conducted at Oak Ridge and the Martin Facility and the installation phase which will be accomplished at the launch site. A report (MND-P-1513) was completed on the first phase and was presented to Oak Ridge National Laboratory on September 11th. Verbal approval of the system was given. A report on the second phase, which includes installation and servicing the unit at the launch site, is being prepared.

A. ASSEMBLY PHASE

The primary piece of equipment required for the assembly phase is the transport vehicle. Two half-power boilers will be supported on the vehicle by gimbaled fixtures which will be used to facilitate loading the isotope into the boiler at the Oak Ridge Hot Cell. The gimbaled fixture will also serve as an assembly jig on the vehicle for tying together the two half-power units and installation of accessories at the Martin Facility.

A cooling system consisting of a bank of radiators and circulating pumps is provided on the vehicle to remove the heat generated in the boilers by the radioisotope. Warning devices will be used to detect a temperature rise in the coolant mercury. A rise could result from pump failure, power supply failure or a system leak. Safety features are included in the event of these failures. Auxiliary pumps and means of re-circulating the mercury are provided. Sumps are placed under the radiator and pumps to catch any mercury which may leak. The mercury would be drained into a reservoir, filtered, and pumped back into the system.

A four section radiator is used, and replacement of any one section is permitted during operation. A pressure sensing device is provided to warn of a mercury drop in the shield container and to sound an alarm. Radiation detectors will also be employed to warn against a rise in radiation level, which would result from a loss of shield mercury.

The transport vehicle as shown in Fig. 43 has a low slung chassis mounted on four dual wheels. An integral elevator system is provided to facilitate loading the power unit into the missile. A steel shell covers the assembled unit for protection during shipment and storage. It is split along the center line and opens like a clam shell for access. The transport skid has been sized so that the unit can be shipped in various aircraft with adequate head and side clearance.

B. INSTALLATION PHASE

The primary equipment required for the installation phase are a nose cone support fixture and a mercury cart to contain the cooling system. The equipment used in the first phase will also be required. Report MND-P-1532 illustrates and describes the equipment for the installation phase.

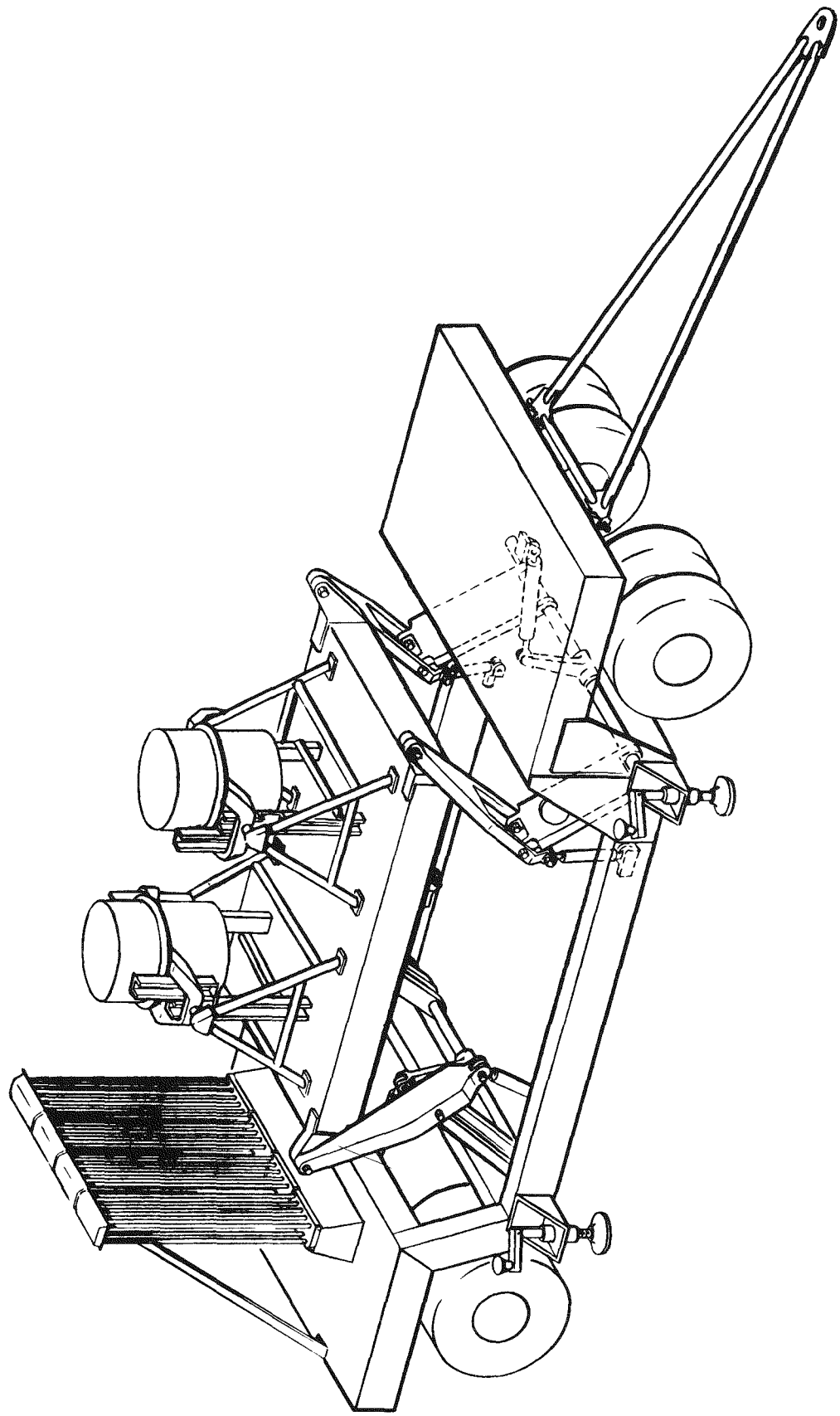

Fig. 43. Transport Vehicle

The nose cone support fixture will hold the nose cone at a proper height so the power unit transport vehicle can be positioned under the nose cone and the power unit elevated directly into it. The fixture will contain leveling and alignment features and will be mounted on casters. (See Fig. 44).

The mercury cart will contain a 116 gallon mercury reservoir, pumps, valves, and a radiator for filling, draining, and cooling the power unit after installation and prior to launching. The cart will be located at the base of the launch pad and will be connected to lines which will run up the umbilical tower to the power unit in the missile.

High pressure nitrogen will charge the reservoir, forcing mercury into the coolant lines, pumps and radiator. Pumps will circulate the coolant mercury. The boiler shield and coolant circuit is drained by purging with the same high pressure nitrogen circuit used for charging. A sump circuit will be provided to collect, filter, and return to the system, any mercury lost by a leak in the radiator or pumps. A warning system similar to that to be incorporated in the transport vehicle will be provided in the mercury cart for detecting abnormal temperature and pressure deviations. The system includes safety features which will prevent siphoning or draining the shield mercury in the event of a line break on the umbilical tower or mercury cart. Auxiliary pumps, circuits, and repair and replacement features incorporated in the transport vehicle cooling system will also be included in the launch pad cooling system.

Fig. 44. SNAP Unit Assembly Stand, Nose Cone and APU

IX. TASK IX - THERMIONIC CONVERSION TECHNIQUES

During this quarter available literature was reviewed. Visits were made to several laboratories conducting experiments in the field of thermionic conversion techniques and to several tube companies that could undertake such investigations.

The objective specification was forwarded to these laboratories with requests to bid on the following: "the development of the unit should culminate in a device that demonstrates capability of meeting all the referenced requirements and can be utilized with a Martin-supplied cylindrical heat source. The program should also show how the techniques employed in developing this unit can be extended to provide power at the 100-watt level."

Power output	1 to 3 watts
Voltage (matched load)	2 volts minimum
Weight	6 pounds
Volume	75 cubic inches
Life	12 months
Heat dump	Radiation only
Efficiency	5 per cent minimum
Maximum temperature of heat source	1000°C
Environment	Zero gravity Shock - 50 G maximum Vibration - 10 to 4000 cps Acceleration 0 10 G maximum

The resulting proposals were evaluated and work statements have been issued for final cost evaluation. Contracts will be awarded in the next quarter.

APPENDIX A

IBM 704 Machine Code

APPENDIX A

IBM 704 Machine Code

This code solves the following differential equation:

$$\left[\frac{\partial^2 T(x,r)}{\partial x^2} + \frac{\partial^2 T(x,r)}{\partial r^2} + \frac{1}{r}\frac{\partial T(x,r)}{\partial r} + \frac{S(x)}{k} = 0\right]_n$$

where: $1 \leq n \leq N$

$2 \leq N \leq 6$

N = number of radial regions

$S(x)_{n>1} = 0$

T = temperature

x = axial position $(0 \leq x \leq L)$

L = core length

r = radial position

k = thermal conductivity

S = volumetric heat production rate

The boundary conditions are:

1. $\frac{\partial T(x,r=0)}{\partial r} = 0$

2. For internal interfaces:

$$T(x,r=R)_{n-1} = T(x,r=R)_n$$

where: R = interface radius

$$\left[k\frac{\partial T(x,r=R)}{\partial r}\right]_{n-1} = \left[k\frac{\partial T(x,r=R)}{\partial r}\right]_n$$

3. For the surface $(n = N)$:

$$\left[k\frac{\partial T(x,r=R)}{\partial r}\right]_n = -k(x)\left[T(x,r=R)-\theta(x)\right]$$

where: h = heat transfer film coefficient

θ = coolant temperature

4. $$\frac{\partial T(x=0,r)}{\partial x} = \frac{\partial T(x=L,r)}{\partial x} = 0$$

The coolant temperature or quality is defined as follows:

1. For $\theta_{in} \leq \theta(x) \leq \theta_{sat}$, $\psi(x)=0$

where: θ_{in} = inlet temperature

θ_{sat} = saturation temperature

ψ = coolant quality

$$\frac{d\theta(x)}{dx} = \frac{2\pi R_N \, h(x) f}{G \, C} \left[T(x,r=R_N) - \theta(x) \right]$$

where: G = coolant mass flow rate

C = coolant heat capacity

f = ratio of tube effective heat transfer area to the surface area of the core (not including the ends).

2. For $\theta(x) = \theta_{sat}$, $0 \; L \; \psi(x) \leq 1$

$$\frac{d\psi(x)}{dx} = \frac{2\pi \, R_N \, h(x) f}{G \, H} \left[T(x,r=R_N) - \theta_{sat} \right]$$

where: H = evaporation enthalpy

3. For $\theta(x) > \theta_{sat}$, $\psi(x) = 1$

$$\frac{d\theta(x)}{dx} = \frac{2\pi \, R_N \, h(x) f}{G \, C \, (x)} \left[T(x,r=R_N) - \theta(x) \right]$$

The heat transfer coefficient is defined by:

1. For $\theta_{in} \leq \theta(x) \leq \theta_{sat} - 300$, $\psi(x) = 0$

$$h(x) = 2.3 \frac{k}{D} \left\{ 1 + 0.1 \left[\frac{G^1 \, DC}{k} \right]^{\frac{1}{2}} \right\}$$

where: k = coolant thermal conductivity

D = equivalent diameter of tube

G^1 = mass flow rate per unit area.

2. For $\theta_{sat} - 300 < \theta(x) < \theta_{sat}$, $\psi(x) = 0$

$$h(x) = \frac{\theta_{sat} - \theta(x)}{300} \left\{ 1 + 0.1 \left[\frac{G^1 DC}{k} \right]^{\frac{1}{2}} \right\} 2.3 \frac{k}{D} + \left[1 - \frac{\theta_{sat} - \theta(x)}{300} \right] \left[A + B\,\zeta(x) + C\,\zeta(x)^2 + D\,\zeta(x)^3 \right]$$

where: A, B, C and D are constants determined by data read into the machine

$$\zeta(x) = T(x, r=R_N) - \theta(x)$$

3. For $0 \leq \psi(x) \leq 0.6$, $\theta(x) = \theta_{sat}$

$$h(x) = A + B\,\zeta(x) + C\,\zeta(x)^2 + D\,\zeta(x)^3$$

4. For $0.6 < \psi(x) < 1$, $\theta(x) = \theta_{sat}$

$$h(x) = \frac{1 - \psi(x)}{0.4} \left[A + B\,\zeta(x) + C\,\zeta(x)^2 + D\,\zeta(x)^3 \right] + \frac{\psi(x) - 0.6}{0.4} \left\{ 0.023 \frac{k(x)}{D} \left[\frac{D\,G^1}{\mu(x)} \right]^{0.8} \left[\frac{\mu(x)\,C(x)}{k(x)} \right]^{0.3} \right\}$$

where: μ = coolant viscosity

and μ, C, and k are vapor properties evaluated at the film temperature.

5. For $\theta(x) \geq \theta_{sat}$, $\psi(x) = 1$

$$h(x) = 0.023 \frac{k(x)}{D} \left[\frac{D\,G^1}{\mu(x)} \right]^{0.8} \left[\frac{\mu(x)\,C(x)}{k(x)} \right]^{0.3}$$

where the properties are evaluated at the film temperature.

APPENDIX B

General Discussion of Use of Radioisotope Heat Source

APPENDIX B

The following is a general discussion of the heat dump and the necessity for it when using a radioisotope heat source and a thermoelectric converter.

The specification requires that P_L watts be available in the load at the end of a specified generator life. To satisfy this requirement there must be a heat flux of P_{Qf} watts available from the fuel or

$$P_{Qf} = \frac{P_L}{\Sigma_f}$$

where: Σ_f is the efficiency at the end of life.

To have P_{Qf} at time, t, one must load P_{Qi}, the initial heat source, which depends upon t and the half-life of the isotope. Consistent with maintaining the specified load power, it is necessary to have maximum efficiency Σ over life, that is, best fuel utilization and lowest fuel cost over life. Thus the difference in junction temperatures, ΔT, must be maximized over the life.

Proposition:

The gradient ΔT should be held constant over the period $t = 0$ to $t = t_f$.

The argument to support this starts with

1. $$P_{Qf} = \frac{P_L \text{ (spec)}}{\Sigma_f \text{ (final } \Sigma)}$$

   a. If P_{Qf} is greater than this, there will be power (and, hence, heat energy) left over above the specification value beyond the life t_f which is wasted with respect to meeting the specification;

   b. If it is less, the specification cannot be met with respect to P_L to t_f;

2. Once the isotope fuel is chosen, P_{Qf} and λ (half-life) determine the initial isotope loading P_{Qi}. The isotope decays according to the law

$$P_Q(t) = P_{Qi} e^{-\lambda t}$$

where: λ is the decay constant (time^{-1}). In one half-life T $P_Q(T) = 1/2\ P_{Qi}$, hence

$$\frac{P_{Qi}}{2} = P_{Qi} e^{-T} \text{ or}$$

$$T = 1/\lambda \ \ln 2$$

also

$$P_{Qf} = P_{Qi} e^{-\lambda t_f} \quad \text{or}$$

$$\frac{P_{Qi}}{P_{Qf}} = e^{-\lambda t_f}$$

Enough equations have been provided to solve for P_{Qi}/P_{Qf} if T or λ and t_f are given.

3. The arguments 1 and 2 imply that to minimize P_{Qi} (which determines the fuel cost) Σ_f must be the greatest possible value. This in turn implies that ΔT_{final} should have the largest possible value; or T_h the greater value and T_c the least value consistent with heat rejection requirements. The statements with respect to T_h and T_c certainly hold if Σ is a monotonically increasing function of $\Delta T = T_h - T_c$. The situation is illustrated graphically in Fig. B-1. The curve P_Q gen(t) which is the heat power passing through the T/E materials must lie somewhere between $P_Q(t)$ and P_{Qf}. It cannot go above by the law of energy conservation and it cannot go below or the specification will not be met at times during the interval 0 to t_f. In practice a line slightly above P_{Qf} would be used. Voltage regulation can then be accomplished by some resistive heat dumping. Maximum utilization of T/E heat rejection area requires that a minimum of heat pass through the T/E materials consistent with supplying the required load P_L. The condition can be accomplished if the temperature T_c is regulated at the lowest possible value, and T_h is kept at the maximum permissible operating temperatures for the thermoelements. Moreover this ΔT is constant over the period $t = 0$ to $t = t_f$ which was the original proposition to be proved.

The discussion and Fig. B-1 show the excess heat power

$$P_Q(t) - P_{Qf} = P_{Qd}(t)$$

must be dumped, that is, dissipated outside of the T/E heat path.

SNAP-III EXAMPLE

It is proposed that in SNAP-III this excess heat be radiated from a surface which is connected to the fuel rod by an insulation which has a thermal

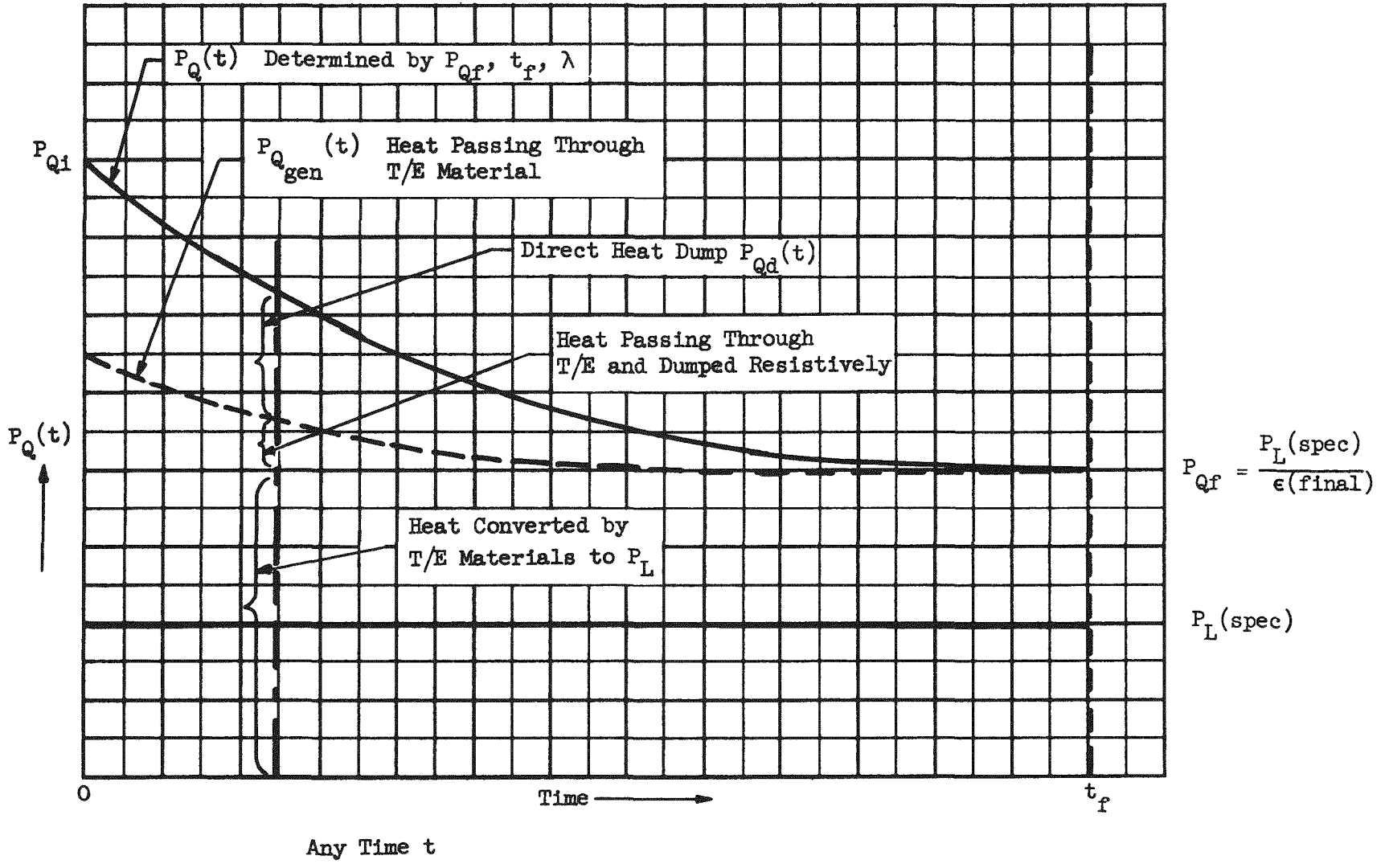

Fig. B-1. Heat Components in T/E System

conductivity which is a function of helium gas pressure in the insulation. The situation is pictured in the following sketch:

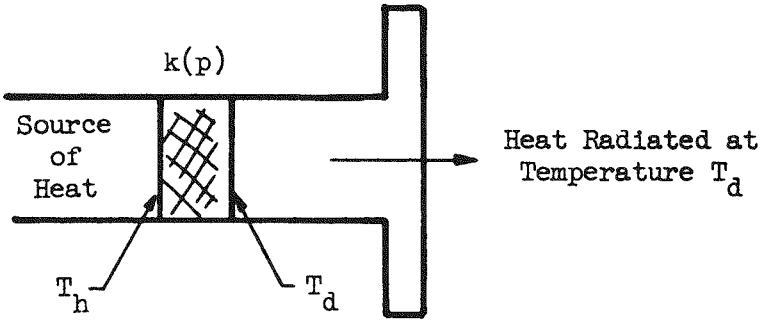

The symbol k is thermal conductivity of the insulation which is dependent upon gas pressure and the type of gas.

The heat flux is determined by the relation

$$P_{Qd}(0) = \frac{k_i A_r}{\ell} \Delta T$$

where:

A_r = radiating area of heat dump in cm^2

k_i = the initial thermal conductivity when P = 1 atmosphere of helium gas

$\Delta T = T_h - T_d$

$P_{Qd}(0)$ = the heat flux at time t = 0 or the initial heat dumped

ℓ = the thickness of the insulating layer

Now $P_{Qd}(0) = P_{Qi} - P_{Qf}$. Although the argument can be carried out in general, it will be more informative to proceed with a numerical example.

Assume $\Sigma(\text{final}) = 1$ per cent

$P_L(\text{spec}) = 3$ watts

$P_{Qf} = \frac{3}{0.01} = 300$ watts

$P_{Qi} = 300 \times 2.45$ for Po^{120} six months - 735 watts

Hence $P_{Qd}(0) = 735 - 300 - 435$ watts.

If $A_r = 50$ in^2, then $P_{Qd}(0) = 8.7$ watts/in^2

To eject this heat at 0.8 emissivity requires a minimum $T_d = 470^\circ$C or 743°K.

Since T_h has been assumed to be 700°C, $\Delta T = 230^\circ$C.

Now from the preceeding equation

$$\frac{P_{Qd}(0)}{A_r} = \frac{k_i \Delta T}{\ell}$$

k_i for santocell at one atmosphere of helium is estimated to be 2.3×10^{-3} watts/cm$^{-\circ}$C.

Hence, $$\ell = \frac{k_i \Delta T}{P_{Qd}(0)} = \frac{2.3 \times 10^{-3} \times 2.3 \times 10^2}{8.7}$$

$$\ell = 0.607 \times 10^{-1} \text{ cm} = 0.6 \text{ mm}.$$

If the helium gas pressure is reduced to ~ 5 mm Hg, a reduction in k of approximately 30 times is expected, that is

$$\frac{k_i}{k_f} = 30.$$

If it is necessary to calculate the heat leakage through the heat dump when k is reduced to k_f (at ~ 5 mm Hg of He gas), that is

$$\frac{P_{Qd}(t_f)}{A_r} = \frac{k_f}{\ell} (T_h - T_{df}),$$

where T_{df} is the final temperature of the heat dump surface, Hence,

$$\frac{P_{Qd}(t_f)}{A_r} = \frac{7.6 \times 10^{-5}}{0.6 \times 10^{-1}} (973 - T_{df})$$

This is solved by plotting the radiation density for 0.8 emissivity as a function of T_{df} for the left side and plotting the right side. The intersection gives $T_{df} = 125^\circ$C

Check: $0.73 = 1.27 \times 10^{-3} (973 - 398)$ watts/in^2

$= 1.27 \times 10^{-3} (575)$

$0.73 = 0.73$

The flux through the dump is 0.73 watt/in^2.

This is to be compared with $\frac{300}{50} = 6$ watts/in^2 out of the T/E radiating area. Under this condition 12 per cent of the heat is dumped with the insulating material in the lowest conductivity state. This may be reduced materially be having the heat dump fins connected to the T/E radiator with about a 50°C gradient in between, then

$$\frac{P_{Qd}(t_f)}{A_r} = 1.27 \times 10^{-3} (973 - 573)$$

$$= 1.27 \times 10^{-3} \times 400$$

$$= 0.508 \text{ watt/in}^2$$

or 8.5 per cent of the total heat is dumped at the time t_f. This can be compared with 8.7 watts initial dump, or a reduction of a factor of 17.